DISSERTATION

submitted to the
Combined Faculty of Natural Sciences and Mathematics
of the Ruperto Carola University Heidelberg, Germany
for the degree of
Doctor of Natural Sciences

Presented by

M.Sc. Bérénice Dorothea Ziegler

born in: Speyer, Germany

Oral examination: 07.05.2021

A Wnt-specific astacin proteinase restricts head organizer formation in *Hydra*

Referees:
apl. Prof. Dr. Suat Özbek
Prof. Dr. Thomas Holstein

“With magic, you can turn a frog into a prince.
With science, you can turn a frog into a Ph.D
and you still have the frog you started with.”

— Terry Pratchett, The Science of Discworld

Table of Contents

Table of Figures

Table of Tables

Digital Supplementary Table of Contents

List of abbreviations

Alp: Alterpaullone; APC: *adenomatous polyposis coli* gene product; Asp: aspartic acid; Azk: Azakenpaullone; BMP: Bone Morphogenetic Proteins; B.Sc.: Bachelor of Science; cDNA: complementary deoxyribonucleic acid; ChIP: Chromatin Immunoprecipitation; CK1: casein kinase 1; DFG: Deutsche Forschungsgemeinschaft; Dkk: Dickkopf; DMEM: Dulbecco's modified Eagle's medium; DMSO: dimethyl sulfoxide; DNA: Deoxyribonucleic acid; ECM: extracellular matrix; et al.: et alia; Fig.: Figure; GFP: Green fluorescent protein; GSK-3: Glycogen synthase kinase 3; gmgc: granular mucous gland cell, hr(s): hour(s); HAS: Hydra Astacin; His: polyhistidin-tag; HL: HL; HPLC: high performance liquid chromatography; HMP: Hydra metalloproteinase; Hy: Hydra; hyp: hypostome; i-cells: interstitial stem cells; ID: Identification; ISH: *in situ* hybridization; LNA: locked nucleic acid; LRP: lipoprotein receptor-related protein; MAM: meprin, A-5 protein, receptor protein-tyrosine phosphatase *μ*; Met: methionine; mRNA: messenger ribonucleic acid; M.Sc.: Master of Science; nematobl: nematoblast, ORF: open reading frame; PBS: Phosphate-buffered saline; PCP: planar cell polarity; PCR: polymerase chain reaction; PDB: Protein Data Bank; Ph.D.: Doctor of Philosophy; RFP: Red fluorescent protein; RNA: Ribonucleic acid; ROR: Receptor tyrosine kinase-like orphan receptor 2; RT: room temperature; RT qPCR: real-time quantitative polymerase chain reaction; SEC: Secretome; smgc: spumous mucous gland cell; SNE: stochastic neighbor embedding; ShKT: Stichodactyla toxin; si(RNA): small interfering (ribonucleic acid); TCF/LEF: T-cell factor/lymphoid enhancing factor; TLL: Tolloid-like; TSP: Thrombospondin; Wnt: wingless/integrated; WISH: Whole-mount *in situ* hybridization; X: *Xenopus laevis*; zmgc: zymogen gland cell.

Abstract

The freshwater polyp *Hydra* is one of the best model organisms to analyze body axis patterning and organizer formation. *Hydra* possesses only one radial-symmetric body axis, which is established and maintained by autocatalytical Wnt/β-catenin signaling in the head organizer. Constant environmental influence, cell flow, as well as injury response can lead to an upregulation of Wnt/β-catenin signaling. A mechanism to restrict Wnt/β-catenin signaling is necessary to ensure the dominance of a single body axis and suppress the formation of ectopic axes and multiple head organizers. So far, only the transcription factor Sp5 (Vogg et al. 2019) has been described as a repressor of Wnt/β-catenin signaling in *Hydra*. Which factors restrict the activity of secreted Wnt ligands at the protein level has been elusive.

In this study, 11 novel *Hydra* astacin metalloproteases (HAS-1 to -11) are described, which were discovered by a secretome analysis for factors showing a proteolytic activity on HyWnt3. All *Hydra* astacins showed a transcriptional profile in endodermal gland cells and either exhibited a ring-like expression pattern under the head region or a graded expression pattern peaking at the tentacle base.

HAS-7 was identified to be a promising candidate to restrict HyWnt3 at the protein level, as *HAS-7* RNAi induced ectopic axis formation in *Hydra*. Importantly, HAS-7 was sufficient to revert double axis formation induced by HyWnt3 mRNA in *Xenopus laevis* embryos. An indirect regulation of *HAS-7* by Wnt/β-catenin signaling was established by experimental promoter analysis and validated by mathematical modelling.

In summary, this work introduces HAS-7 as a negative regulator of HyWnt3 in the classical sense of the Gierer-Meinhardt activator-inhibitor model, and therefore plays an important role in *Hydra* axis formation and maintenance.

Zusammenfassung (German Abstract)

Der Süßwasser Polyp *Hydra* ist einer der am besten geeigneten Modellorganismen zur Untersuchung der Körperachsen- und Organisatorbildung. *Hydra* besitzt nur eine radial-symmetrische Körperachse, die durch den Wnt/β-Catenin-Signalweg im Kopforganisator induziert und autokatalytisch aufrechterhalten wird. Stetig wirkende Umwelteinflüsse, konstante Zellmigration, sowie Verletzungen können zu einer Hochregulierung des Wnt/β-Catenin-Signalwegs führen. Ein Mechanismus zur Regulierung dieses Signalwegs ist hierbei essentiell, um das Entstehen mehrerer Kopforganisatoren und Achsen zu verhindern. Bislang ist nur der Transkriptionsfaktor Sp5 (Vogg et al. 2019) als ein Repressor für den Wnt/β-Catenin-Signalweg auf Trankriptionsebene in *Hydra* beschrieben worden. Ein Faktor, welcher die Aktivität von sezerniertem Wnt auf Proteinebene limitiert, war bislang nicht bekannt.
In dieser Arbeit wird erstmals eine Gruppe von Astacin-Metalloproteasen (HAS-1-11) in *Hydra* beschrieben, die durch eine Sekretomanalyse des Kopfgewebes im Hinblick auf HyWnt3-prozessierende Faktoren entdeckt wurde. Alle untersuchten Astacine zeigten eine Expression in endodermalen Drüsenzellen, entweder in Form eines Ringes unterhalb der Kopfregion oder als aufsteigenden Gradienten von der Körpermitte bis zur Tentakelregion.
HAS-7 stellte sich als vielversprechender Kandidat für die Regulierung von HyWnt3 auf Proteinebene heraus, da ein *HAS-7* Knockdown mittels siRNA zu ektopischer Achsenbildung infolge erhöhter Wnt-Aktivität führte. Zudem konnte eine durch HyWnt3 mRNA induzierte Doppelachsenbildung in *Xenopus laevis*-Embryonen durch die zusätzliche Injektion von HAS-7 mRNA revertiert werden. Eine indirekte Regulation von *HAS-7* durch TCF/β-Catenin konnte durch experimentelle Promotoranalysen nachgewiesen und durch ein mathematisches Modell der Achsenbildung verifiziert werden.
Die vorliegende Arbeit führt mit HAS-7 einen Inhibitor von HyWnt3 im klassischen Sinn des Gierer-Meinhardt Aktivator-Inhibitor Modells ein, der eine wichtige Rolle in der Achsenentstehung und -erhaltung von *Hydra* spielt.

Introduction

Hydra as a model organism for regeneration

Hydra is a freshwater polyp that belongs to the phylum Cnidaria. Cnidarians are basal metazoans that represent a sister group to the Bilaterians (Fig. 1 a) (Trembley, 1744) (Weismann, 1883) (Technau et al., 2012). Cnidarian comprises four subphyla: Hydrozoa, Anthozoa, Scyphozoa and Cubozoa.

Hydra is a convenient model organism due to its uncomplicated culture conditions and reproduction strategy. Under favorable conditions, *Hydra* polyps mainly reproduce asexually by budding, which results in a clonal culture. Specific environmental conditions, in particular stressors, such as low temperatures or starvation, can induce sexual reproduction in *Hydra*. Individual animals can be dioecious, where each individual can produce eggs or sperm, or monoecious, where they are hermaphroditic. *Hydra* has a very simple body plan with one radially symmetric body axis (Fig. 1 b). The basal disc is located within the peduncle zone at the most basal end of the polyp. The budding zone is located in the lower third of the body column, which extends from the basal end to the tentacle zone. Located at the apex, the head is situated with the hypostome, which harbors the organizer that expresses *HyWnt3* from a small population of endo- and ectodermal cells (Broun & Bode, 2002) (Nakamura et al., 2011). Furthermore, the hypostome surrounds the mouth, the only opening into the gastric cavity of the animal. The head structure is surrounded by tentacles which are populated by nematocytes, the stinging cells used for prey capture. *Hydras* are diploblastic and consist of endodermal and ectodermal cell layers separated by the mesoglea (Fig. 1 c; Supplementary Fig. 2) (Sarras et al., 1991) (Technau et al., 2012). The ectoderm comprises ectodermal epithelial cells, sensory and ganglion neurons, as well as mature nematocytes. Neurons and nematocytes descend from interstitial stem cells (i-cells), which are multipotent stem cells that also give rise to germline stem cells for sexual reproduction (Bosch & David, 1987) (Nishimiya-Fujisawa & Kobayashi, 2012) (David, 2012). I-cells also give rise to endodermal ganglion neurons and gland cells (Fig. 1 d), which are located in the endodermal cell layer together with endodermal epithelial cells (Murphy, 1977) (H. R. Bode et al., 1987).

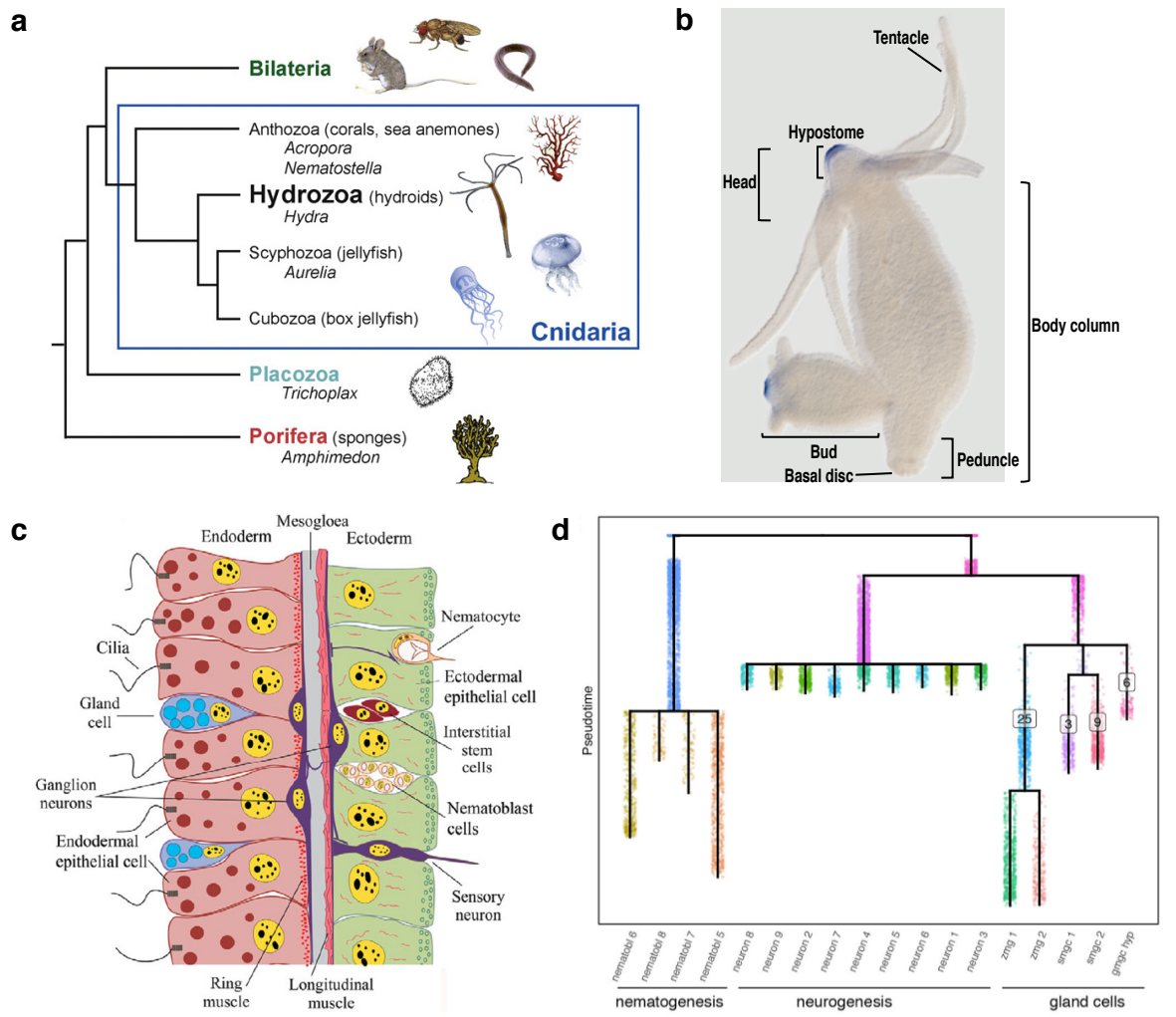

Figure 1. Phylogenetic classification of Cnidaria and *Hydra* body plan.

(a) Adapted from Augustin et al., 2010 (Augustin et al. , 2010). Simplified phylogenetic tree of the lower metazoan. *Hydra* is a genus from the family of Hydridae which belongs to the class of Hydrozoa and to the phylum of Cnidaria. Cnidaria is a sister group to Bilateria. (b) mRNA detection of *HyWnt3* by whole-mount *in situ* hybridization in *Hydra vulgaris* to illustrate *Hydra* anatomy. *HyWnt3* mRNA detection occurs at the hypostomal head organizer, which is located at the tip of the mouth opening (Broun & Bode, 2002). The head is surrounded by tentacles. The body column reaches from the tentacles to the basal end. The budding zone is located at the lower third of the polyp, where asexual reproduction takes place. At the most basal end is the peduncle zone, with the basal disc at the very end. (c) Adapted from Technau & Steele, 2012 (Technau & Steele., 2012). Ectodermal and endodermal cell layers with specific cell types separated by the mesoglea. (d) Adapted from Siebert et al., 2019 (Siebert et al., 2019). URD differentiation tree of the interstitial lineage into nematocytes, neurons and gland cells. Colors represent URD segments and do not correspond to the colors in the t-SNE blots (Fig. 6). Gmgc: granular mucous gland cell; hyp: hypostome; nematobl: nematoblast; smgc: spumous mucous gland cell; zmgc: zymogen gland cell. Numbers indicate different cell populations within a cluster.

Hydra gland cells are part of the endodermal epithelium and arise, as mentioned, from the i-cells, but are also generated via self-renewal (H. R. Bode et al., 1987) (Schmidt & David, 1986). There are three different types of gland cells in *Hydra*: spumous mucous gland cells (smgc), zymogen gland cells (zmgc), and granular mucous gland cells (gmgc) (Fig. 1 d). Gland cells in *Hydra* have phenotypic plasticity, therefore they undergo transdifferentiation when they change their position. This means that they partly change their gene expression in response to the positional-value of the signaling gradient (Siebert et al., 2008) (Augustin et al., 2006). For instance, zmgc inhibit the expression of HyDKK1/2/4c and start expressing HyTSR1 when moving from x to y (Siebert et al., 2019). Moreover, zmgc located in the body column can re-locate to the head region and thereby be transdifferentiated into gmgc. The constant cell flow observed in *Hydra* is not only responsible for these positional changes described above, but also contributes to the astonishing regenerative ability of the organism (Campbell, 1967).

The “Hydra of Lerna” of the Greek mythology served as an eponym for *Hydra* due to its regenerative ability (Pseudo-Apollodorus, n.d.) (Hesiod, 1914). *Hydra’s* high regenerative capacity is well described and is another strong impetus to study *Hydra* as a model organism (T. W. Holstein et al., 2003). Astonishingly, *Hydra* is even able to regenerate its complete body from a single cell cluster (Sato et al., 1992) (Vogg et al., 2019): a process that involves *de-novo* axis establishment and *de-novo* patterning (Miljkovic-Licina al., 2007). In addition, the activity of i-cells play a key role in regeneration by either being paused in G2- or traversing S-phase (Sato et al., 1992) (Vogg et al., 2019); the cycling of which is controlled by injury response (Cummings & Bode, 1984) (Vogg et al., 2019) (Buzgariu al., 2014). Moreover, the Wnt signaling pathway is crucial for axis establishment, as well as patterning in *Hydra.*

The Wnt signaling pathway

Mouse Wnt1, a secreted glycoprotein belonging to the *Wnt* gene family, was first described in 1982 and named in 1991 by Nusse et al. (Nusse & Varmus, 1982) (Nusse et al., 1991). The name “Wnt” is a concatenate of *int-1* and the *wingless* gene from *Drosophila melanogaster* (Rijsewijk, 1987). During evolution, the Wnt gene family initially arose in metazoans during the transition from unicellular to multicellular

eukaryotes (Paps & Holland, 2018) (Reviewed in (T. W. Holstein, 2012)). In metazoans, Wnt is responsible for the evolutionary first polarized development, leading to axis formation by providing the system positional information (Reviewed in (Petersen & Reddien, 2009)).

The Wnt signaling pathways are separated into the canonical Wnt signaling pathway (Fig. 2 b) (Torres et al., 1996) and three non-canonical Wnt signaling pathways, which include the non-canonical Wnt planar cell polarity (PCP) pathway (Fig. 2 a) (Reviewed in (Strutt, 2003)), Wnt/Ror2 pathway (Schambony & Wedlich, 2007) (Unterseher et al., 2004) and the non-canonical Wnt/calcium pathway (Fig. 2 c) (Reviewed in (De, 2011)) (Kühl et al., 2000) (Gordon & Nusse, 2007) (Huelsken, 2002). The canonical Wnt signaling pathway is β-catenin dependent, whereas the non-canonical pathways are β-catenin independent. However, the canonical and non-canonical Wnt signaling pathways are closely interconnected by their utilization of the Frizzled receptors (Weidinger & Moon, 2003).

In a nutshell, the canonical Wnt signaling pathway is based on a β-catenin accumulation in the cytoplasm and its re-location into the nucleus (Fig. 2 b, d). β-catenin acts in concert with TCF/LEF (T-cell factor/lymphoid enhancing factor) as a transcription factor to induce Wnt-active gene transcription (Kühl et al., 2000) (Gordon & Nusse, 2007). β-catenin can also form transcription factor complexes with other transcription factors like Pygopus, although Pygopus can also drive gene transcription independent of β-catenin (Kramps et al., 2002) (Mosimann et al., 2006) (van Tienenet al., 2017). Canonical secreted Wnt ligands are required in the extracellular matrix to ensure an accumulation of β-catenin. At the outer cell surface, Wnt binds to the receptor Frizzled and its co-receptor LRP5/6, which leads to the binding of cytoplasmic Dishevelled (Dsh) on the inner surface. Axin is then recruited and thereby disables the destruction complex (MacDonald et al., 2009) (Kramps et al., 2002). The destruction complex consists of the scaffolding protein Axin, the tumor suppressor *adenomatous polyposis coli* gene product (APC), casein kinase 1 (CK1), and glycogen synthase kinase 3 β (GSK3β). CK1 and GSK3β are required for β-catenin phosphorylation, which leads to the ubiquitination and subsequent targeting of β-catenin for proteasomal degradation (Kramps et al., 2002) (Mosimann et al., 2006). Upon inhibition of the destruction complex, β-catenin is not targeted for degradation and accumulates, which ultimately drives autocatalytic β-catenin/Wnt signaling.

13 different Wnt gene subfamilies have been described in vertebrates. Three of the members belong to the canonical Wnts (Wnt1, Wnt3a, Wnt8) (Reviewed in (Miller, 2002)) (Kusserow et al., 2005) (Shimizu et al., 1997) and play important roles in several developmental processes such as in pattern formation and organizer setup; an example is the formation of the Spemann organizer in *Xenopus* (Shimizu et al., 1997) (Clevers, 2006).

Wnt signaling in Hydra

As mentioned before, *HyWnt3* is expressed alongside other HyWnts in the hypostomal head organizer in *Hydra* and plays an important role in axis maintenance and setting up the hypostomal head organizer (Miller, 2002) (Kusserow et al., 2005). Canonical Wnt signaling was first described in *Hydra* by Hobmayer et al., 1996 (E. Hobmayer et al., 1996) (B. Hobmayer et al., 2000). 11 *Wnt* genes were found in *Hydra*: *HyWnt1, 2, 3, 5, 7, 8, 9/10a-c, 11 and 16* (Lengfeld et al., 2009). Furthermore, 7 out of 11 *Wnt* genes in *Hydra* (*HyWnt1, 3, 7, 9/10a, 9/10c, 11, 16*) showed an expression in the hypostomal head organizer, whereas *HyWnt3* is the earliest Wnt gene expressed during head regeneration (Lengfeld et al., 2009). The other 4 *Wnt* genes have varying spatial and temporal expression patterns: *HyWnt5* and *HyWnt8* are expressed in the tentacles, *HyWnt9/10b* is only expressed during *Hydra* embryonal development, and *HyWnt2* is expressed transiently during the early stages of bud formation (Lengfeld et al., 2009).

A disturbance of the Wnt signaling pathway in *Hydra* can have severe implications for pattern formation. For instance, Alsterpaullone treatment leads to ubiquitous β-catenin accumulation and results in ectopic tentacle formation (Broun, 2005). Furthermore, transplantation of a hypostome, harboring HyWnt3 expressing cells, from one animal to the body column of a separate *Hydra* host results in secondary axis formation in the host animal (Broun & Bode, 2002) (Browne, 1909) (Yao, 1945), which strongly speaks for an involvement of hypostome-specific *HyWnt* expressing cells in axis establishment (Lengfeld et al., 2009). Due to the importance of proper Wnt signaling in normal development, regulation is not only important but required.

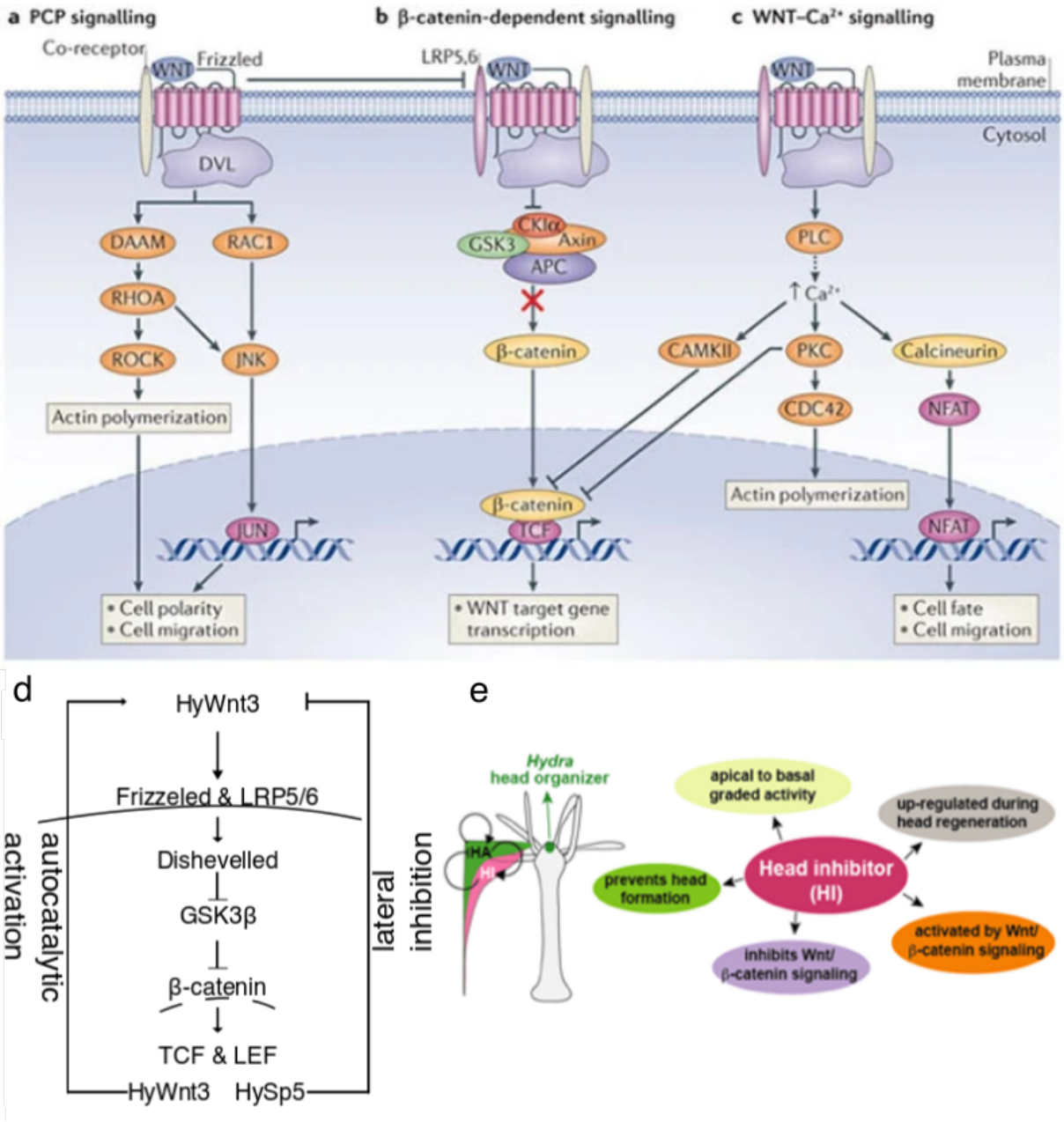

Figure 2. Wnt signaling pathway in Hydra – the reaction diffusion system.

(a-c) Adapted and modified from Niehrs, 2012 (Niehrs, 2012). In (a) the non-canonical Wnt planar cell polarity (PCP) pathway is depicted. (b) shows the canonical Wnt pathway which is dependent on β-catenin signaling. The non-canonical Wnt-Calcium pathway is presented in (c). (d) Adapted from Guder et al., 2006 (Guder et al., 2006). The canonical Wnt pathway appears to be autocatalytic with lateral inhibition as the Turing model with Gierer & Meinhardt extension proposed for pattern formation. For instance, if HyWnt3 is present in the medium, it binds to the co-receptors Frizzled and LRP5/6 which leads to binding of Dishevelled on the inner surface. Dishevelled recruits Axin and thereby inhibits GSK3β by disassembling the destruction complex. β-catenin, which is no longer targeted for degradation by the destruction complex, accumulates in the cytoplasm and relocates into the nucleus where it acts with TCF and LEF as transcription factors to activate, for instance,

HyWnt3 as an autocatalytic feedback loop or HyWnt inhibitors like HySp5 (Vogg et al., 2019) or HydKK1/2/4 (Guder et al., 2006).
(e) Adapted from Vogg et al., 2019 (Vogg et al., 2019). Short-range head activator (HA) situated in the hypostomal head organizer of *Hydra* and long-range head inhibitor (HI) yet unknown. Both act in the reaction diffusion system described by Turing (Turing, 1952) and Gierer & Meinhardt (Meinhardt & Gierer, 2000). Proposed requirements for a proposed head inhibitor in *Hydra*.

In *Hydra*, regulation can occur at the transcriptional level: two examples are regulation by HySp5 with repressor activity (Vogg et al., 2019) (Nakamura et al., 2011) and by HyDkk1/2/4, a Wnt antagonist expressed in the *Hydra* body column (Guder et al., 2006).
In search of a suitable candidate for head inhibition, requirements were postulated by Vogg et al., 2019 (Vogg et al., 2019) (Fig. 2 e). The head inhibitor should fulfill the criteria of being: "(1) expressed in an apical to basal graded pattern, (2) upregulated during head regeneration, (3) able to prevent head formation, (4) activated by canonical Wnt signaling and (5) able to inhibit canonical Wnt signaling" (Vogg et al., 2019). Furthermore, the Inhibitor should be secreted to fulfill the criteria stated in the reaction diffusion system postulated by Turing (Kondo et al., 2010). Sp5 fulfills criteria 1-5 but is not a secreted factor, which means that Sp5 is not a suitable candidate for head inhibition after the reaction diffusion model by Turing because it does not diffuse.

Astacin metalloproteases

Metalloproteases are proteolytic enzymes that require a metal ion for activation, predominantly zinc ions, but cobalt, manganese or nickel ions are also able to activate certain metalloproteases (Chang & Lee, 1992) (Beninga et al., 1998). According to the MEROPS database, 103 families are grouped as metallopeptidases or metalloproteases (https://www.ebi.ac.uk/merops/cgi-bin/family_index?type=P), which are further divided into clans. Metalloproteases are involved in tissue repair (Gajendrareddy et al., 2013), morphogenesis (Detry et al., 2012), protein turnover and regulation, as well as cell growth (Reviewed in (Turunen et al., 2017)). Malfunctions in metalloproteases can lead to fatal consequences like cancer (Reviewed in (Turunen et al., 2017) (Grasso & Bonnet, 2014)).
A highly conserved family of metalloproteases is the metalloendopeptidase astacin family, belonging to the metzincin clan (Bode et al., 1993) (Stöcker & Bode, 1995)

(Gomis-Rüth, 2009) (Reviewed in (Gomis-Rüth, 2003)). Astacins are grouped into the M12 family in the MEROPS database (https://www.ebi.ac.uk/merops/cgi-bin/famsum?family=M12) and are either secreted or are membrane-bound metalloproteases that are activated by Zn^{2+}. Astacin was named after the first member found by Sonneborn et al. in *Astacus astacus*, the European crayfish (Sonneborn et al. , 1969). After mRNA translation astacin is a zymogen with an NH_2-terminal hydrophobic signal peptide required for secretion and a pro-domain which is cleaved to activate the catalytic site that harbors the active site cleft with the central zinc ion (Fig. 4 a, b) (Reviewed in (Gomis-Rüth et al., 2012) (Bond & Beynon, 1995)) (Sarras, 1996). In humans and mice, one member of the astacin metalloprotease family is bone morphogenetic protein-1 (BMP-1), which is able, inter alia, to induce ectopic bone formation in mice (Wozney et al., 1988). Furthermore, five more astacin metalloproteases can be found in human and mouse: *ovastacin*, *meprin1-α*, *meprin1-β*, *tolloid like-1*, *tolloid like-2* (Reviewed in (Gomis-Rüth et al., 2012)) (Karmilin et al., 2019) (Kessler et al., 1996) (Dumermuth et al., 1991) (Stöckert al., 2009). Prominent members of the astacin metalloproteases family in other organisms are *Drosophila melanogaster* Tolloid (Shimell et al., 1991), its *Xenopus* homologue Xolloid (Piccolo et al., 1997), and Medaka low and high choriolytic enzymes (LCE and HCE) (Bond & Beynon, 1995) (Sarras, 1996). Furthermore, in *Xenopus,* a new metalloprotease of the TIKI family was discovered and grouped into the M96 family in the MEROPS database (Zhang et al., 2016). TIKI is expressed in the Spemann organizer and was shown to be required for head formation via cleavage and inactivation of Wnt ligands, especially XWnt8 (Zhang et al., 2013) (Zhang et al., 2016).

Among other things, astacins play an important role in ECM assembly, axis establishment, cell differentiation during development (Shimell et al., 1991) (Nguyen et al., 1994) (Blader et al., 1997) (Maéno et al., 1993) (Piccolo et al., 1997), as well as processing of growth factors (Reviewed in (Bond & Beynon, 1995)). For instance, an important role in ECM formation plays BMP-1, which is described to maturate fibrillar collagen by cleaving off C-peptides from procollagen I-III (Kessler et al., 1996) (Li et al., 1996). Furthermore, BMP-1/TLL growth factors activate growth and differentiation factor 8 (GDF8), as well as GDF11 by cleaving the pro domain, which lead to downstream signal transduction by releasing the mature proteins (Wolfman et al., 2003) (Ge et al., 2005). BMP-1 and TLL1 are also responsible for inhibiting chordin,

which is a main player during early embryonal development in dorsal-ventral pattern formation. This inhibition is caused by removing an EGF motif, which results in a conformational change of chordin, which cause an accessibility for Chordinase (Pappano et al., 2003) (Garrigue-Antar et al., 2004).

In *Hydra,* two astacin metalloproteases have been described, hydra metalloproteinase 1 (HMP1) (Yan et al., 1995) and hydra metalloproteinase 2 (HMP2) (Yan et al., 2000). An important role during *Hydra* head regeneration was described for HMP-1 (Yan et al., 1995) (Yan et al., 2000). Whereas, HMP2 is crucial for foot morphogenesis in *Hydra* (Yan et al., 2000).

Reaction diffusion systems

Turing model and Gierer-Meinhardt extension

One of the most intriguing questions in nature is how can groups of cells with the same genetic information can give rise to different types of organs. More specifically in the case of *Hydra*, how is *Hydra* able to regenerate an entire polyp from a single cell cluster? And how does *Hydra* maintain axis patterning when experiencing constant cell flow? A mathematical model published in 1952 by Turing described a reaction diffusion model for pattern formation based on asymmetric signal concentrations in different parts of an organism, which is the foundation of morphogenesis (Turing, 1952). The model depends on the existence of two secreted, interacting morphogens; one is a short-range activator and the other one a long-range inhibitor, the activity of which results in oscillating morphogen concentrations. Based on the reaction diffusion system, the aspect of autocatalytic activation and lateral inhibition was added to the model by Gierer and Meinhardt (Gierer & Meinhardt, 1972) (Reviewed in (Meinhardt & Gierer, 2000) and (Kondo et al., 2010)). More precisely, the autocatalytic activation means that the activator promotes self-production, as well as the production of its fast diffusing inhibitor which results in a lateral inhibition of the activator itself (Fig. 2 d) (Kondo, 2017). During *Hydra* head regeneration, the organizer has to be formed *de-novo,* as well as in reaggregation experiments, axis patterning must be re-established, which is orchestrated by Wnt/β-catenin signaling. HyWnt3 is fulfilling the most criteria to be regarded as the head activator in *Hydra* (Vogg et al., 2019). Whereas the search of the head inhibitor is still proceeding.

Aim of the work

To date, the regulation of HyWnts, especially HyWnt3, is poorly understood. HyWnt3 regulation has only been described on the transcriptional level by the repressing transcription factor HySp5 (Vogg et al., 2019) and the HyWnt antagonist HyDkk1/2/4 (Guder et al., 2006). Initial experiments performed by Sumit Kumar, Ph. D. revealed a proteolytic activity of recombinant HyWnt3 in *Hydra* HL (HL). After proteomic analysis, HyWnt3-processing samples unveiled astacin metalloproteases as possible HyWnt3 regulators on the protein level. The research goal of this described study was to investigate the involvement of the astacin metalloproteases, above all HAS-7, in HyWnt regulation, and their roles as head inhibitors and in axis establishment and maintenance.

Results

Proteomic approach to identify HyWnt3 proteolytically active candidates in Hydra HL

Initial HyWnt3 stability assays, as well as the sample preparation for mass spectrometry, were performed by Sumit Kumar, Ph. D. (see Supplementary Fig. 1 a). Hydra head lysates were fractionated by cation exchange chromatography and the peak fractions were further analyzed regarding their ability to process recombinant HyWnt3 ((Ziegler et al., 2020) in preparation). Fractions 1 to 5 were able to process HyWnt3 whereas fraction 2 and 3 were also able to partially process Hydra cadherin, which was used as a control (see Supplementary Fig. 1 b). To eliminate background of unspecific proteases like serine or cysteine proteases fractions 1 to 3 were excluded. Remaining fractions (4 and 5), which were able to process HyWnt3 in a 6 hrs time frame, were henceforth called HyWnt3 (+) and pooled, whereas fractions (6 and 7), which were not able to process HyWnt3, were henceforth called HyWnt3 (-) and pooled as well. Both sample pools were analyzed by orbitrap mass spectrometry, which was performed by the Genomics and Proteomics core facility of the DKFZ in Heidelberg. Protein hits were selected for having a signal peptide for secretion and for having at least two peptide hits, which resulted in the HyWnt3 (+) and HyWnt3 (-) secretomes (see Digital Supplementary Table 1 a, b). The largest protein family found in HyWnt3 (+) secretome was the astacin metalloprotease family, the second largest diverse miscellaneous enzymes and the third largest group were diverse secreted factors (Fig. 3 a). In contrast, the content of the HyWnt3 (-) secretome showed top hits in diverse miscellaneous enzymes as well as extracellular matrix (ECM) proteins and receptors (Fig. 3 a). 12 metalloproteases from the astacin family were detected in the HyWnt3 (+) secretome while 6 of them were also found in HyWnt3 (-) secretome but with lower protein hit scores.

Protein stability assay in hydra body part lysates

For further analysis, lysates from different hydra body parts were prepared according to the cutting lines shown in Figure 1 a (black lines) and their concentrations were adjusted to 4 mg/ml using a NanoDrop photometer and α-Tubulin Western blotting (Fig. 3 b, e). Recombinant HyWnt3-His was degraded after 4 hrs in hydra head lysate (HL) and after 6 hrs in hydra upper body part lysate (Fig. 3 b). For control, 1 μg of BSA was not processed during 24 hrs incubation with hydra HL (Fig 3 b). HyWnt3-His processing in 1 x PBS was detectable only after 24 hrs (Fig. 3 b). Longer incubation of HyWnt3-His in 1 x PBS was not tested. Surprisingly, HyWnt3-His was stable at all time points during a 24 hrs time span when incubated with hydra tentacle or hydra lower body part lysates (Fig. 3 b).

To verify the specificity of the hydra HL for HyWnt3, I analyzed the proteolytic activity in the respective body lysates for the Wnt antagonist HyDkk1/2/4. Recombinant HyDkk1/2/4-His was incubated with hydra body lysates as stated above, not showing any processing for any of the respective time points (Fig. 3 b).

Furthermore, HL was incubated with HyWnt3-His together with chelators like EDTA and 1,10-Phenanthroline demonstrating a complete block of the proteolytic activity over a time frame of 24 hrs (Fig. 3 c). The specific matrix metalloprotease inhibitor Batimastat (Rasmussen & McCann, 1997) was also able to inhibit HyWnt3-His proteolysis by hydra HL over 24 hrs (Fig. 3 c), although a slight degradation of HyWnt3-His after 24 hrs could be observed in this case.

To substantiate the hypothesis that the active factor in the HL is an astacin metalloprotease I used Fetuin-B in the next experiment. Fetuin-B was recently described by Karmilin et al., in 2019 (Karmilin et al., 2019) to block specifically astacin metalloproteases like ovastacin. Interestingly, Fetuin-B inhibited the processing of HyWnt3-His by the hydra HL in a dose-dependent manner.

A concentration of 1 μM Fetuin-B completely blocked the proteolytic activity and 0.5 μM reduced the half-life of HyWnt3-His to approximately 8 hrs compared to the control incubation without Fetuin-B, which showed a half-life for HyWnt3-His of approximately 2 to 4 hrs in the used hydra HL batch (Fig. 3 e).

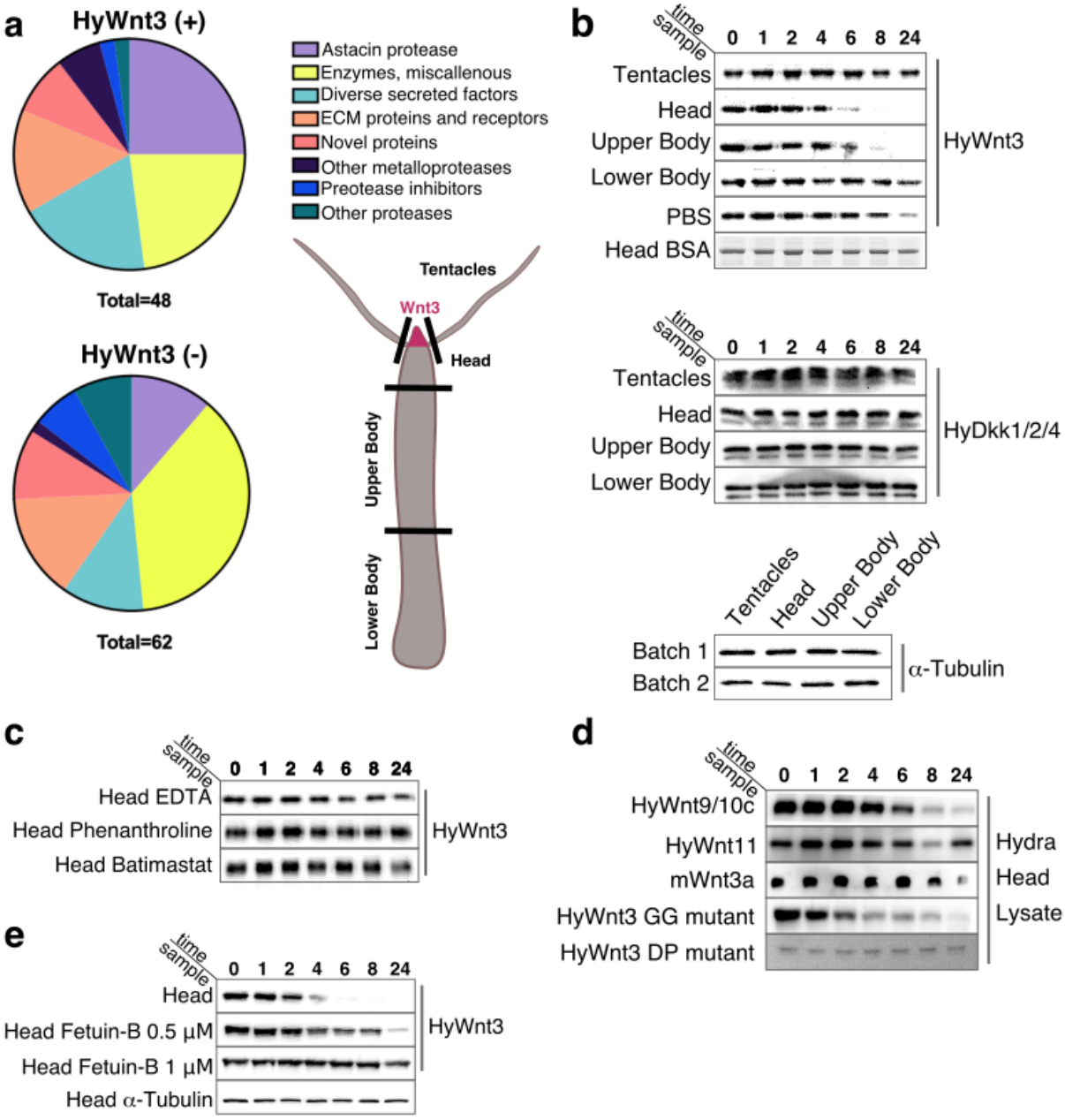

Figure 3. HyWnt-His processing in hydra tissue lysates.

Modified from (Ziegler et al., 2020), in preparation. (a) Distribution of protein classes in *Hydra* HL secretome identified in HyWnt3(+) and HyWnt3(-) fractions as indicated. The full dataset is given in Digital Supplementary Table 1 a, b. Schematic representation of body plan. Cutting lines are marked with black bars. Body parts used for lysates in b-f are indicated. The hypostomal organizer, which harbors HyWnt3 expressing cells, is marked in red. (b) Seven time points were tested during the proteolysis assays: 0, 1, 2, 4, 6, 8 and 24 hrs (b-e). Cleavage of recombinant HyWnt3-His, analyzed by Western blotting with anti-His antibody, reached roughly half-maximal levels after ~4 hrs incubation in HL and after ~6 hrs in upper body lysate. No cleavage was observed during incubation in tentacle and lower body lysates, while incubation in the PBS control showed slight unspecific degradation after 24 hrs. No proteolysis of 1 *µ*g BSA was detectable in hydra HL over the time period of 24 hrs as analyzed by SDS-PAGE and Coomassie staining. No cleavage was observed for the

recombinant Wnt antagonist HyDkk1/2/4-His in the respective body tissue lysates during a 24 hrs incubation time frame. Note that the double band appearing in the blot analysis is due to an SDS-PAGE artifact. The total protein concentration of different hydra body part lysates as indicated in the scheme (a) were adjusted by tubulin Western blotting. (c) Hydra HL proteolytic activity for HyWnt3-His was blocked by the addition of metal ion chelators EDTA and Phenanthroline and the matrix metalloproteinase inhibitor Batimastat. (d) Proteolysis assay for different Hydra Wnts and HyWnt3-His mutants in hydra HL monitored by Western blotting with anti-His antibody. (e) HyWnt3-His processing by hydra HL is inhibited by mouse Fetuin-B in a dose-dependent manner as compared to the control incubation without Fetuin-B.

To analyze the specificity of the hydra HL for HyWnt3-His, other recombinant HyWnts as well as mouse Wnt3a were tested in the stability assay. Compared to HyWnt3-His (4 hrs), HyWnt9/10c-His showed a slightly increased stability when incubated with HL whereas HyWnt5-His showed a similar kinetics as HyWnt3-His (Fig. 3 d). HyWnt11-His stayed stable during the 24 hrs incubation time, indicating that there is no general Wnt proteolysis by the HL (Fig. 3 d). mWnt3a also stayed stable in hydra HL with partial loss of signal after 24h (Fig. 3 d). To verify the predicted DP astacin cleavage motif in HyWnt3 the respective dipeptide was mutated by inserting two point mutations: D187A and P188A (Fig. 3 d). Incubation of the recombinant HyWnt3-DP/AA-His in HL showed no processing in the given 24 hrs time frame. To preclude further a serine protease to be the active component in hydra HL, a dibasic motif adjacent to the DP motif was mutated as well: R189G; K190G. HyWnt3-RK/GG-His was processed by hydra HL with the same kinetics as wildtype HyWnt3-His (Fig. 3 d). In summary, the hydra HL showed a specific proteolysis of HyWnt3 that is likely based on metalloprotease activity. Point mutations of a predicted cleavage site as well as the blocking of cleavage by Fetuin-B strongly indicated that astacin proteases could be responsible for HyWnt3 processing in hydra's head region.

Characterization of the HyWnt3 (+) secretome

The HyWnt3 (+) secretome contained 12 unique astacin sequences, which were called HAS (*Hydra* astacin) (see Table 3 for accession numbers with respective HAS numbers). HAS-1 and HAS-7 had the highest protein score in the orbitrap mass spectrometry (see Digital Supplementary Table 2). Astacins start at the NH_2-terminal end with a signal peptide for secretion followed by a pro-domain, which is cleaved to activate the catalytic domain (Fig. 4 b). An alignment of the pro-domain and catalytical protein regions shows a high conservation of crucial motifs like the aspartate switch region (Asp switch, Fig. 4 a in green), methionine turn (Met-turn: SxMHY, Fig. 4 a in blue) and zinc-binding motif (Zn-binding: HExxHxxGxxH, Fig. 4 a in orange) compared to already described astacins and meprins (Fig. 4 a) ((Ziegler et al., 2020) in preparation). Interestingly, in HAS-1 and Has-7 to -11 the substrate-binding site (S'_1, Fig. 4 a in purple) shows a higher similarity to meprins starting with an isoleucine (I) and a glycine (G), whereas the HAS-2 to -6 S'_1 sites show are more similar to the originally described astacin from crayfish (Fig. 4 a) ((Ziegler et al., 2020) in preparation). Furthermore, up to 6 C-terminal ShKT (*Stichodactyla* toxin) domains were found in the detected *Hydra* astacins. While HAS-1-4 have no ShKT domains, HAS-5 and HAS-6 have one. Two C-terminal ShKT domains were found in HAS-7 to -10 and HAS-11 has 6 ShKT tandem repeats (Fig. 4 b) ((Ziegler et al., 2020) in preparation). No transmembrane motifs were found in any of the analyzed HAS sequences (see Supplementary Fig. 4).

All detected HAS proteinases share similar signal peptide and pro-domain structures as well as highly conserved regions mentioned above. Discrepancies emerged within the S'_1-sites as well as in the number of ShKT domains at the C-terminal end. A phylogenetic tree (Fig. 4 c ((Ziegler et al., 2020) in preparation)) shows that the *Hydra* astacins cluster together with astacins from *Podocoryne carnea* (PMP1) (Pan, Gröger, Schmid, & Spring, 1998) and *Hydractinia echinata* HEA2 (Möhrlen, Maniura, Plickert, Frohme, & Frank, 2006) (Fig. 4 c ((Ziegler et al., 2020) in preparation)). HMP-2 (Yan et al., 2000) is related to astacins in human (hMEPa/ß: Meprin α and β *Homo sapiens*), mouse (mMEPa/ß: Meprin α and β *Mus musculus*) and zebrafish (zMEPa1 and 2/ß: Meprin-1 α, -2 α and β *Danio rerio*) (Fig. 4 c ((Ziegler et al., 2020) in preparation)).

HMP-1 clusters together with astacins found in *Hydractinia echinata* (HEA-1, -3, -4) (Fig. 4 c ((Ziegler et al., 2020) in preparation)).

a

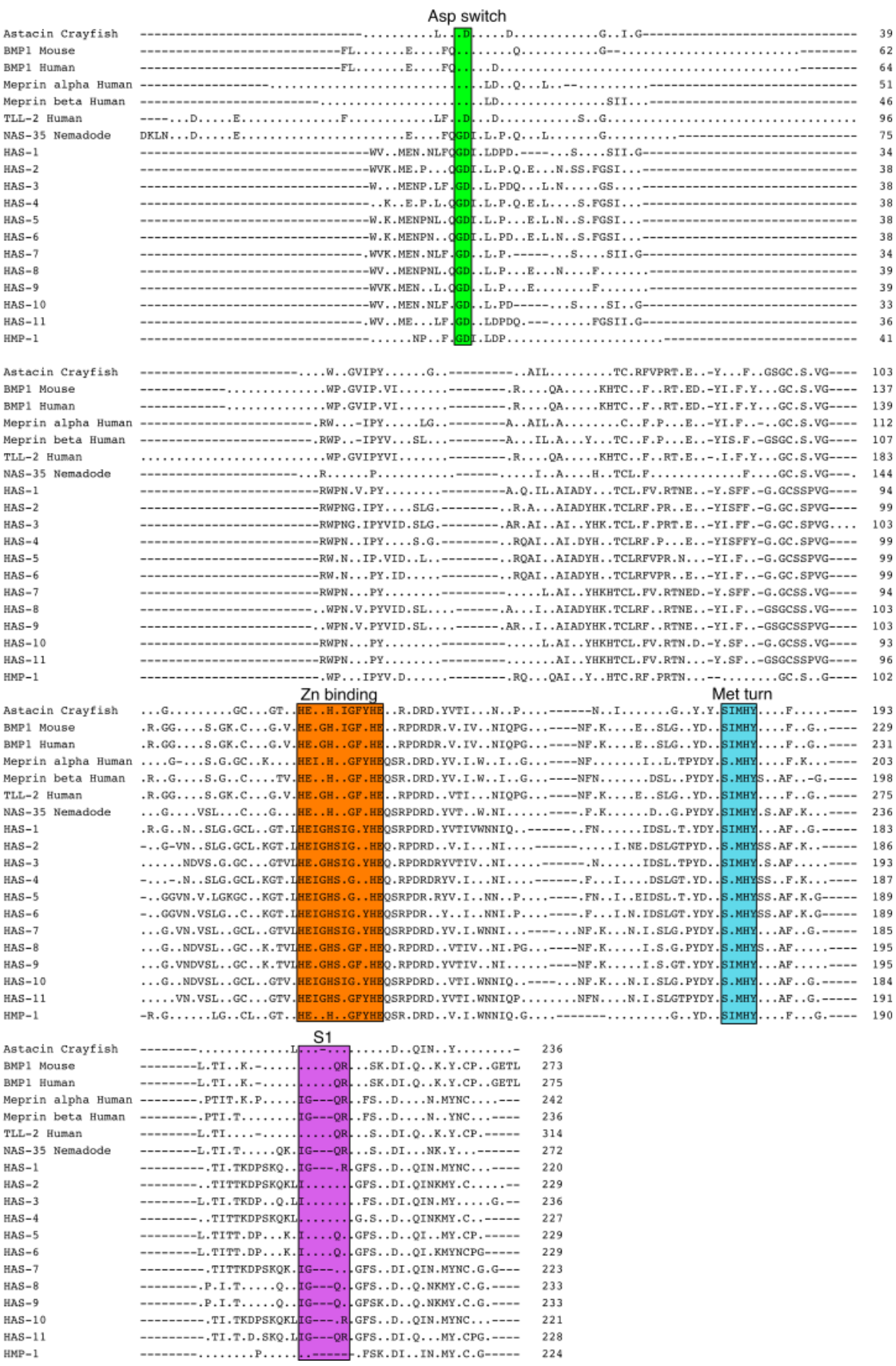

b

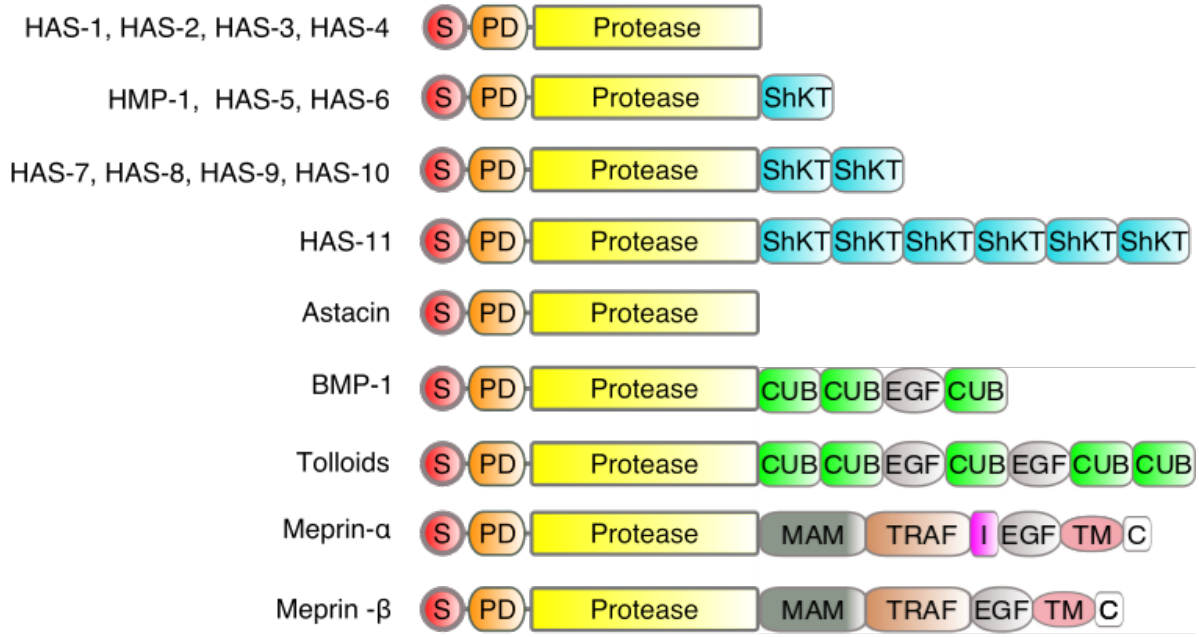
HAS-1, HAS-2, HAS-3, HAS-4
S PD Protease
HMP-1, HAS-5, HAS-6
S PD Protease ShKT
HAS-7, HAS-8, HAS-9, HAS-10
S PD Protease ShKT ShKT
HAS-11
S PD Protease ShKT ShKT ShKT ShKT ShKT ShKT
Astacin
S PD Protease
BMP-1
S PD Protease CUB CUB EGF CUB
Tolloids
S PD Protease CUB CUB EGF CUB EGF CUB CUB
Meprin-α
S PD Protease MAM TRAF I EGF TM C
Meprin -β
S PD Protease MAM TRAF EGF TM C

c

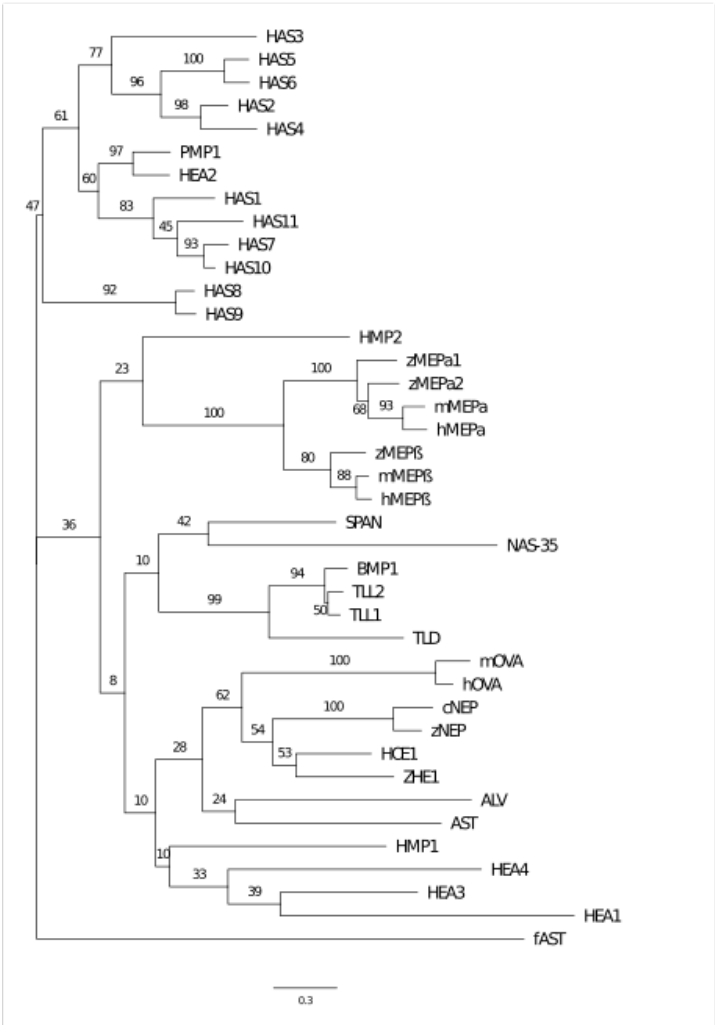
HAS3
HAS5
HAS6
HAS2
HAS4
PMP1
HEA2
HAS1
HAS11
HAS7
HAS10
HAS8
HAS9
HMP2
zMEPa1
zMEPa2
mMEPa
hMEPa
zMEPß
mMEPß
hMEPß
SPAN
NAS-35
BMP1
TLL2
TLL1
TLD
mOVA
hOVA
cNEP
zNEP
HCE1
ZHE1
ALV
AST
HMP1
HEA4
HEA3
HEA1
fAST
0.3

Figure 4. Sequence features of astacin genes found in HyWnt(+).

Modified from (Ziegler et al., 2020), in preparation. (a) Alignment of multiple pro-domain and catalytic domain sequences of HAS and astacin sequences from diverse species outside the cnidarian phylum. Gene ID numbers are as follows: Astacin *Astacus astacus* (P07584), Bone morphogenetic protein 1 *Mus musculus* (BMP-1 Mouse) (NP_033885.2), Bone morphogenetic protein 1 *Homo sapiens* (BMP-1 Human) (NP_001190.1), Meprin-α *Homo sapiens* (Q16819), Meprin-β *Homo sapiens* (Q16820), Tolloid-like protein 2 *Homo sapiens* (TLL2 Human) (AAH13871.1), NAS-35 *Caenorhabditis elegans* (P98060); *Hydra*: HAS-1 (XP_012565441.1), HAS-2 (XP_002162822.1), HAS-3 (XP_002166229.3), HAS-4 (XP_002162738.1), HAS-5 (XP_002164800.1), HAS-6 (XP_002157397.2), HAS-7 (XP_012560086.1), HAS-8 (XP_002153855.1), HAS-9 (XP_002161766.1), HAS-10 (XP_002159980.2), HAS-11(XP_012561076.1), HMP1 (NP_001296695.1).
The aspartate switch residue in the pro-peptide is given in green, the zinc-binding motif is marked in orange and the Met-turn in blue. The residues forming the S1′ (substrate binding site) are indicated in purple. (b) Domain structures of astacins. Cnidarian astacins detected in HyWnt3(+) HL fractions. (S) in red: signal peptide; (PD) in orange: pro-domain; Protease: Proteolytic active domain in yellow. C-terminal domains: (ShKT) in blue: *Stichodactyla* toxin domain; (CUB) in green: for complement C1r/C1s, Uegf, Bmp1; (EGF) in light gray: epidermal growth factor-like ; (MAM) in dark gray: meprin, A-5 protein, receptor protein-tyrosine phosphatase *μ*; (TRAF) in brown: domain found in intracellular signaling proteins; (I) in pink: inserted domain , (TM) in light red: transmembrane anchor; (C) in white: cytosolic domain. (c) Phylogenetic tree HAS-1 (XP_012565441.1), HAS-2 (XP_002162822.1), HAS-3 (XP_002166229.3), HAS-4 (XP_002162738.1), HAS-5 (XP_002164800.1), HAS-6 (XP_002157397.2), HAS-7 (XP_012560086.1), HAS-8 (XP_002153855.1), HAS-9 (XP_002161766.1), HAS-10 (XP_002159980.2), HAS-11(XP_012561076.1), HMP-1 (NP_001296695.1), HMP-2 (NP_001296648.1), HEA-1 *Hydractinia echinata* astacin 1 (Q2MCX9), HEA-2 *Hydractinia echinata* astacin 2 (Q2MCX8), HEA-3 *Hydractinia echinata* astacin 3 (Q2MCX7), HEA-4 *Hydractinia echinate* astacin 4 (Q2MCX6), *Podocoryne carnea* PMP1 (CAA06314.1).

Hydra astacin gene expression patterns

To investigate whether the analyzed proteolytic activity in the HL can be associated with gene expression patterns, whole-mount *in situ* hybridization (WISH) was performed for all HAS genes detected in the HyWnt3(+) secretome. Conventional WISH, using a sense (control) and antisense probe were carried out for *HAS-1*, *HAS-7* and the previously described *HMP1* (Blader et al., 1997) (Yan et al., 1995) (Fig. 5 a-c'). Locked nucleic acid (LNA) probes were designed for the remaining HAS genes. LNAs were used in the WISH assay because of their eminent target specificity for highly similar gene sequences (LNA WISHs were performed by Svenja Kling under supervision) (Fig. 5 d-i). All analyzed astacin genes showed an endodermal gene

expression pattern mainly in the upper part of the body column. Four genes were expressed in a narrow ring beneath the tentacle base (*HAS-5*, *HAS-9*, *HAS-10, HAS-11*) (Fig. 5 e-h). A gradient-like gene expression pattern starting at the tentacle base and fading towards the central body column was observed for *HAS-2*, *HAS-7* and *HMP1* (Fig. 5 a, b, d). *HAS-1* was homogenously expressed in large endodermal cells all over the body column (Fig. 5 c). *HAS-7*, *HAS-2* and *HAS-5* expression reached partly in between the tentacles so that a jagged line appeared in WISH (Fig. 5 a, d, e, Supplementary Fig. 2). Sense probe controls for conventional WISH as well as the scrambled LNA probe showed no coloring reaction (Fig. 5 a', b', c', i). LNA WISH for *HAS-3, HAS-4, HAS-6* and *HAS-8* showed no specific and reproducible staining applying a maximum coloring reaction of 5 days at 37 °C. Also, using hybridization temperatures varying between 50 °C and 60 °C did not yield any detectable staining pattern.

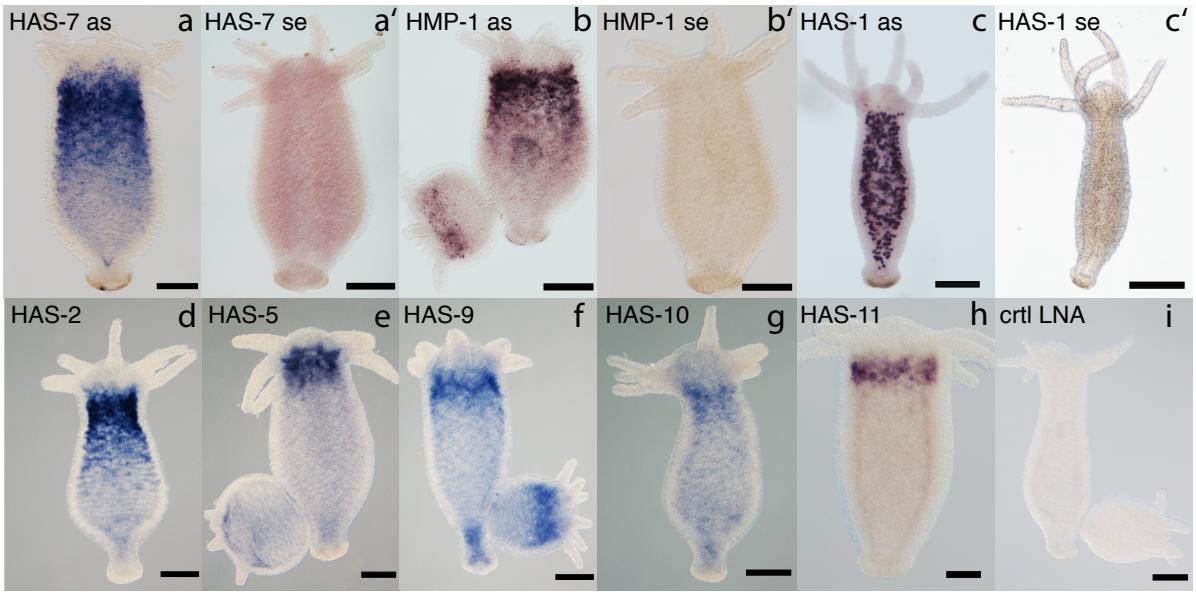

Figure 5. Astacin mRNA expression pattern analyzed by whole-mount in situ hybridization.

(a-c') WISH experiments using antisense DIG-labeled probes (a, b, c) and sense DIG-labeled probes as a negative control (a', b', c'). A graded endodermal gene expression starting under the tentacle base and fading towards the middle of the body column was detected for *HAS-7* and *HMP-1* (a, b) (d-i) WISH experiment with LNAs showed a ring-like expression pattern at the border between head and body column for *HAS-5*, *HAS-9*, *HAS-10* and *HAS-11* (e-h). *HAS-2* also showed a graded mRNA expression as described above (d). The obtained scrambled LNA probe was used as a control, which did not show any coloring reaction (i). Representative of ~ 20 hydras examined. Scale bars: 200 *µ*m: a-c'; 100 *µ*m: d, f-i; 50 *µ*m: e.

To obtain a higher resolution concerning the cell type-specificity of the newly found *Hydra* astacin metalloproteases, the respective genes were analyzed using the recently published single-cell sequencing data from the Juliano Lab (University of California, Davis, USA) (Siebert et al., 2019).

Data was recovered from the official *Hydra* single-cell transcriptome homepage: https://singlecell.broadinstitute.org/single_cell/study/SCP260/stem-cell-differentiation-trajectories-in-hydra-resolved-at-single-cell-resolution. Scatter plots showed that all analyzed genes were contained in the i-cell cluster (Supplementary Figure 3). More specifically, all cell-specific expression signatures were found in i-cell-derived gland cells (Fig. 6). I therefore integrated the Wnt antagonist *Dkk1/2/4* in the analysis as it was described previously to be expressed by gland cells in the body column (Guder et al., 2006). *HAS-1* showed an expression signature in the zymogen gland cell population 2 (zmg2) whereas *Dkk1/2/4* showed expression in zmg2 as well as in zymogen gland cell population 1 (zmg1) and the transition zone between zmg1 and zmg2. An expression in zmg1, zmg2 and in granular mucous gland cell head population (gmgc_head) was detected for *HAS-2*, *HAS-7, HAS-10* and *HMP1*. *HMP1* showed a few hits in zmg2, whereas *HAS-10* scored low in zmg1 and gmgc head cell types. Strikingly, the highest expression counts for *HAS-2*, *HAS-7* and *HMP1* were detected in the transition zone between zmg1 and gmgc_head cell types. *HAS-3* showed expression hits in zmg2 and gmgc_head cells. Furthermore, *HAS-9* showed an expression profile in zmg1 and gmgc_head as well as in the transition zone between both cell types. *HAS-8* showed an expression signature in zmg1 cells as well as a few counts in the transition zones to zmg2 and gmgc_head cells. *HAS-4, HAS-5* and *HAS-6* showed expression counts in gmgc_head cells, as well as a few counts in the transition zone between zmg1 and zmg2. *HAS-4* and *HAS-5* also showed a few expression counts in granular mucous gland cell hypostome population (gmgc_hyp), whereas *HAS-6* showed most expression counts in gmgc_hyp for all analyzed genes. *HAS-11* showed overall a very weak expression signature mainly in gmgc_head with even fewer counts in the transition zone from gmgc_head to zmg1. None of the analyzed genes showed an expression signature in the two spumous mucous gland cell populations (smgc1, smgc2; Fig. 6; Supplementary Fig. 3).

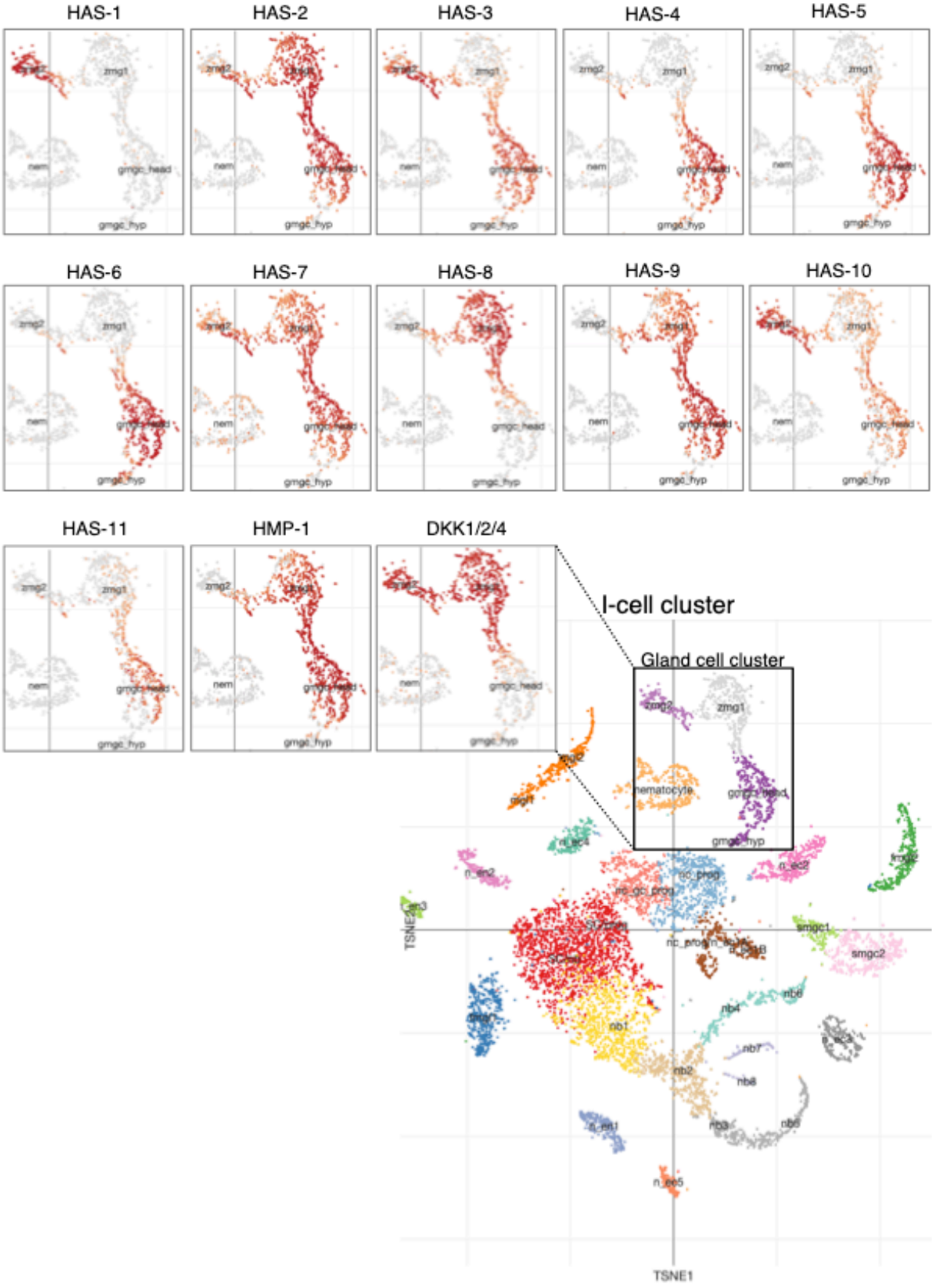
HAS-1
HAS-2
HAS-3
HAS-4
HAS-5
HAS-6
HAS-7
HAS-8
HAS-9
HAS-10
HAS-11
HMP-1
DKK1/2/4
I-cell cluster
Gland cell cluster
zmg1
zmg2
nem
gmgc_head
gmgc_hyp
hematocyte
smgc1
smgc2
nb1
nb2
nb3
nb4
nb5
nb6
nb7
nb8
nb9
TSNE1
TSNE2

Figure 6. Transcriptional profiles obtained by analyzing astacin gene expression in the single-cell sequencing data for the interstitial cell cluster.

The expression profile for all HyWnt3(+) astacin genes as well as for *HyDkk1/2/4* was clustered in the gland cell cluster of the i-cell cluster. Zoomed-in window to the gland cell cluster in the i-cell cluster of the t-SNE blot is as indicated (for overview see Supplementary Fig. 3). The cells in the t-SNE plots were colored based on expression levels for the respective gene using the online tool provided by the Juliano Lab (University of California, Davis, USA) at https://singlecell.broadinstitute.org/single_cell/study/SCP260/stem-cell-differentiation-trajectories-in-hydra-resolved-at-single-cell-resolution (Siebert et al., 2019). The transcript IDs are given in Table 2 "Single cell sequencing IDs". Cluster label abbreviation key is as follows: bat: battery cell, fmgl: female germ-line, gc: gland cell, gmgc: granular mucous gland cell, hyp: hypostome, id: integration doublet, mgl: male germline, nb: nematoblast, nc: neuronal cell, nem: nematocyte, nurse: nurse cells, prog: progenitor, SC: stem cell, smgc: spumous mucous gland cell, zmg: zymogen gland cell. Numbers indicate different cell populations within a cluster.

All analyzed genes showed an endodermal expression in the upper body column in some instances in a gradient pattern starting at the tentacle base.

The expression signature for the analyzed genes were detected in zymogen gland cells as well as in granular mucous gland cell, which all derive from i-cells. Interestingly, the Wnt antagonist *Dkk1/2/4*, also showed an expression signature in this cluster.

HAS-7 knockdown is detectable on the protein level and leads to double axis formation

HAS-7 was chosen to be investigate further because of its high protein score in the mass spectrometry in the HyWnt3 (+) secretome. Furthermore, the graded mRNA expression pattern of *HAS-7* which reflected the observed gradient of HyWnt3-His proteolysis (Fig. 3 b) and thus hinted to a link to pattern formation (Fig. 5 a), was intriguing to further set the focus on this astacin.

To further investigate HAS-7 on the protein level, a polyclonal HAS-7 antibody was raised against a unique epitope in the HAS-7 primary sequence located between the catalytic domain and the N-terminal ShKT domain (APPTAGPTISPT) ((Ziegler et al., 2020) in preparation). This antibody was used in Western blots for HAS-7 detection with different hydra body part lysate samples as well as a full hydra lysate sample. The Western blots showed a band at ~40 kDa (Fig. 7 a), which was the most prominent in the hydra head lysate sample and weaker in the hydra upper and lower body part

lysate samples mirroring the proteolytic activity on HyWnt3 along the hydra body axis. Hydra upper and lower body part lysate samples, as well as full hydra lysate sample showed additional bands at ~70 kDa. Furthermore, a weak band at ~55 kDa was detected in the upper body part and in the full hydra lysate sample. A recombinant HAS-7-His protein sample received from the Stöcker Lab (University of Mainz, Germany) showed a band at ~40 kDa comparable to the band observed in the hydra HL sample (Fig. 7 b). Recombinant HAS-7 showed a slightly higher (~1-2 kDa) apparent MW due to the additional tag sequences.

Then I investigated whether a *HAS-7* siRNA knockdown induced any phenotypical effect. Three siRNAs for *HAS-7* were designed: siHAS7_1 for the pro-domain, siHAS7_2 the catalytical domain and siHAS7_3 a less conserved region in the C-terminal ShKT domain (Table 1: "siRNA sequences"). To confirm that the siRNA knockdown was successful I used the *Hydra vulgaris endo::GFP ecto::RFP* strain and applied a *GFP* siRNA in combination with the target siRNAs and monitored the knockdown effect in the endodermal layer by fluorescence microscopy. The obtained endodermal knockdown of the transgenic *GFP* was half-sided as expected by the transversal electroporation method (see Digital Supplementary Fig. 1, white arrow).

To analyze the *HAS-7* knockdown on the protein level I performed Western blots detecting HAS-7 with full hydra lysates from siGFP treated animals as well as animals electroporated with two siRNA combinations for HAS-7 (1+2 and 2+3). The bands obtained from the siGFP treated hydra lysate showed no difference compared to the full hydra lysate described above (Fig. 7 a, c). Lysates from siGFP and siHAS-7 treated animals were analyzed by Western blot after adjusting total protein concentration using a NanoDrop photometer and α-tubulin detection as loading control. Silencing of HAS-7 using siRNAs 1+2 showed a moderate decrease of the assumed HAS-7 band intensity at ~40 kDa as compared to the siGFP control (Fig. 7 c). Silencing of HAS-7 using siRNAs 2+3 completely eliminated the bands at ~40 as well as at ~70 kDa (Fig. 7 c). I additionally validated the detected knockdown by analyzing transcript levels using quantitative RT-PCR. I checked the transcript level of *HAS-7* in the HLs of steady-state *Hydra vulgaris* (AEP), in HLs after *GFP* and *HAS-7* (2+3) RNAi treatment. A *GFP* RNAi led to no significant changes in the *HAS-7* transcript level (Fig. 7 d) compared to the transcript level of steady state wild type *Hydra* samples.

Strikingly, after *HAS-7* RNAi a significant decrease of *HAS-7* transcripts in the HL could be observed (Fig. 7 d) when compared to the wild type transcript level. The relative quantity after *HAS-7* knockdown was RQ ~0.25 compared to steady state hydras (RQ 1) or to samples after a knockdown with siGFP which showed a relative quantity of ~1 (Fig. 7 d).

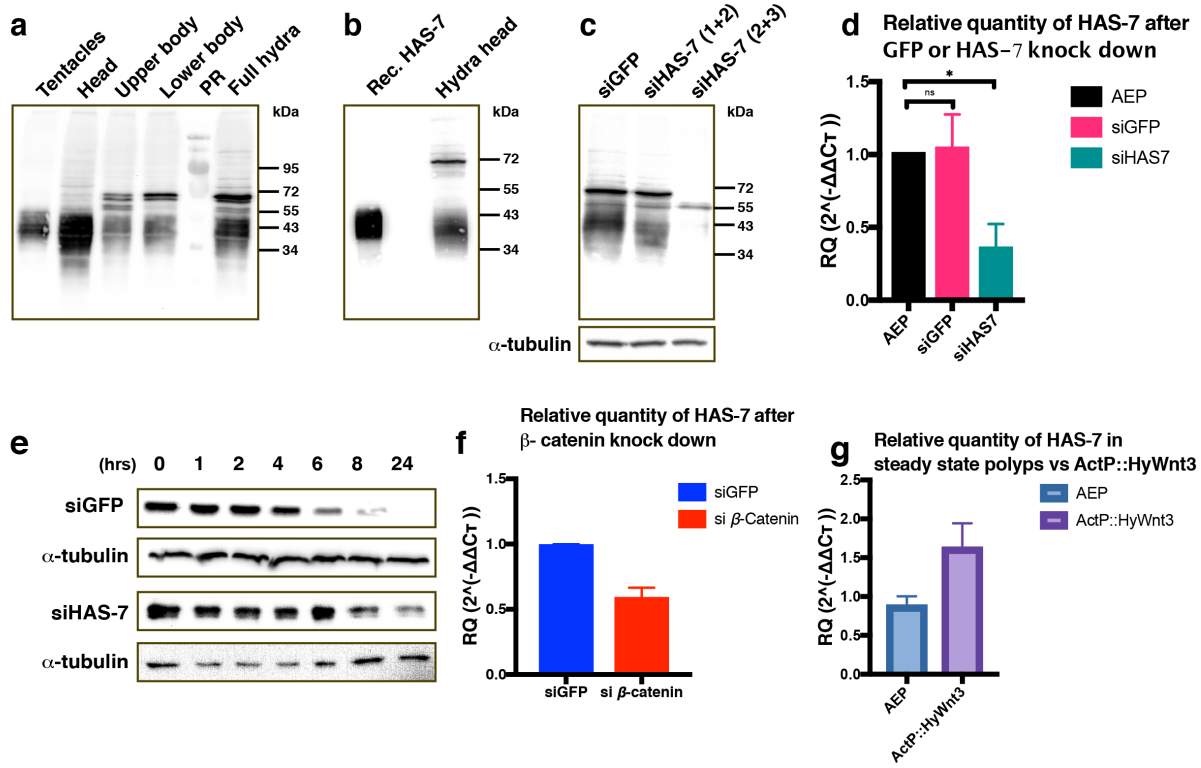

Figure 7. siRNA knockdown of *HAS-7* detected on protein and mRNA level.

Modified from (Ziegler et al., 2020), in preparation. Protein MW is given in kDa (a-c). (a) Western blotting for HAS-7 detection in body lysate samples using a polyclonal HAS-7 antibody. HAS-7 was weakly detected in the tentacles at ~40 kDa while the HL showed a strong signal at ~40 kDa. The upper and lower body part show a weaker signal at ~40 kDa, addtional bands at ~55 kDa and ~70 kDa. The full hydra lysate showed every band described above. PR = protein marker. (b) Recombinant HAS-7 protein expressed in High Five cells (obtained from the Stöcker Lab (University of Mainz, Germany)) (left) compared to native protein in *Hydra* HL as detected by HAS-7-specific antibody (right). Note that that the slightly higher apparent molecular mass is due to the introduced histidine tag in recombinant HAS-7. (c) Analysis of HAS-7 protein levels by Western blotting with HAS-7 antibody in full hydras after treatment with different HAS-7 siRNA combinations as indicated. α -tubulin Western blot detection was used as loading control of the respective hydra lysates. For siHAS-7 combination 1+2 the HAS-7 band at ~40 kDa was weaker, whereas the ~70 kDa and 55 kDa band were unaffected. Moreover, after a HAS-7 knockdown with siRNA

combination 2+3 the ~40 kDa as well as the ~70 kDa bands vanished, whereas the protein band at 55 kDa was unaffected. The distinct band at 70kDa in a-c likely represents a dimer of processed HAS-7. (d) Quantitative real-time PCR analysis of *HAS-7* expression in head tissues confirms the decreased expression in siHAS-7 (siRNA2+3) treated animals compared to siGFP treated and untreated (steady-state AEP animals). Results are given in relative quantity (RQ) ($2^{(-\Delta\Delta CT)}$) and represent mean +/– standard deviation from three biological and respective three technical experiments, analyzed by t-tests. *$p < 0.05$. ns: not significant (e) Proteolysis of HyWnt3-His in hydra HL of *HAS-7* siRNA2+3 treated animals was extended to > 8 hrs whereas a *GFP* knockdown did not have any effects on the proteolysis of HyWnt3-His in the respective HL. α-tubulin was used as loading control for concentration adjustment of the respective HLs applied for each time point. (f) Quantitative real-time PCR analysis of *HAS-7* expression in head tissues obtained from β-catenin RNAi animals compared to *GFP* knock down controls. Results are given in relative quantity (RQ) ($2^{(-\Delta\Delta CT)}$) and represent mean +/– standard deviation from three biological and respective three technical experiments, analyzed by t-tests. *$p < 0.05$. (g) Quantitative real-time PCR analysis of *HAS-7* expression in whole steady state polyps (AEP) versus whole transgenic *Actin::HyWnt3* animals confirms an increased expression of *HAS-7* by increased β-catenin activity. Results are given in relative quantity (RQ) ($2^{(-\Delta\Delta CT)}$) and represent mean +/– standard deviation from three biological and respective three technical experiments, analyzed by t-tests. *$p < 0.05$.

The siRNA knockdown for *HAS-7* using the combination of siRNAs 2+3 was most effective, both at protein level as well as transcript level and was therefore used for all further assays. Next, I analyzed the effect of a *HAS-7* knockdown on HyWnt3-His proteolysis using the respective HLs. HyWnt3-His was degraded after 6 hrs when incubated in HLs from siGFP treated hydras. In comparison, HyWnt3-His proteolysis was significantly retarded in the HL of siHAS-7 treated hydras (Fig. 7 e).

Additionally, I observed morphological changes after RNAi. After *HAS-7* knockdown an ectopic axis formation was observed in about 40% of the hydras (Fig 8 o, q). No ectopic axis formation was observed after *GFP* mRNA depletion via knockdown (Fig. 7 a, b, q). To verify that the ectopic axes are a result of increased Wnt3 activity, I challenged *HAS-7* RNAi treated hydras with Azakenpallone (Azk), which increases the β-catenin concentration globally by inhibiting GSK3-β. siGFP/Azk treated control animals showed ectopic tentacle formation along the body column as expected but no increased ectopic axis formation when compared to siGFP/DMSO treated controls (Fig. 8 b, q). Ectopic tentacles induced by Alsterpaullone (Alp) in the body column were shown to be functional tentacles, which harbor mature nematocytes (Fig. 8 s) as evidenced by CPP-1 staining (Fig. 8 s, s''), as well as in bright field close-up (Fig. 8 s').

Azk treatment after siHAS-7 knockdown led to ectopic axis formation in about 80% of the animals (Fig. 8 c, q). The observed ectopic axis showed a secondary organizer as evidenced by *HyWnt3* reporter expression (Fig. 8 r, arrowheads) at the ectopic hypostome in a transgenic *HyWnt3P::GFP* line. The spot is wider and brighter than ectopic tentacle spots indicative of *HyWnt3* expression along the body column of ALP-treated animals (Fig. 8 r). Furthermore, the ectopic forms a functional head which can capture prey with its tentacles (Fig. 8 p). This phenotype could be completely rescued by a HAS-7/HyWnt3 double knockdown (Fig. 8 g, q). Moreover, a steady-state polyp of *Hydra vulgaris* transgenic strain *ActP::HyWnt3* also showed ectopic axis formation (Fig. 8 e). RNAi silencing of the Wnt antagonist HyDkk1/2/4 followed by an Azk pulse led to ectopic axis formation in ~20% of the animals (Fig. 8 f, q). A *HMP-1* RNAi treatment led in ~45% of the animals to ectopic axis formation after a subsequent Azk pulse (Fig. 8 d, q), indicating some redundancy among Wnt-specific astacins. *HAS-1* siRNA treatment with a subsequent Azk pulse did not lead to ectopic axis formation (Fig. 8 h, q). Nodal-related (Ndr) is required for organizer formation during budding (Meinhardt, 1993) (Watanabe et al., 2014). To analyze if the ectopic axis formation after *HAS-7* depletion requires nodal signaling, a double knockdown of *HAS-7* and *Ndr* was performed, which completely reversed the ectopic axis phenotype (Fig. 8 i, q). A knockdown of *HAS-7* together with *HyWnt8*, which is involved in tentacle formation (Meinhardt, 2012), interestingly resulted in reduced ectopic tentacle formation and in multiple axis formation in 7% of the animals (Fig. 8 j, q). This suggests that ectopic tentacle formation occurs at the expense of ectopic axis formation. To validate this, I performed a long-term treatment using a low concentration of Alp as previously shown by Lengfeld “Der Wnt/ß-Cateninsignalweg und die axiale Musterbildung im Süßwasserpolyp Hydra” (Doctoral thesis 2009). 21 days after the Alp treatment the animals showed ectopic axis formation without ectopic tentacles (Fig. 8 n).

To investigate whether *HAS-7* RNAi showed an effect during the regeneration process, hydras were bisected at 50% body length 6 days after RNAi treatment. During 5 days of regeneration neither the foot regenerates (Fig. 8 k) nor the head regenerates (Fig. 8 l) showed any phenotypical alterations and regenerated normally. This indicates that is not involved in the de novo formation of the head organizer but is rather involved in maintaining the dominance of a single organizer in steady-state animals.

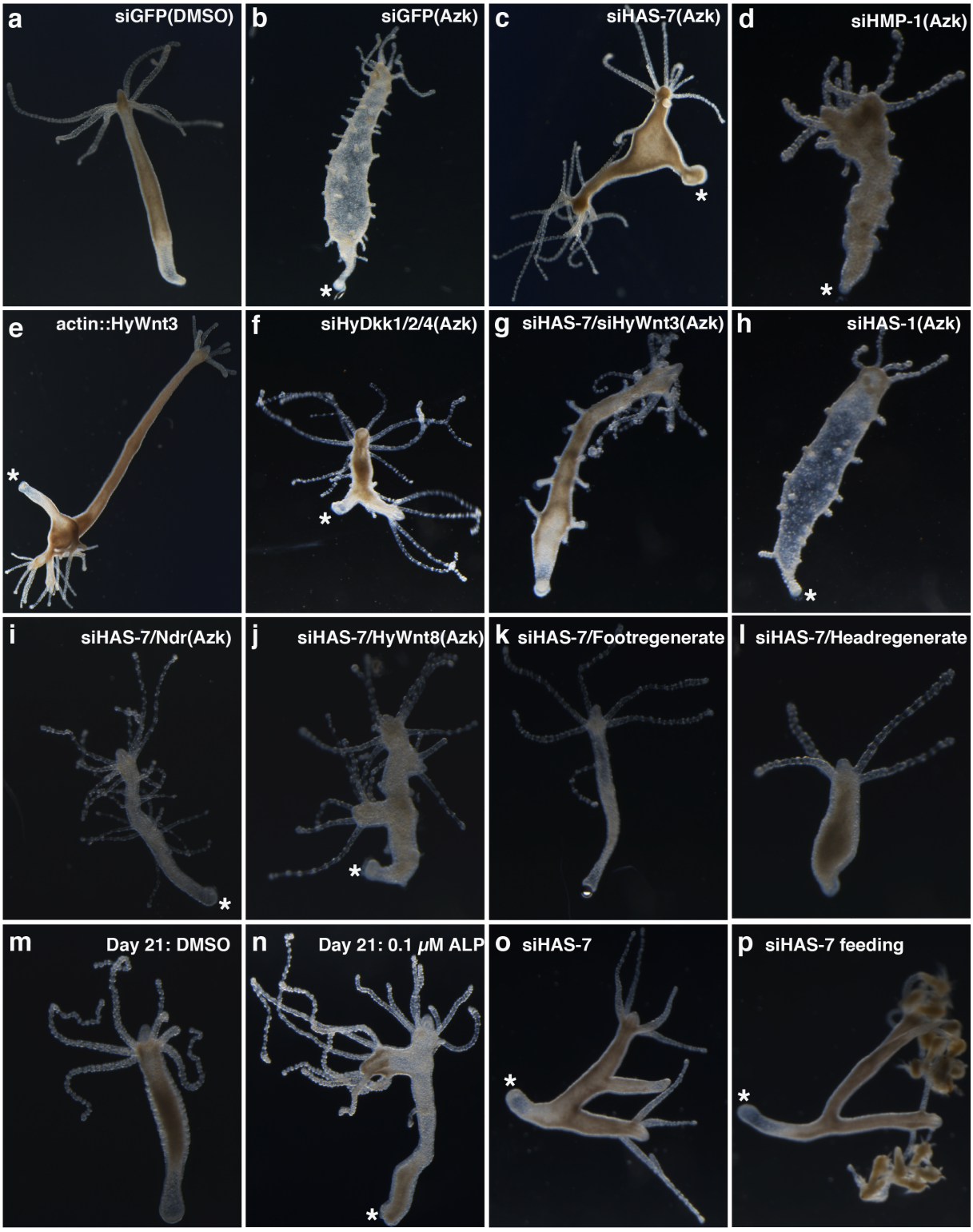
a siGFP(DMSO)
b siGFP(Azk)
c siHAS-7(Azk)
d siHMP-1(Azk)
e actin::HyWnt3
f siHyDkk1/2/4(Azk)
g siHAS-7/siHyWnt3(Azk)
h siHAS-1(Azk)
i siHAS-7/Ndr(Azk)
j siHAS-7/HyWnt8(Azk)
k siHAS-7/Footregenerate
l siHAS-7/Headregenerate
m Day 21: DMSO
n Day 21: 0.1 μM ALP
o siHAS-7
p siHAS-7 feeding

q

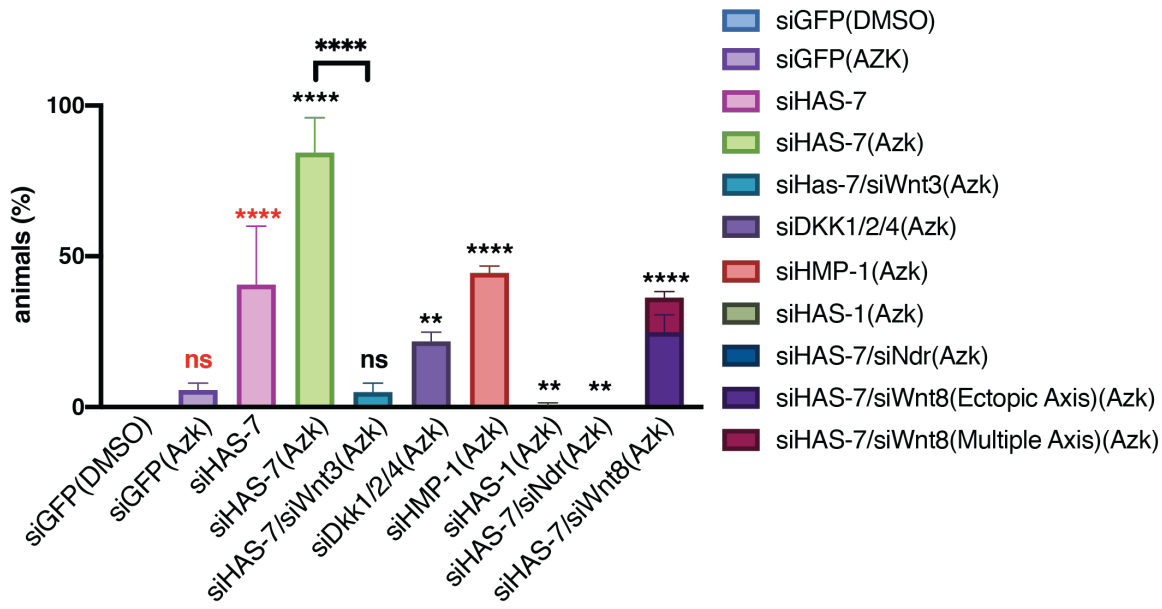
Ectopic axis formation
animals (%)
100
50
0
ns
****
****
ns
**
****
**
**
****
siGFP(DMSO)
siGFP(AZK)
siHAS-7
siHAS-7(Azk)
siHas-7/siWnt3(Azk)
siDKK1/2/4(Azk)
siHMP-1(Azk)
siHAS-1(Azk)
siHAS-7/siNdr(Azk)
siHAS-7/siWnt8(Ectopic Axis)(Azk)
siHAS-7/siWnt8(Multiple Axis)(Azk)

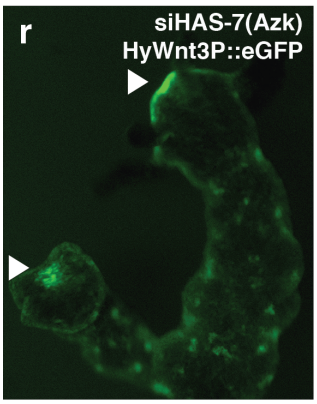
r
siHAS-7(Azk)
HyWnt3P::eGFP

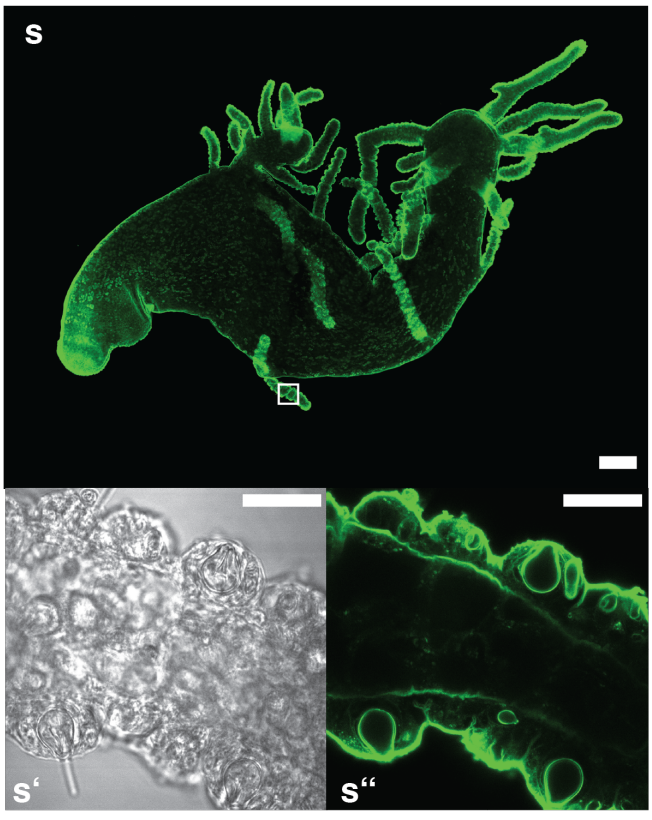
s
s‘
s“

Figure 8. Functional assay of *HAS-7* knockdown by siRNA.

Modified from (Ziegler et al., 2020), in preparation. (a) *GFP* knockdown with DMSO treatment without dissolved Azk showed no phenotypical anomalies compared to steady-state polyps. (b) *GFP* knockdown with Azk pulse showed ectopic tentacle formation along the body column. (c) *HAS-7/GFP* knockdown with a subsequent Azk pulse led to ectopic axis formation with less ectopic tentacle formation along the body column. (d) *HMP-1/GFP* knockdown with a subsequent Azk pulse led to ectopic axis formation with a double head. (e) Ectopic axis formation of transgenic *Hydra vulgaris ActinP::HyWnt3*. (f) *HyDkk1/2/4 / GFP* knockdown with a subsequent Azk pulse led to ectopic axis formation. (g) *GFP/HAS-7/HyWnt3* co-knockdown with subsequent Azk pulse led to a normal, rescued Azk pulse phenotype with ectopic tentacles but no ectopic axis formation. (h) *HAS-1/GFP* with Azk treatment did not lead to ectopic axis formation but ectopic tentacle formation. (i) *HAS-7/HyNdr* co-knockdown with a subsequent Azk pulse led to no ectopic axis formation but showing ectopic tentacles. (j) *HAS-7/HyWnt8* co-knockdown led after an Azk pulse to ectopic axis formation, as well as ectopic tentacle formation. (k, l) 6 Days after *HAS-7* RNAi Hydras were bisected. No ectopic axis formation was observed in the foot and head regenerates after 5 days. (m, n) Long-term Wnt modulation experiment with 0.1 μM Alp and DMSO as a control. 21 days after DMSO treatment start, the *Hydras* showed no morphological change. *Hydras* treated for 21 days with 0.1 μM Alp showed ectopic axis formation. (o, p) Feeding experiment after *HAS-7* RNAi to analyze functional ectopic heads. Ectopic axis formation after *HAS-7* RNAi before feeding (o) and after feeding with *Artemia salina* (p). Both heads were able to catch prey with their tentacles (p). (q) Rate of double axis phenotypes in hydras after electroporation with siGFP or combinations of siGFP with siRNAs as indicated. In animals without subsequent Azk treatment, double axes were counted 6 days after electroporation. In animals treated additionally with Azk, incubation was started 6 days after electroporation and the numbers of double axes in each group were counted 5 days after Azk pulse. Quantity of animals “n” in each group were with a representative picture: (a) siGFP/DMSO = 192, (b) siGFP/Azk = 230, (c) siHAS-7 /siGFP/Azk = 248, (d) siHMP-1/siGFP/Azk = 204, (f) siHyDkk1/2/4/siGFP/Azk = 290, (g) siHAS-7 /siHyWnt3/siGFP/Azk = 203, (h) siHAS-1/siGFP/Azk = 150, (i) siHAS-7/HyNdr = 63, (j) siHAS-7/HyWnt8 = 61, (k) Footregenerates = 25, (l) Headregenearates = 25,(m) 21 Days DMSO = 43, (n) 21 Days 0.1 μM Alp = 41, (o) siHas-7/siGFP = 186. RNAi results from at least three independent experiments are shown. Each column represents the total percentage of one group, bars indicate the mean ± S.E.M. **** P-value < 0.0001; *** P-value < 0.0005; ** P-value < 0.001; * P-value < 0.05; ns: not significant. The data were analyzed for significance using an unpaired parametric T-test with Welch’s correction followed by pairwise multiple comparisons of each group with the other group as indicated. (r) Transgenic *Hydra vulgaris HyWnt3P::GFP* showed hypostomal HyWnt3 expression (white arrowheads) after a *HAS-7* knockdown with following Azk treatment. Smaller spots along the body column are small ectopic organizers which usually give rise to ectopic tentacles, for instance as in (b). (s) CPP-1 immunofluorescence staining of a whole animals 5 days after Azk treatment to analyze if ectopic tentacles have nematocyte capsules and are therefore classified as real tentacles. White box indicates close up zone. (s’, s’’) Close up zone zoom as bright field (s’) and CPP-1 detection (s’’) showing nematocyte capsules in the ectopic tentacle. Scalebars: s = 200 μm, s’ and s’’ = 20 μm. siRNA combination 2+3 was used to document *HAS-7* knockdowns (c, g, i-l, o, p, r). Transgenic *Hydra vulgaris endo::GFP ecto::RFP* were used in (a-p) unless indicated otherwise. Asterisk marks the peduncle region (b-f, h-l, n-p).

To further validate the inhibition of HyWnt3 by HAS-7 *in vivo* I performed co-injections in *Xenopus laevis* embryos. An injection of 10 pg codon-optimized *HyWnt3* mRNA induced double axis formation in ~15% of the embryos compared to a 10 pg *XWnt8* injection, which led to double axis formation in ~60% of the injected animals as detected in the tail bud stage (Fig. 9 b, d). ~60% double axis formation was reached after an injection with a total of 100 pg of codon-optimized *HyWnt3* mRNA. This phenotype could be rescued by a co-injection of 100 pg codon-optimized *HAS-7*, which led to a significantly reduced double axis formation of ~3% (Fig. 9 d). Uninjected embryos as well as injection with scrambled mRNA did not show double axis formation (Fig. 9 a, d). 5% of the animals which showed a secondary axis showed more severe ectopic axis formation phenotypes with a dorso-anterior index of 8 (DAI 8) (Kao & Elinson, 1988) (Fig 9 c).

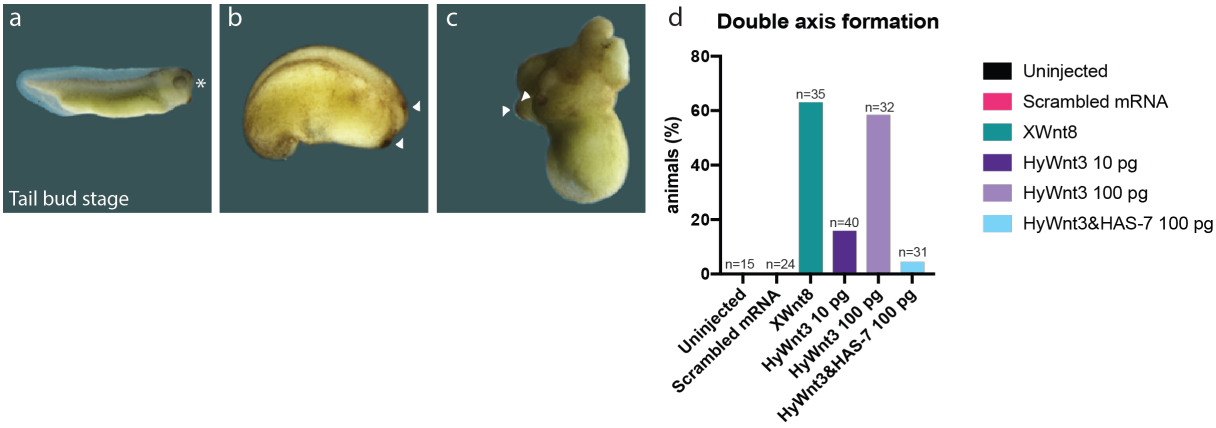

Figure 9. Double axis assay in *Xenopus laevis* embryos.

(a) *Xenopus laevis* tail bud stage 24. Staging after (Gurdon, 1995). (b, c) Injection with 10 pg or 100 pg of codon-optimized *HyWnt3* mRNA led to comparable ratios of double axis formation with two cement glands, respectively (arrowheads). (d) Uninjected as well as scrambled mRNA injections did not lead to doubles axis. 10 pg *XWnt8* as well as 100 pg codon-optimized *HyWnt3* led to doubles axis formation in ~60% of injected embryos. ~20% double axis formation was documented for injections with a total amount of 10 pg codon-optimized *HyWnt3* mRNA. Co-injection of codon-optimized *HAS-7* mRNA inhibited *HyWnt3* mRNA induced ectopic axis formation in *Xenopus laevis.* DAI was categorized by Kao et al., 1988 (Kao & Elinson, 1988). The quantity of animals analyzed for each experiment is indicated in “n” and each column represents the total percentage of one group.

β-catenin dependency of *HAS-7* expression

For investigation of a possible β-catenin/TCF dependency of *HAS-7,* the expression pattern after β-catenin upregulation with Alp (Watanabe et al., 2014). WISH showing *HAS-7* mRNA detection 24 hrs and 48 hrs after Alp pulse (Fig. 10 b, c) compared to control (time point = 0) (Fig. 10 a, Fig. 5 a). In transgenic *ActP::HyWnt3* hydras WISH showed a strong *HAS-7* mRNA expression pattern in the whole endodermal layer of the body column (Fig. 10 f). WISH experiments (Fig. 10 a-e) were perfomed by Benjamin Trageser and Ann-Katrin Heilig.

Furthermore, I analyzed whether *HAS-7* is regulated by Wnt signaling, a *β-catenin* RNAi was performed and *HAS-7* transcript levels were analyzed using quantitative real-time PCR. A significant decrease in *HAS-7* transcript level can be observed after β-catenin silencing when compared to *HAS-7* transcript levels after *GFP* RNAi (Fig. 7 f). The RQ of samples for *GFP* RNAi was ~ 1 and the RQ of samples after *HAS-7* RNAi was ~0.6.

To validate this β-catenin dependency, I also analyzed *HAS-7* transcript levels from a *Hydra* transgenic line which overexpresses HyWnt3 (*ActP::HyWnt3*), which leads to an ubiquitous β-catenin signaling in WISH (Fig. 10 f) and compared it to wild type hydras by RT qPCR. In transgenic *ActP::HyWnt3* hydras a significant increased level of *HAS-7* transcripts could be detected compared to wild type animals (Fig. 7 g).

A RQ of ~ 1.7 for *HAS-7* could be detected for full body samples of transgenic HyWnt3 overexpressing Hydras, whereas the RQ of samples from wild type Hydras was ~ 1.

As a further investigation of a possible β-catenin/TCF dependency via a predicted TCF binding site upstream of the *HAS-7* coding region, a chromatin immune precipitation (ChIP) using a *Hydra* TCF-specific antiserum (Lommel et al., 2018) (Gufler et al., 2018) was performed by the Hartl Lab (University of Innsbruck, Austria). Upon examination of the *HAS-7* promoter region for regulatory elements, a single putative TCF binding element with the conserved sequence motif 5'CTTTGTT3' was identified (Fig. 10 g), similar to those experimentally confirmed in the *HyWnt3* (Nakamura et al., 2011) and *HmTSP* (Lommel et al., 2018) promoters (CTTTGWW, W=A or T). Chromatin was taken from control polyps and Alp treated animals. No PCR product was obtained with primers flanking the identified TCF binding element in the *HAS-7* promoter in control

and Alp conditions (Fig. 10 g). In contrast, as control an amplification of the TCF binding element in the *HmTSP* promoter yielded the expected PCR product from both samples (Fig. 10 h) ((Ziegler et al., 2020) in preparation). In summary, *HAS-7* gene expression follows β-catenin activity, but is not directly regulated by TCF.

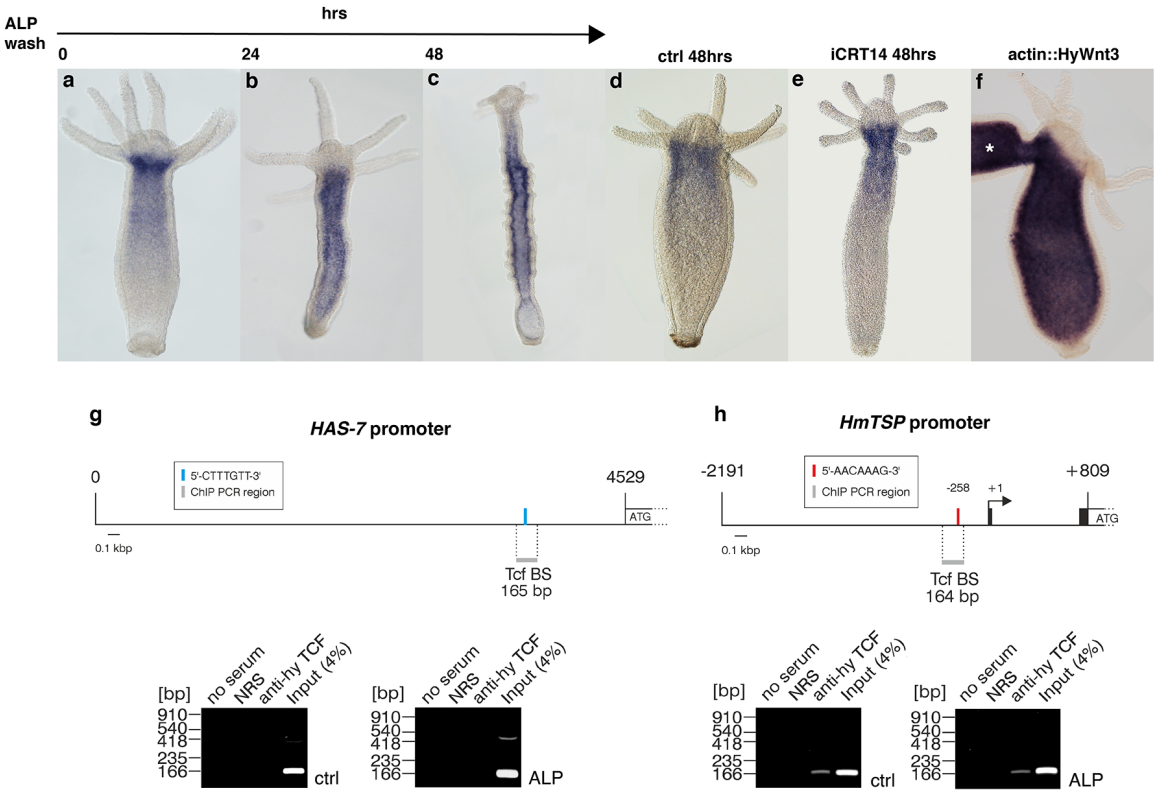

Figure 10. Inactive TCF-binding site and β-Catenin dependent *HAS-7* expression.

Adapted from (Ziegler et al., 2020), in preparation. (a-c) ISH analysis of *HAS-7* expression after Alp treatment shows a global upregulation after 24hrs and a shift towards the developing ectopic organizers along the body column after 48hrs as compared to DMSO-treated controls (d). At 0h after Alp wash (a) no change of the *HAS-7* expression pattern compared to untreated controls (compare d and Fig. 2a) was evident. (f) *HAS-7* expression is globally upregulated in the gastric region of transgenic actin::HyWnt3 animals. The asterisk marks a secondary axis. Representatives of 10 hydras examined. (g-h) No detectable binding of *Hydra* TCF to the *HAS-7* promoter. (g) ChIP analysis of the *Hydra magnipapillata HAS-7* promoter. Upper site: Topography of the *HAS-7* 5'-untranslated region (nt 1 to 4529). The ATG indicates the translation start site. The position of a canonical TCF binding motif (5'-CTTTGTT-3') is indicated by a blue bar. The localization of the 165-bp DNA segment flanked by the specific ChIP primer pair is visualized with a grey bar. Lower site: ChIP analysis of the *Hydra HAS-7* promoter region using chromatin from untreated whole hydra animals (ctrl), and from animals treated with Alp. A polyclonal antibody directed against *Hydra* TCF was used for precipitation, followed by PCR amplification of the indicated

fragment from the *HAS-7* regulatory region. Reactions with normal rabbit serum (NRS) or total chromatin (Input) were used as controls. PCR products were resolved by agarose gel electrophoresis and visualized by ethidium bromide staining. (h) ChIP analysis of the *HmTSP* promoter performed under the same conditions as in (g) and used as a positive control. Upper site: Topography of the 3,000-bp *HmTSP* promoter (nt -2191 to +809). Black boxes depict the first two exons of the *HmTSP* gene. The arrow indicates the transcription start site of the *HmTSP* mRNA, and ATG the translation start site. The position of the tested canonical TCF binding motif (5'-AACAAAG-3') is indicated by a red bar. The localization and size of a 164-bp DNA segment flanked by specific ChIP primer pair is visualized with a grey bar. Lower site: ChIP analysis as described under (g) ((Ziegler et al., 2020) in preparation). WISHs (a-e) were done by Benjamin Trageser and Ann-Katrin Heilig. ChIP was performed by the Hartl Lab (University of Innsbruck, Austria).

Discussion

Summary of the main results

A proteomic analysis of the Hydra head secretome performed in this work revealed a group of novel *Hydra* astacin metalloproteases, HAS1-HAS11, which are partly involved in the proteolytic deactivation of HyWnt3 (Fig. 3 a). The identified *Hydra* astacin metalloproteases possess a signal peptide for secretion, a pro-domain, and the catalytical domain, which harbors the active cleft with the zinc-binding motif (Fig. 4 a). Seven of the HAS enzymes possess between one and six C-terminal ShKT domains (Fig. 4 b).

To further characterize the *Hydra* astacins, protein stability assays were performed using lysates from different body regions of *Hydra* and recombinant HyWnt3. These assays demonstrated that the proteolytic activity targeting HyWnt3 varies depending on the location within the organism. Lysates from tentacles as well as lower body parts were not able to cleave HyWnt3 in the given 24-hour time frame (Fig. 3 b). Conversely, head and upper body part lysates showed high proteolytic activity on HyWnt3.

The addition of chelators, such as EDTA and 1, 10-Phenanthroline, to the HL inhibited HyWnt3 proteolysis (Fig. 3 c). Furthermore, specific inhibitors, as well as physiological inhibitor, namely Batimastat and Fetuin-B, likewise inhibited the HyWnt3-specific proteolytic activity of the HL (Fig. 3 c).

The hydra head lysate was shown to have proteolytic activity also on HyWnt9/10c; however, HL showed no cleavage of HyWnt11, mouse Wnt3a, and the Wnt antagonist HyDkk1/2/4. Furthermore, proteolysis was inhibited after mutating a predicted astacin cleavage motif in HyWnt3 (Fig. 4 d). However, mutation of an adjacent serine protease cleavage site in HyWnt3 did not lead to an inhibition of proteolytic activity by HL (Fig. 4 d). The expression patterns for all new *Hydra* astacin metalloproteases were analyzed by whole-mount *in situ* hybridization (WISH) (Fig. 5) and single-cell sequencing data (Fig. 6), and revealed an endodermal expression for all HAS in the zymogen and granular mucous gland cells, as well as in the transition zones between the gland cell populations. Ring-like gene expression patterns were detected in the upper body column underneath the tentacle base (HAS-5, HAS-9, HAS-10, HAS-11)

or in graded expression pattern in the upper body column, starting below the tentacle base and fading toward the middle of the body column (HAS7, HMP-1). *HAS-1* deviated in exhibiting a homogenous expression pattern throughout the body column. *HAS-7* knockdown led to decreased HyWnt3 proteolytic activity of the respective HL (Fig. 7 e). The knockdown was detectable at the protein level (Fig. 7 c) as well as on the transcriptional level (Fig. 7 d). Furthermore, ectopic axis formation was induced by HAS-7 knockdown, similar to the phenotype observed by silencing of the Wnt inhibitor Dkk1/2/4. The presence of an active TCF binding site could not be confirmed by ChIP (Fig. 7); but gene expression patterns of *HAS-7* after β-catenin modulation (Fig. 10 b, c), as well as *HAS-7* transcript level analysis of *β-catenin* RNAi hydras (Fig. 7 f) and transgenic HyWnt3 overexpressing hydras (Fig. 7 g) indicated an indirect β-catenin dependency.

Characterization of *Hydra* astacins identified in this work

In *Hydra*, HyWnt3 plays an important role in axis maintenance and pattern formation during early development, budding, and regeneration (Miller, 2002) (Kusserow et al., 2005) (Lengfeld et al., 2009). Regulation of HyWnt3 at the transcriptional level by Sp5 was recently described by Vogg, et al. in 2019 (Vogg et al., 2019); additionally, Guder, et al. demonstrated the suppression of Wnt/β-catenin signaling by HyDkk1/2/4 in *Hydra* in 2006 (Guder et al., 2006). However, how HyWnt3 activity is restricted at the protein level remained largely unknown.

To better understand Wnt regulation in *Hydra* at the protein level, the first investigative focus was set on discovering which factor in the HL was responsible for the specific HyWnt3 proteolytic activity. Analysis of the HyWnt3(+) secretome revealed a group of novel *Hydra* astacin metalloproteases (HAS-1 to HAS-11). Six of these were also found in the HyWnt3(-) secretome (HAS-1, HAS-2, HAS-3, HAS-6, HAS-9, HAS-11). Interestingly, HAS-1, HAS-9, and HAS-11 did not show a graded gene expression pattern in WISH (Fig. 5 c, f, h). HAS-1, HAS-9, and HAS-11 were therefore excluded from the list of promising candidates involved in pattern formation. Unfortunately, the used LNA probes were not able to detect mRNA for HAS-3, HAS-4, HAS-6, and HAS-8 under any applied conditions in WISH, which could be due to either low transcript numbers or an insufficient optimization of the WISH protocol for these particular.

The graded gene expression of *HAS-7, HMP1* and *HAS-2* (Fig. 5 a, b, d) in gland cells is similar to the expression pattern of *SEC-1* in gland cell subpopulations, which was described by Schmidt and David in 1986. SEC-1 is a marker of gland cells, which do not directly descend from undifferentiated i-cells, but arise from other gland cells by transdifferentiation (Schmidt & David, 1986). Furthermore, the graded gene expression pattern is also comparable to *Hydractinia HEA1* and *HEA2* that are expressed in gland cells located in the upper body column of polyps during metamorphosis (Möhrlen et al., 2006).

A validation of WISH was achieved by comparing the expression patterns to single cell sequencing data. HAS-7 and HAS-2 showed similar spatial expression in WISH (Fig. 5 a, d), as well as similar transcriptional profiles in the single cell sequencing data (Fig. 6). However, the sequence similarity of HAS-7 and HAS-2 is only 40%, indicating a low probability for cross-reactions of the respective *in situ* probe
(see Digital Supplementary "HAS_Similarity" created with the help of https://www.ebi.ac.uk/Tools/psa/emboss_needle/).

Hence, the single cell sequencing transcriptional profiles help to predict the expression patterns of *HAS-3*, *HAS-4*, *HAS-6*, and *HAS-8* due to their transcriptional profiles in the interstitial cell cluster (Fig. 6). *HAS-3* most likely has an expression pattern reminiscent of *HAS-10*. Furthermore, *HAS-4* and HAS-6 show single cell sequencing profiles comparable to *HAS-5* (Fig. 5 e). A prediction for *HAS-8* can be made solely on the basis of single cell sequencing data, which show an expression in the gland cells of the upper body part of the animal (Fig. 6).

Interestingly, the previously described *HMP-1* (Yan et al., 1995) (Yan et al., 2000) and the main candidate that I investigated further, HAS-7, have similar apical to basal graded WISH patterns, as well as similar transcriptional profiles in the single cell sequencing analysis, indicating related functional roles in morphogenesis. HMP-1 was shown to have an important role in head regeneration. When HMP-1 is blocked by antibodies or by antisense oligonucleotides head regeneration is inhibited (Yan et al., 1995) (Yan et al., 2000). Hence, the graded apical to basal gene expression pattern for HAS-7 emphasizes an involvement in pattern formation and together with its high abundance in the HyWnt3(+) secretome and absence in the HyWnt3(-) secretome, being a strong candidate as a potential candidate for HyWnt3 proteolysis.

Interestingly, the substrate binding sites of HAS-1, HAS-7, and HAS-11 are highly conserved (S1 ‘, Fig. 4 a) when compared with Meprin-α or -β (*Homo sapiens*), SPAN (*Strongylocentrotus purpuratus*), HCE-1 (*Oryzias latipes*), NAS-35 (*Caenorhabditis elegans*), and ZHE-1 (*Danio rerio*). In contrast, HAS-2 to HAS-6 have less conserved substrate binding sites. One can speculate that the different binding sites mutated during evolution to bind different substrates, for instance different Wnts in *Hydra*. Additionally, the hypothesize is that Astacin from *Astacus astacus* and *Hydra* HAS-2 to HAS-6 split from the remaining *Hydra* astacins (HAS-1 and HAS-7 to HAS-11). As shown in Fig. 4 c, an earlier evolutionary branching of HAS-8 and HAS-9 occurred. Later on, the remaining HAS split into two groups: HAS-2 to HAS-6 and HAS-1, HAS-7, HAS-10 and HAS-11, indicating potentially different functions, correlating with different substrates.

However, the evolution of Wnts, the assumed substrates of *Hydra* astacin, could account for the presence of two different substrate binding sites and the absence of one of these substrate binding sites group in *Homo sapiens* or *Danio rerio* (Janssen et al., 2010) (T. W. Holstein, 2012). This hypothesis can be supported by the evolution of a signaling protein and its regulators inside a protein interaction network by co-evolution (Fraser et al., 2002).

Substrate specificity of the HAS-7 proteinase

To investigate the substrate specificity of HAS-7 contained in the *Hydra* head lysate, different HyWnts were used in a protein stability assay. The results revealed that the active factor in the HL and upper body part specifically targets HyWnt3, indicating specific cleavage sites for astacin metalloproteases in the primary sequence (Fig. 3 b, d). Putative cleavage sites for astacins were recently shown to have a preference for aspartate in the P1’ position (first amino acid C-terminal of the cleavage site) and proline in P2’ or P3’ in substrate peptides (Philipp et al., 2009).

In HyWnt3, only D187 followed by Pro188 fulfills this criterion. Furthermore, HL also was able to cleave HyWnt9/10c (Fig. 3 d), which has a DA motif at this position, which was shown to be an even more favored cleavage site for astacin metalloproteases by a proteomic study (Becker-Pauly et al., 2011).

To support the cleavage site prediction, a structural homology model was designed by Jörg Stetefeld (Department of Chemistry, University of Manitoba) and Walter Stöcker (University of Mainz, Germany). The structural model (Fig. 12 a) showing the interaction of HAS-7 and HyWnt3 was built on the basis of the X-ray crystal structure of crayfish astacin (Bode et al., 1992) (Gomis-Rüth et al., 1993) and zebrafish hatching enzyme (ZHE-1) (Okada et al., 2010), as well as *Xenopus* Wnt8 (Janda et al., 2012). In the model the binding of the catalytic zinc ion for HAS-7 occurs at the bottom of the active site cleft (Fig. 11 a). A trigonal bipyramidal sphere is built around the central zinc ion by associating with the hydroxyl group of Tyr191, as well as the imidazole component of His132, His136 and His142. HyWnt3 most likely binds in an anti-parallel manner into the active cleft of HAS-7 ((Ziegler et al., 2020) in preparation) (Fig. 11 b). According to the model, the elongated KKRK*__**DP**__RKIM motif would be an efficient cleavage site in HyWnt3 ((Ziegler et al., 2020) in preparation) (Fig. 11 c). The positively charged arginine (R217) located in the substrate binding site of HAS-7 would link to the negatively charged aspartic acid (P1', D187) of HyWnt3 (Fig. 11 b) (Philipp et al., 2009) (Guevara et al., 2010). Interestingly, the DP cleavage motif is not conserved in HyWnts expressed more distally towards the body, like HyWnt7 and HyWnt16, or in non-canonical, tentacle-related HyWnts, like HyWnt5 and HyWnt8 (Philipp et al., 2009) ((Ziegler et al., 2020) in preparation). The substrate specificity of HAS-7 is thus comparable to that of Meprin-α and crayfish astacin because they all have a proline located at the P2' position (Philipp et al., 2009) (Guevara et al., 2010).

Mutation of the postulated DP cleavage site (D187A, P188A) blocked proteolysis by the HL, confirming the cleavage site prediction (Fig. 3 d). Mutation of a di-basic serine protease cleavage site in close vicinity to the DP motif in HyWnt3 did not inhibit cleavage by HL, indicating that the active factor in HL is likely not a serine protease (Fig. 3 d). Furthermore, I investigated BSA stability in HL ruling out unspecific proteolysis by the HL as a cause for HyWnt3 proteolysis (Fig. 3 b).

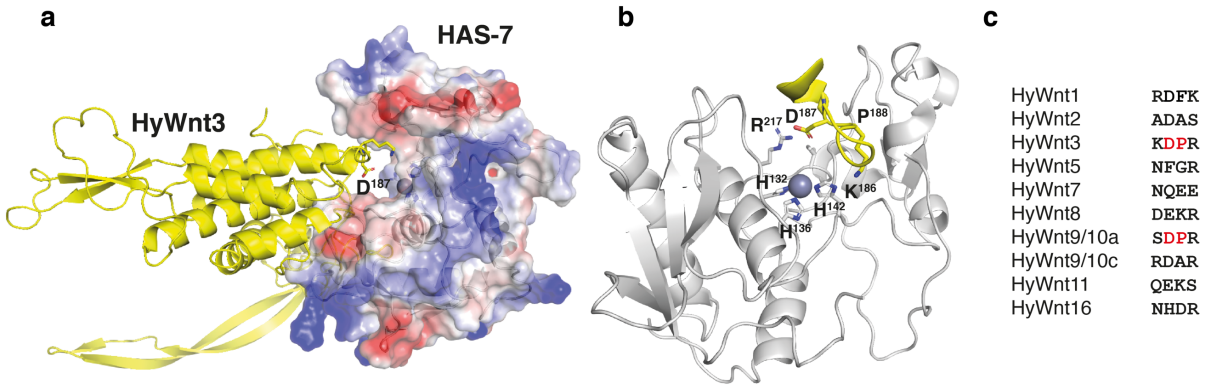

Figure 11. Structural model of the putative HyWnt3: HAS-7 complex.

Adapted from (Ziegler et al., 2020), in preparation. Structural modeling was built by Jörg Stetefeld (Department of Chemistry, University of Manitoba) and Walter Stöcker (University of Mainz). (a) Overview of HAS-7 (3D-surface in red, white and blue) complexed with HyWnt3 (3D-confirmation cartoon in yellow) at D187. The active site of HAS-7, harboring the activating Zn-ion, is indicated in pink. (b) Zoomed view of the active cleft of HAS-7 (3D-confirmation cartoon in white), shown while interacting with the DP site of HyWnt3 (3D-confirmation cartoon in yellow). (c) Different *Hydra* Wnt protein amino acid sequence alignments including the putative DP cleavage motif in HyWnt3 and the putative DA cleavage motif in HyWnt9/10c.(Ziegler et al., 2020) in preparation.

Furthermore, the proteolytic activity of the HL was shown to be specific for *Hydra* Wnt ligands: HyDkk1/2/4, a major Wnt antagonist, remained stable in HL (Fig 3 b). Additionally, the proteolytic ability of the HL on HyWnt3 showed species specificity by not being active on mouse Wnt3a, in which the DP motif is not conserved (Fig. 3 d).
An additional point confirming the hypothesis that HyWnt3 proteolysis in the HL is due to a metalloprotease activity is that chelators like EDTA and 1,2-Phenantroline inhibited HyWnt3 proteolysis. Chelators hinder metalloprotease activity by keeping the activating ions, for example zinc, captive. A specific antagonist for matrix metalloproteases, Batimastat (Beattie et al., 1994) (Reviewed in (Rasmussen & McCann, 1997)), also inhibited the proteolytic activity of the HL on HyWnt3. Batimastat inhibits matrix metalloproteases by mimicking their substrate and thereby blocking the active cleft of the matrix metalloprotease and reversibly suppressing the interaction with intrinsic substrate (Beattie et al., 1994) (Reviewed in (Rasmussen & McCann, 1997)).

Furthermore, I showed that Fetuin-B inhibited the proteolytic activity of the HL on HyWnt3 in a dose dependent manner (Fig. 3 e). Fetuin-B is a physiological inhibitor for human meprin metalloproteases, crayfish astacin and ovastacin, which is an astacin found in mammalians (Karmilin et al., 2019). Hence, the proteolytic activity of the HL very likely arises from an astacin metalloprotease with a predicted cleavage site in HyWnt3 opposite to the Frizzled binding sites.

Validation of HAS-7 anti body specificity

To analyze HAS-7 at the protein level a polyclonal peptide antibody was raised. The antibody recognized a band at the expected size of ~ 40 kDa (Fig. 7 a) in HL. A combination of different mature and immature HAS-7 forms could be the reason for the broad, heterogenous band pattern of HAS-7 in the HL ((Ziegler et al., 2020) in preparation). In addition, a ~ 70 kDa band was detected, which might indicate HAS-7 dimerization, as previously described for meprin-α (Hengst & Bond, 2004) and meprin-β (Schlenzig et al., 2015).

However, HAS-7 does not contain an uneven number of cysteines nor harbors a MAM domain (meprin, A-5 protein, receptor protein-tyrosine phosphatase *μ*), which would allow dimerization. In the meprin α and β subunit, homo- and hetero dimerization is established by disulfide bonding between the MAM-domains (Sterchi et al., 1988) (Eldering et al., 1997). However, also non-covalent interaction in meprins results in oligomerization (Becker et al., 2003), which also could be the case in HAS-7, suggesting that the band at ~ 70 kDa may be the result of SDS-resistant non-covalent HAS-7 dimers.

Recombinant HAS-7 protein including a histidine-tag, which was expressed in insect cell line High Five, could be detected by the specific Has-7 antibody (Fig. 7 b), with a slightly higher molecular mass due to the added tag sequence (1.7 kDa) when compared to the HAS-7 protein band of the HL ((Ziegler et al., 2020) in preparation).

To investigate HAS-7 function *in vivo*, I performed siRNA knockdown experiments, which could be verified at the protein level (Fig 7 c). The protein band at ~ 40 kDa, as well as the protein band at ~ 70 kDa, were no longer detected after *HAS-7* RNAi. The absence of the ~ 70 kDa protein band after knockdown of HAS-7 could also be an

indication that the band at ~ 70 kDa is a result of dimerization. It should be noted that HAS-7 detection showed an additional protein band at 55 kDa after both RNAi treatments, which indicates that this band is the result of antibody binding to an unspecific antigen.

HAS-7 suppresses ectopic axis in steady-state *Hydra*

HAS-7 knockdown by siRNA electroporation led to a significant increase in ectopic axis formation (Fig. 8 o, q), which indicates an involvement in axis formation by HyWnt3 proteolysis. After a subsequent Alp pulse, which globally stimulates the Wnt/β-catenin signaling pathway, the HAS-7 RNAi animals showed an increased number of ectopic axes, but no ectopic tentacle formation as usually induced by Alp (Fig. 8 c, q). *HyWnt3* was expressed in both hypostomal organizers of double axis animals (Fig. 8 r) and both ectopic axes had functional tentacles able to capture (Fig. 8 p). Hence, the induced ectopic axis harbors a functional head with a hypostomal organizer.
Furthermore, significant ectopic axis phenotypes were also observed in HyDkk1/2/4 RNAi animals (Fig. 8 f, q), as well as in a transgenic strain overexpressing HyWnt3 (Fig. 8 e), which validates the assumption that *HAS-7* knockdown leads to ectopic axis formation as a result of increased Wnt/β-catenin signaling compared to steady state polyps. This hypothesis was further bolstered by a rescue experiment using a double knockdown of *HAS-7* and *HyWnt3* followed by treatment with Azk*,* which led to a reversal of the ectopic axis phenotype (Fig. 8 g, q), indicating that excessive HyWnt3 activity is responsible for inducing a secondary axis (Fig. 12 b).

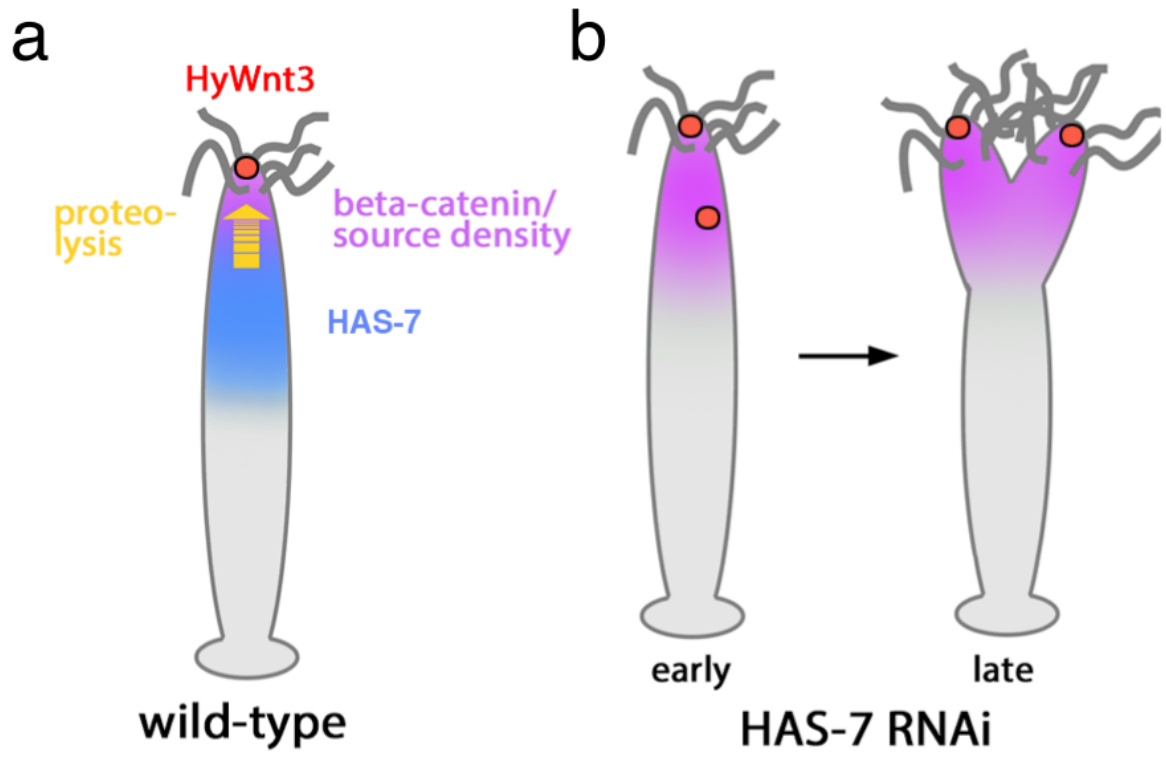

Figure 12. Schematic representation of the role of HAS-7.

Adapted from (Ziegler et al., 2020), in preparation. Schematic representation of HAS-7 role in (a) steady state *Hydra* polyps. HAS-7 (blue) expression shows a graded pattern starting under the tentacle base acting as a proteolysis barrier. HyWnt3 (red) is expressed in the hypostomal head organizer in an autocatalytic feedback loop expressing β-catenin (purple). (b) After HAS-7 silencing Hydras showed ectopic axis formation with a second HyWnt3 hypostomal organizer with a wider β-catenin source density.

Furthermore, I was able to induce double axis formation in *Xenopus laevis* by injecting codon-optimized HyWnt3 mRNA at the 4-cell stage, which was phenotypically comparable to *XWnt8* mRNA injection (Steinbeisser et al., 1993), as well as *Hyβ-catenin* mRNA injection (B. Hobmayer et al., 2000). This finding indicates that *HyWnt3* can act in *Xenopus* as a morphogen to induce Wnt/β-catenin signaling. Importantly, the double axis phenotype was rescued by co-injection of codon-optimized *HAS-7* mRNA, which confirms that HAS-7 is sufficient to inhibit *HyWnt3* in the context of a different organism.

An active TCF binding site in the promotor region of *HAS-7* could not be verified by ChIP analysis in steady state compared to Alp treated Hydras (Fig. 9 g, h), although WISH analysis after Alp treatment as well as in transgenic Act::HyWnt3 transgenic hydras showed upregulation as a consequence of increased β-catenin

signaling (Fig. 9) This was additionally confirmed by RT qPCR analysis of Act:: HyWnt3 transgenic hydras showing increased transcript levels of *HAS-7* (Fig. 7 g) and animals electroporated with β-catenin siRNAs showing reduced transcript levels of *HAS-7* (Fig. 7 f).This led to the notion that HAS-7 could be indirectly regulated by β-catenin signaling by additional factors that remain to be identified.

However, the indirect β-catenin dependency of *Has-7* is likely the manifestation of an extended Gierer-Meinhardt model with two separate patterning systems governing body axis and head organizer as suggested by a mathematical model proposed recently by Moritz Mercker and Anna Marciniak-Czochra (Moritz Mercker, 2020, in preparation). To investigate the role of HAS-7 during axis and head pattern formation in *Hydra*, Moritz Mercker and Anna Marciniak-Czochra from the Institute for Applied Mathematics, Interdisciplinary Center for Scientific Computing (University of Heidelberg, Germany) built a model describing HAS-7-HyWnt3 spatio-temporal dynamics as an extension of the classical activator-inhibitor models of Gierer and Meinhardt. As a framework, a hypothetical two-component activator-inhibitor concept based on current experimental evidence of HyWnt3 and β-catenin/TCF dynamics was applied and employed to the experimental findings presented here. Hereby the previous models were extended by explicitly distinguishing between β-catenin/TCF and HyWnt3 driven pattern formation ((Ziegler et al., 2020) in preparation).

A simulation of a steady state Hydra polyp, the undisturbed system, shows one body axis with one hypostomal head organizer surrounded by tentacles and HAS-7 expression below in a ring-like pattern beneath the tentacles (Fig 13 b) which is comparable and thereby verified by the WISH detection of *HAS-7* (Fig. 5 a). Simulations of Wnt/β-catenin signaling modulation assuming higher starting values of the source density resulted in ectopic tentacle formation and a broader HAS-7 expression in the body column (Fig. 13 c), which was verified by the experimental data showing that after Alp treatment *HAS-7* is ubiquitously expressed in the *Hydra* body column (Fig. 10 c). Wnt modulation in connection with HAS-7 silencing showed indeed ectopic axis formation (Fig. 13 d), confirming the phenotypes obtained through RNAi assays of *HAS-7* depletion (Fig. 8 c). Simulation of HyDkk1/2/4 depletion in connection with Wnt modulation resulted in ectopic axis formation but also in ectopic tentacles (Fig. 13 e), which is supported by the *HyDkk1/2/4* RNAi assays (Fig. 8 f). This finding might be explained by the fact that HyDkk1/2/4 silencing increases the responsiveness

of target cells to HyWnt3, but does not have an effect on overall HyWnt3 levels, which are supposed to inhibit the tentacle system. When *HyWnt3* overexpressing animals were simulated, the results showed a wider HyWnt3 patch in the head as well as an ubiquitous expression of *HAS-7,* but no ectopic axes. This result partly contradicts the experimental data, the model describes each pattern formation system by an activator-inhibitor model and an inherent mathematical property of this class of models does not allow increased activator production to cause an increase in the number of resulting heads, explaining this discrepancy between model and experimental data.

In summary, the mathematical model by Moritz Mercker and Anna Marciniak-Czochra validates the experimental finding and supports the hypothesis that HAS-7 prevents the formation of multiple *HyWnt3* spots. In particular, the dominance of a single organizer is ensured by the degradation of canonical Wnt ligands by HAS-7. I assume that this task is especially important when β-catenin/TCF levels are increased, which may occur in *Hydra* under natural conditions.

Importantly, HAS-7 fulfills all requirements for a head inhibitor postulated by Vogg et al. in 2019 (Vogg et al., 2019)(numbers in brackets indicating criteria points): I showed that *HAS-7* has an apical to basal graded gene expression pattern (1) (Fig. 5 a, Fig 13 b). Furthermore, HAS-7 is able to prevent head formation (3) (Fig. 8 c; Fig. 13 d) by inhibiting canonical Wnt signaling (2) (Fig. 3 b, d). Finally, HAS-7 is dependent on β-catenin/TCF signaling (4) (Fig. 8 h, f; Fig. 7 f, g; Fig. 13 f) and, different than Sp5, is a diffusible factor.

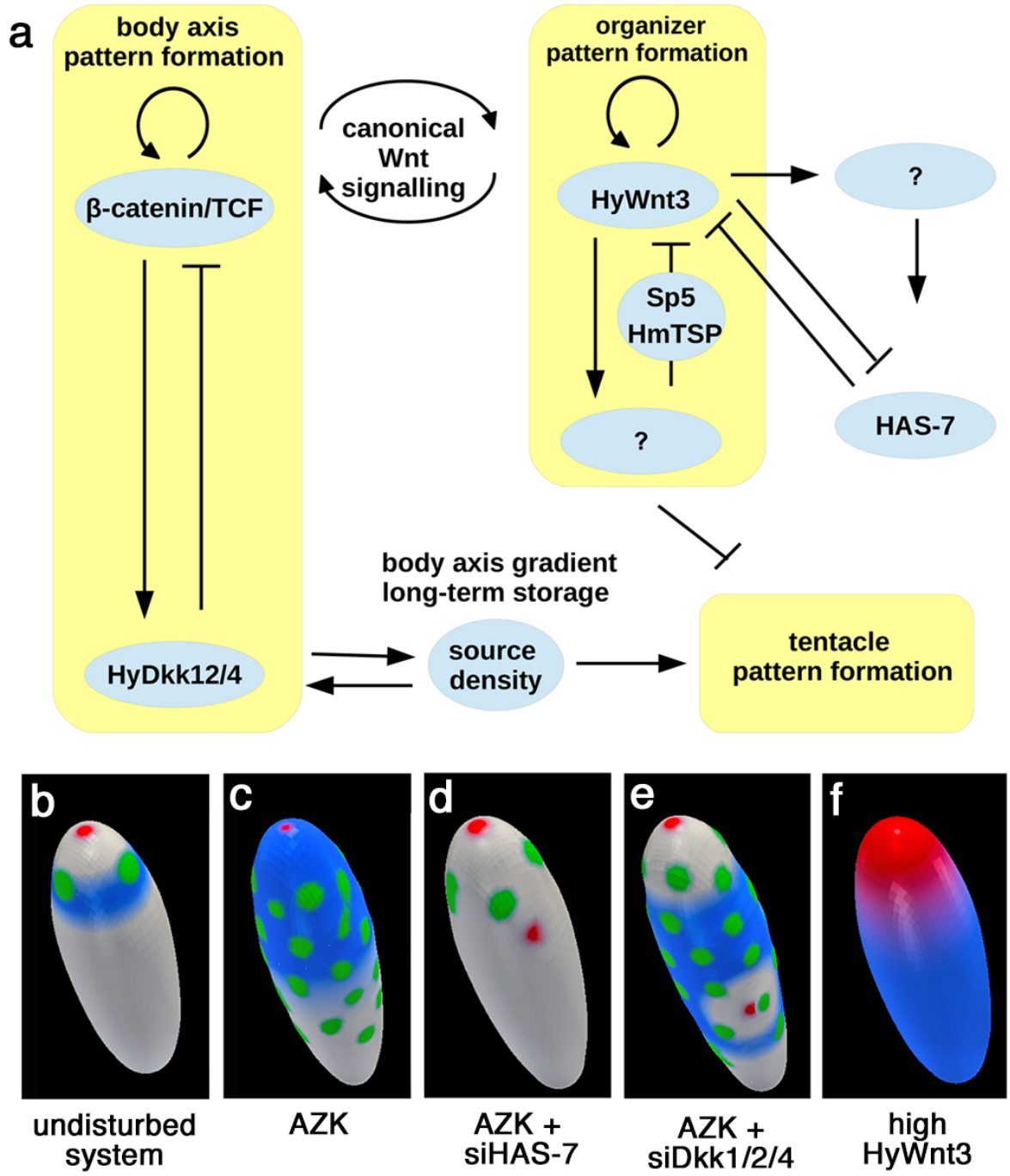

Figure 13. Mathematical model of HAS-7 function.

Adapted from (Ziegler et al., 2020), in preparation. Moritz Mercker and Anna Marciniak-Czochra from the Institute for Applied Mathematics, Interdisciplinary Center for Scientific Computing (University of Heidelberg, Germany) built and designed this mathematical model. (a) A schematic representation of the reaction diffusion system model (Fig.2 a; see "In Hydra, two astacin metalloproteases have been described, hydra metalloproteinase 1 (HMP1) (Yan et al., 1995) and hydra metalloproteinase 2 (HMP2) (Yan et al., 2000). An important role during *Hydra* head regeneration was described for HMP-1 (Yan et al., 1995) (Yan et al., 2000). Whereas, HMP2 is crucial for foot morphogenesis in *Hydra* (Yan et al., 2000).

Reaction diffusion systems"). Auto-catalytic feedback loop responsible for pattern formation in Hydra (in yellow) consisting a long-range inhibitor and a short-range activator. (b)-(f) Different experimental scenarios result in finite element simulations, showing a connection between HAS-7 (blue), HyWnt3 (red) and spots of tentacle formation (green) ((Ziegler et al., 2020) in preparation).

A developmental balance between axis and tentacle formation

During β-catenin/Wnt signaling modulation by Alp, the organizer-potential induced by the *HyWnt3* spots normally results in ectopic tentacle formation, but occasionally can also give rise to ectopic axes (Broun, 2005). To investigate if ectopic tentacle and ectopic axes formation are interrelated, I used the established RNAi assay to silence *nodal-related* (*Ndr*), as well as *HyWnt8*, which are essential factors of bud or tentacle development (Watanabe et al., 2014) (Philipp et al., 2009). A double knockdown of *HAS-7* and *Ndr* with a subsequent AKP pulse led to ectopic tentacle formation without ectopic axis (Fig. 8 i). *Ndr* is expressed during early bud development and is essential for this process (Watanabe et al., 2014). The experiments indicate that Ndr/pitx signaling is adopted for ectopic axis formation. This supports Gierer and Meinhardt's hypothesis that *Hydra* head and bud formation require the same patterning process and are independent of the tentacle system (Gierer & Meinhardt, 1972).

HAS-7 and *HyWnt8* double knockdown led to the formation of multiple ectopic axes and dramatically reduced ectopic tentacle numbers after subsequent AZK treatment. This indicates that tentacle and organizer development in this case compete with each other and are part of a developmental balance. When tentacle formation is inhibited by *HyWnt8* RNAi and HyWnt3 activity is increased by *HAS-7* RNAi the "organizer potential" of the epithelial cells in the body column is apparently invested into the establishment of ectopic axes (Fig. 8 j). This notion is further supported by Alp treatment at a low level over an extended period of time, which induces ectopic axis formation without ectopic tentacles (Fig. 8 n).

The formation of ectopic tentacles by a global increase of β-catenin might therefore be at the expense of the axis-forming potential. This suggests a competition between tentacle and head formation at regions of high positional value as predicted by Meinhardt's model of pattern formation.

Conclusion

In conclusion, this study identifies a novel family of *Hydra* astacin metalloproteases (HAS). The presented experimental results illustrate that HAS-7 has a negative regulatory effect on HyWnt3 and restricts canonical Wnt ligand activity at the protein level to the hypostomal organizer.

This regulative effect prevents the formation of ectopic organizers and maintains the dominance of a single body axis in steady state *Hydras* (Fig. 12 a). An indirect β-catenin regulation of HAS-7 suggests an extension of the Gierer-Meinhardt model of body axis patterning by an activator-inhibitor interaction.

Methods

Hydra culture

Hydra handling

Hydra vulgaris was cultured in hydra medium (Hydra medium: 1 mM $CaCl_2$, 0.1 mM $MgCl_2$, 0.1 mM KCl, 1 mM NaH_2CO_3, pH 7.8) at 18 °C. The hydras were fed two to three times a week with freshly hatched *Artemia salina nauplii*. Remaining *Artemia* were washed out ~5 hrs after the feeding. For the washing of the hydras, the animals were tilted in their hydra medium through a finely woven tea sieve which was stored in 2-Propanol and washed with *Hydra* medium beforehand.

Artemia salina nauplii eggs were incubated for hatching in saltwater at 21 °C for about 24 hrs. 24 hrs after the remaining *Artemia* from the feeding process were washed out, the hydra culture boxes were deep cleaned with the help of 2-Propanol. Before experiments, animals were starved for 24 hrs unless indicated otherwise.

Hydra strains

The wild type *Hydra vulgaris* (AEP) strain was used for hydra body part lysate production for protein stability assays or Western blotting unless indicated otherwise. Transgenic *Hydra vulgaris* which express in the endodermal layer GFP and in the ectodermal layer RFP (endo::GFP; ecto::RFP) (Carter et al., 2016) were used for small interfering RNA (siRNA) knockdown experiments unless indicated otherwise. Another used transgenic *Hydra vulgaris* strain was *ActP::HyWnt3* (Nakamura et al., 2011) in which HyWnt3 is ubiquitously expressed under the *Actin* promotor which was used to generate RNA sampled for cDNA synthesis used in RT-qPCR and as a comparison in the documentation process of siRNA silenced animals. The transgenic strain *Hydra vulgaris HyWnt3P::eGFP* (Nakamura et al., 2011) which expresses eGFP under the *HyWnt3* promotor was used in siRNA knockdown assays.

siRNA knockdown

The knockdown experiment was carried out as described in Lommer et al., 2018 (Lommel et al., 2018) with changes. The transgenic *Hydra* strains *Hydra vulgaris endo::GFP ecto::RFP*, provided by Robert Steele's Lab (University of California, Irvine, USA), and *Hydra vulgaris HyWnt3P::eGFP* were used for small interfering RNA knockdown experiments.

siRNA design and order

siRNAs were designed with the help of http://sirna.wi.mit.edu. The mRNA sequence was received by accession numbers (see Table 1: "siRNA sequences"). Furthermore, I chose siRNAs with a length of 21 bases. I let the tool design an "AAN19TT" pattern, changed the GC percentage to: 30 to 50%, and excluded patterns with more than 3 T or A in a row and ended the siRNA with NN. I aimed for a negative thermodynamic value to avoid secondary structure formation. After the siRNA design, I checked in the Hydra 2.0 database for possible off-targets. For each gene of interest target three siRNAs were designed and used in different combination to get more efficient knockdown results. The siRNAs were obtained from Sigma-Aldrich in HPLC grade with an UU overhang.

siRNA electroporation and electroporated hydra handling

All hydra handling was done with Pasteur glass pipettes which were flamed at the tips to avoid sharp edges. 20 *Hydra vulgaris endo:GFP ecto:RFP* or *Hydra vulgaris HyWnt3P::eGFP* which starved for 24 hrs were used per electroporation and transferred into a 0.4 cm electroporation cuvette (Biorad). The hydra medium was removed and replaced by a solution of 170 µl RNAse/DNAse free water with 30 µl of siRNA mix with a total siRNA concentration of 3 µM (for instance a combination of 1 µM siGFP, 1 µM siHAS-7_001 and 1 µM siHAS-7_002) (see Table 1:"siRNA sequences"). The hydras were incubated in the cuvette in the final siRNA solution for about 2 min until the hydras relaxed and elongated. Afterwards the electroporation pulse was applied as a single square pule with 250 V for 25 ms in the electroporator chamber. Immediately after the pulse ~500 µl ice cold restoration buffer (Restoration

buffer: 80% (v/v) Hydra medium with 20% (v/v) Dissociation medium (Dissociation medium: 12.5 mM TES, 6 mM CaCl2, 6 mM Na-Citrate, 6mM Pyruvate, 3.6 mM KCl, 4 mM Glucose, 1.2 mM $MgSO_4$, 0.10 g/L Streptomycin, 0.05 g/L Rifampicin, 0.05 g/L Kanamycin; pH 6.9); Dissociation medium can be stored at -20 °C in aliquots) was added and the animals were kept, still in the cuvette, on ice for about 10-15 min. The animals were carefully transferred with a flamed Pasteur glass pipette into a petri dish which was filled beforehand with restauration buffer. I prevented that the Hydras were too close to each other in the petri dish and I avoided needless movement of the petri dishes. The recovering hydras were kept on 18 °C overnight. The following day, the restoration buffer was carefully replaced by hydra medium and cell debris was discarded. The RNAi treated hydras were fed one time two days after the electroporation. The hydra medium was exchanged daily and every three days the hydras were transferred into a fresh petri dish.

Assays after siRNA knockdown

6 days after the electroporation the hydras were either used for hydra body part lysate preparation (see "Protein Stability Assay"), Western blot sample preparation (see "Wnt proteolysis assay"), RNA isolation (see "RNA isolation"), documented or a subsequent Azk treatment was done. For the Azk pulse treatment (Kunick et al., 2004) the Hydras were transferred into a new petri dish and the hydra medium was exchanged for hydra medium containing 50 nM Azk. Azk was dissolved initially in Dimethyl sulfoxide (DMSO). DMSO had a final concentration of ~1:1000 in hydra medium, so a control with 1:1000 DMSO in hydra medium was carried along. The hydras were incubated for ~16 hrs in Azk and afterward, the hydra medium containing the Azk was removed and the hydras were washed 3 x 5 min in hydra media. The hydras were observed over time and documented. For the phenotypical documentation, the hydras were anesthetized by Linanool (Sigma-Aldrich) (Goel et al., 2019). Linanool was previously diluted 1:10 in 100% Ethanol absolute (Merck) and diluted right before use 0.1% (v/v) in hydra medium. 6 days after the Azk was removed from the animals, the phenotypical documentation was done. The documentation was done with Nikon SMZ 25 stereomicroscope equipped with a 0.5x AHR Plan Apo objective and a Nikon DS-Ri2 high definition camera. Phenotypical documentation of fluorescent *Hydra vulgaris*

HyWnt3P::eGFP or *Hydra vulgaris endo::GFP ecto::RFP* was done with the use of UV LED light. The NIS Elements software was used for microscope controlling. Cropping and scale bar implementation were later applied by Fiji.

Regeneration assay

6 days subsequently to the siRNA knockdown *Hydras* were bisected at 50% body length. Both *Hydra* parts were washed afterwards 3 x 10 min in Hydra medium and kept separately at 18°C. The Hydras were washed daily and documented at day 11 post RNAi using Linanool as stated in "Assays after siRNA knockdown".

Long-term Wnt modulation assay

24 hrs starved *Hydras* were either incubated in 1.5 *µ*M Alsterpaullone ((Alp)Sigma-Aldrich) in Hydra medium (Condition 1) or in DMSO in Hydra medium (Condition 2) (DMSO volume equal to total Alp volume used for Condition 1) for ~21 days. The media of all conditions were exchanged daily and the animals were fed once a week. Documentation was carried out in Linanool.

Immunofluorescence staining

6 days after a HAS-7 RNAi, a subsequent Azk pluse was done. The animals were relaxated 5 days after the Azk pulse in 2% urethan. Afterwards, the *Hydras* were fixated Lavdovsky's fixative (50% ethanol absolute, 36% ddH_2O, 10% formaldehyde, 4% acetic acid). The fixated animals were washed 3 x 10 min with 1 x PBS with 0.1% Triton X-100 (Sigma-Aldrich). The first antibody against Cpp1(Eurogentec) was diluted 1:200 in 1 x PBS with 0.1% Triton X-100 and 1% BSA (Carl Roth) and the incubation was done overnight at 4 °C. The following day, 3 x 10 min washing steps with 1 x PBS with 0.1% Triton X-100 were carried out to remove unbound antibodies. The used secondary antibody Alexa 488 anti-rabbit was diluted 1:400 in 1 x PBS with 0.1% Triton X-100 and 1% BSA. The incubation with the secondary antibody was done for 2 hrs at RT. Afterwards, the samples were washed 3 x 10 min with 1 x PBS and mounted using Mowiol solution as described in "*In situ* hybridization (conventional or LNA *in situ* hybridization)". The documentation was done using a with the Nikon A1R confocal laser-scanning microscope. The image processing as well as the image stitching was performed with Nikon NIS Elements.

Gene expression assays

Real-time quantitative PCR

RNA isolation

The RNA isolation was done after Petersen et al., 2015 (Petersen et al., 2015) and Chomczynski & Sacchi, 1987 (Chomczynski & Sacchi, 1987) and the TRIzol™ (Thermo Fisher Scientific) instruction protocol with changes: 10 hydras or 60 hydra heads from steady-state polyps or after HAS-7 or GFP knockdown were dissolved by pipetting up and down in 200 µl TRIzol. Afterward, the samples can be frozen away at -20 or -80 °C or used for extraction right away. 100 µl TRIzol was added additionally and left 5 min at room temperature (RT). Afterward, 60 µl Chloroform (Merck) was added and vortex for 5 seconds (sec) and left for 3 min at RT. The samples were centrifugated at 11000 rpm for 15 min at RT. After the centrifugation, the upper aqueous phase was transferred into a new tube and the lower organic phase was discarded. To the aqueous phase sample 150 µl 2-Propanol was given and vortexed for 5 sec and incubated for 10 min at RT. The samples were again centrifugated at 11000 rpm for 10 min at RT. The liquid was carefully removed and the well visible pellet was dissolved in 50 µl RNAse/DNAse free water. The pellet dissolving process can be optimized by placing the tube with an open lid into the Thermomixer which was set to 65 °C with the lowest rotation (300 rpm) for 3 min. This additional process allows also the evaporation of the remaining 2-Propanol. Afterward, 7.5 µl 2 M Sodium Acetate (Sigma-Aldrich), pH 4.1 was added. The same volume, therefore 57.5 µl Phenol-Chlorophorm-Isoamylalcohol mixture (Merck, BioUltra) was added and vortexed for 5 sec. The samples were centrifuged at 11000 rpm for 5 min at RT. The lower organic phase was discarded by pipetting the lower phase carefully out of the sample with the help of a fine-tipped pulled Pasteur glass pipette. To the remaining upper aqueous phase, 100 µl Chloroform/Isoamyl alcohol (a mixture of 24:1, for instance, 24 µl Chlorophorm and 1 µl Isoamylalcohol which were mixed beforehand) was added and vortexed for 5 sec. The samples were centrifuged at 11000 rpm for 5 min at RT. The upper aqueous phase was carefully transferred into a new tube and the lower organic phase was discarded. A volume 2.7x the volume of the upper aqueous phase of 100% Ethanol was added to the kept upper aqueous phase (for instance 46 µl of the upper

aqueous phase were transferred into a new tube, so 124.2 µl 100% Ethanol was added) and vortexed for 5 sec. Afterward, the samples were kept overnight at -20 °C. The next day the samples were centrifuged at 13000 rpm for 20 min at RT. The liquid was carefully removed and exchanged with 75% (v/v) Ethanol with 25% RNAse/DNAse free water to wash, not dissolve the pellet. The samples were again centrifuged at 13000 rpm for 10 min at RT. The liquid was carefully removed and the pellet was dissolved in 30 µl RNAse/DNAse-free water by placing the tube with an open lid into a thermomixer which shakes at 300 rpm at RT. The concentration was measured by NanoDrop (230 nm) (see "NanoDrop") and for the RNA quality control, a 1% (w/v) Agarose gel (see "Agarose gel") was performed.

cDNA synthesis

cDNA synthesis was done with the SensiFAST cDNA Synthesis Kit (Bioline) as described in the instruction protocol unless stated otherwise: Per reaction 1 µg (calculated from the NanoDrop results) total RNA from the RNA isolation, 4 µl 5x TransAmp Buffer and 1 µl Reverse Transcriptase was mixed by pipetting up and down. The reaction volume was filled up to 20 µl with RNAse/DNAse free water (for instance a concentration of 0.29 µg/µl RNA was measured, so 3.5 µl was added, as well as 11.5 µl RNAse/DNAse free water). The reactions were put into the PCR machine with the settings:

- Primer annealing: 25 °C for 10 min
- Reverse Transcription: 42 °C for 15 min
- Reaction inactivation: 85 °C for 5 min
- End: 4 °C on hold

The synthesized cDNAs were afterward diluted 1:5 in RNAse/DNAse free water and stored at -20 °C until "Real-time quantitative PCR" started.

Real-time quantitative PCR

The RT-qPCR was carried out after the instructions and with the SensiFAST SYBR-Hi-ROX Kit (Bioline), optimized as follows: Per well sample 5 µl synthesized cDNA template (from the 1:5 diluted cDNA, see above), 0.4 µl forward primer (final concentration of 200 nM, see Table 3 "RT-qPCR Primer"), 0.4 µl respective reverse

primer (final concentration of 200 nM, see Table 3 "RT-qPCR Primer"), 10 µl 2x SensiFAST SYBR Hi-ROX Mix and 4.2 µl RNAse/DNAse free water (for a total sample volume of 20 µl) were mixed per well from a 96-well plate (96 Fast PCR-Platte half skirt DNA-/DNAse-/RNAse-/PCR inhibitor-free (Sarstedt)). If the pipetting process was finished a MicroAmp ™ Optical Adhesive Film PCR/REAL-time PCR compatible (Applied Biosystems by Thermo Fisher Scientific) was applied to the open surface of the well plate to seal all wells tight. The plate was shortly centrifuged for 10 sec at RT in a plate centrifuge (PeQLab Perfect Spin P). The RT-qPCR machine (Applied Biosystems StepOnePlus™ Instrument) was set to "Relative Quantification Settings" and to a 2-step cycle:

- Cycle 1 (Polymerase activation): 95 °C for 2 min
- Cycle 2-40 (Denaturation, Annealing/Extension; (Repeat)): 95 °C for 5 sec, 60 °C for 30 sec

The plate was afterward kept at 4 °C for potential product analysis on a 1% (w/v) Agarose gel ("Agarose gel"). The whole experiment was done in biological and respectively technical triplicates as well as with water controls. HAS-7 primers were picked exon-exon junction spanning (see Table 3: "RT-qPCR Primer"). The analysis was done by the $\Delta\Delta C_{(T)}$-Method with Elongation Factor 1-α (EF-1α) as a house keeping gene for normalization. The obtained data was transformed into relative quantity by $2^{(-\Delta\Delta C(T))}$ for analysis and presentation.

In situ hybridization

In conventional *in situ* hybridization, a sense (control probe) and an antisense probe were used. For LNA *in situ* hybridization locked nucleotide acids (LNAs) were ordered and designed by Quiagen (see Table 4: "

Accession numbers can be used to obtain protein amino acid sequences by blasting the accession number: https://blast.ncbi.nlm.nih.gov/Blast.cgi?PROGRAM=blastp&PAGE_TYPE=BlastSearch&BLAST_SPEC=&LINK_LOC=blasttab&LAST_PAGE=blastn

Transcript IDs were obtained by https://research.nhgri.nih.gov/hydra/sequenceserver/ and used to gain single sequencing data https://portals.broadinstitute.org/single_cell/study/stem-cell-differentiation-trajectories-in-hydra-resolved-at-single-cell-resolution.

In situ probes"). *In situs* with LNA probes were done by Svenja Kling, B. Sc. during a lab rotation under supervision.

Probe synthesis (conventional in situ hybridization)

The genes were subcloned into a pGEMT easy (Promega) vector by Jutta Tennigkeit ("Plasmids and constructs"). The orientation of the insert was determined by sequencing service (Eurofins).

M13 PCR amplification

As first step, a PCR was run from the plasmids to get the linearized double stand sequence.

Per reaction:

1 µl of the plasmid (10-20 ng/µl)
1 µl dNTPs (0.2 mM of each)
1 µl M13 forward (5 pmol/µl)
1 µl M13 reverse (5 pmol/µl)
5 µl 10x DreamTaq Buffer
1 µl Dream Taq DNA Polymerase (1.25 U)
40 µl RNAse/DNAse free water (Total reaction volume of 50 µl)

PCR machine settings:

95 °C for 5 min	
35 Cycle	95 °C for 30 sec
	55 °C for 30 sec
	72 °C for 1 min (1 min for 1000 bp)
	72 °C for 2 min
4 °C hold	

Agarose gel

The PCR product was controlled on an agarose gel. 1% (w/v) Agarose (Carl Roth) was shortly heated in 1 x TAE (50 x TrisAcetate-EDTA: 2 M Tris, 1 M anhydrous acetic acid, 50 mM EDTA disodium salt) with ddH_2O (double distilled water). To the completely dissolved 100 ml mixture of 1% (w/v) Agarose in 1 x TAE which was still hot, 5 µl Midori Green (NIPPON genetics EUROPE) was added. The solution was given into an agarose gel carriage with previously sealed edges with a 12 slot gel-comb inserted beforehand. For RNA gels a preincubation of the gel carriage, gel chamber and the comb with 3% (v/v) H_2O_2 (Merck) was performed for 24 hrs at RT. After the gel cooled down and formed a gelation, the gel carriage was inserted into the gel running chamber and filled up with 1 X TAE until the gel was covered. The samples were pipetted into the pockets caused by the comb. A 1 kb Plus DNA ladder (Thermo Scientific) was used to determine the base pair (bp) size and the concentration of the tested samples. For RNA gels a ssRNA ladder was applied. The tested volume of PCR products was 1 µl and 5 µl in a total volume of 15 µl with ddH_2O and 5 x loading dye (Thermo Fisher). For RNA samples a 6 x Formamide loading dye (6 x Formamide loading dye: 750 µl Formamide, 40 µl 0.5% (w/v) Bromphenol blue with 0.5% (w/v) Xylen Cyanol, 170 µl DNAse/RNAse free water) was used. RNA samples were incubated for 5 min at 65 °C together with the 6 x Formamide loading dye. The gel was run at 100 V for ~1 hr at RT. The documentation was done with a Safe Imager Blue-Light Transilluminator (Thermo Fisher).

PCR product clean-up

The PCR product clean-up was done with Wizard ® SV Gel and PCR Clean-Up System Kit from Promega with changes:

To 50 µl PCR sample 50 µl membrane binding solution was added. The whole mixture was incubated in the minicolumn for 1 min at RT: The samples were centrifugated at 16000 x g for 1 min at RT. The flowthrough which was collected in collection tubes was discarded. 700 µl membrane washing solution (with previously added Ethanol 100% absolute) was added unto the minicolumn and again centrifugated at 16000 x g for 1 min at RT. The Flowthrough was discarded and the washing step was repeated with

500 µl membrane washing solution. The centrifugation step was done at 16000 x g for 5 min. The flowthrough was discarded again and the empty minicolumn was centrifugated again with an open lid at 16000 x g for 1 min to allow the remaining Ethanol to evaporate. The minicolumn was transferred into a 1.5 ml Eppendorf tube and into the column 20 µl DNAse/RNAse free water was added carefully onto the membrane. The columns in the tubes were incubated for 3 min at 45 °C in the thermomixer shaking at 300 rpm. Afterward, the minicolumns were centrifugated at 16000 x g for 1 min at RT. This elution process was repeated once, that the final volume of the elution added up to 40 µl in total. The samples were stored at -20 °C. The PCR product clean up quality was checked on a 1% (w/v) Agarose gel ("Agarose gel") to verify that there are unique products at the expected size and the quantity was checked by NanoDrop ("NanoDrop") to estimate the concentration.

NanoDrop

The NanoDrop machine (NanoDrop ® ND-1000 Spectrophotometer (peQLab) Biotechnologie GmbH) was set to measure DNA/RNA (230 nm) or Proteins (280 nm). The machine was blanked with 1 µl of the buffer used to elute or dilute the sample. 1 µl of the sample tested sample was applied to the machine.

Probe synthesis

The cleaned-up PCR product ("PCR product clean-up") was used for *in situ* probe synthesis for sp6 and T7 amplification as follows:

2 µl PCR product clean-up 250 ng/µl (total of 500 ng)
2 µl Digoxygenin-labelled RNA nucleotides
2 µl RNAse Inhibitor
2 µl 10 x reaction buffer
2 µl sp6 or T7 polymerase
10 µl DNAse/RNAse free water (Total reaction volume of 20 µl)
The incubation was done for 3.5 hrs at 37 °C.

A subsequent ammonium acetate precipitation was done as follows:

20 µl probe synthesis mix

405 µl 100% Ethanol absolute
135 µl 7.8 M Ammonium acetate
95 µl DNAse/RNAse free water
The incubation was done for 45 min at RT. The samples were centrifugated at 14000 rpm for 20 min at 4 °C in the cooling centrifuge (Herdeus Biofuge fresco (Thermo Fisher Scientific)). The supernatant was carefully discarded and unto the pellet 300 µl 70% (v/v) Ethanol absolute with 30% DNAse/RNAse free water was added. Afterward, the samples were again centrifugated at 14000 rpm for 20 min at 4 °C. The supernatant was discarded and the dry pellet was dissolved in 20 µl DNAse/RNAse free water by placing it into the shaking (300 rpm) Thermomixer at RT for 5 min.
1 µl of the sample was diluted with 9 µl DNAse/RNAse free water and used for quality control on a 1% (w/v) agarose gel (see "Agarose gel"). From the diluted sample 1, 2.5 and 5 µl were used as samples to put unto the gel together with a ssRNA ladder (Bio Labs) to estimate the correct size and the concentration of the probe.
The remaining probe was diluted 1:1 with Formamide and stored at -80 °C.

In situ hybridization (conventional or LNA *in situ* hybridization)

In situ hybridization was done after Grens et al., 1996 (Grens et al., 1996) and Bode et al., 2008 (H. Bode et al., 2008) with changes: *Hydras vulgaris* which were fed the day before were collected in a 50 ml tube in 20 ml hydra medium. Hydras handling and solution exchange was done with Pasteur glass pipettes which were flamed at the tips to avoid sharp edges. 20 ml 4% (w/v) Urethan in hydra medium was added (end concentration of 2% (w/v) Urethan in hydra medium) for 90 sec to relax the animals. The Urethan solution was replaced by 4% (w/v) Paraformaldehyde (PFA) in 1 x PBS and washed for 5 min under rotation to remove the remaining Urethan. The PFA solution was exchanged by fresh 4% (w/v) PFA in 1 x PBS and the tube was rotate overnight at 4 °C for fixation. On the next day, the PFA solution was removed and 100% Methanol was given to the fixated hydras. The hydras were then either stored at -20 °C or the 100% Methanol was replaced after 15 min at RT by 75% (v/v) Methanol in 1 x PBS. After 5 min two further 5 min rehydration steps with 50% (v/v) and 25% (v/v) Methanol in 1 x PBS were carried out. Afterwards 3 x 5 min washing steps with 1 x PBS-T (1 x PBS with 0.1% (v/v) Tween-20 (Carl Roth)) were done. A 7 min incubation with pre-tested 1 x Proteinase K (1 µg Proteinase K per ml PBS-T, Sigma-Aldrich) in

PBS-T followed at RT. The Proteinase K treatment was briefly stopped by replacing the Proteinase K solution with 1 x Glycine (Labochem international) in PBS (1 x Glycine: 4 mg Glycine per ml PBS). Afterward, the solution was exchanged with fresh 1 x Glycine in PBS and incubated for 10 min under rotation at RT. The animals were washed 2 x 5 min with 0.1 M TEA (0.1 M Triethanolamine (Merck) in DNAse/RNAse free water) while rotating at RT. An additional 5 min incubation step with 0.25% (v/v) acetic anhydride (Grüssing) in 0.1 M TEA followed. The Hydras were washed afterward 2 x 5 min with 1 x PBS-T while rotating at RT. A refixation with 4% (w/v) PFA in PBS-T was done for 20 min while rotating at RT. To wash out the fixative 5 x 5min washing steps with PBS-T were done while rotating at RT. To initiate the pre-hybridization the hydras were incubated for 10 min at RT with 1:1 hybridization mix in 1 x PBS-T ((50 ml hybridization mix: 25 ml Formamide, 12.5 ml 20 x SSC, 5 ml DNAse/RNAse free water, 5 ml 1% (w/v) Chaps (Roche) in DNAse/RNAse free water, 1 ml 50 x Denhardt's, 1 ml 200 µg/ml Yeast RNA in DNAse/RNAse free water, 500 µl 10 mg/ml Heparin (Carl Roth), 50 µl Tween-20); (20 x SSC: 3 M Sodium chloride (Sigma-Aldrich), 0.3 M Sodium citrate (Sigma-Aldrich) in DNAse/RNAse free water); (50 x Denhardt's: 1% (w/v) BSA (Carl Roth), 1% (w/v) Ficoll 400 (Sigma-Aldrich), 1% (w/v) Polyvinylpyrrolidone (Sigma-Aldrich) in DNAse/RNAse free water)). The animals were then transferred and split into 2 ml tubes to test different probes (different LNA probes and/or sense and antisense probes, respectively) and incubated in 100% hybridization mix for 10 min while rotating at RT. The pre-hybridization was done in freshly exchanged hybridization mix for 2 hrs under 300 rpm shaking in the thermomixer at 55 °C. For conventional *in situ* hybridization, 1 µl of 5 ng/µl sp6 or T7 probes were diluted in 100 µl hybridization mix. For LNA *in situ* hybridization 1 µM LNA probes were diluted in 100 µl hybridization mix. Both probe variant mixtures were heated for 10 min at 70 °C and afterward, the mixtures were given unto the hydras. The hybridization of the hydras together with the probes was done for ~ 65 hrs in the thermomixer at 55 °C. The probes were washed out with fresh hybridization mix for 5 min in a 300 rpm rotating thermomixer at 55 °C. To wash out remaining probes 3 x 5 min washing steps at 55 °C with 75% (v/v), 50% (v/v) and 25% (v/v) Hybridization mix in 2 x SSC were done. Afterward, the Hydras were washed 4 x 20 min at 55 °C in a 300 rpm rotating thermomixer with 2 x SSC with 0.1 % (w/v) Chaps. The Hydras were subsequently washed 2 x 10 min under rotation at RT with Maleic acid buffer (MAB: 100 mM Maleic

acid (Merck), 150 mM NaCl; pH 7.5). The blocking step was done by 1% (w/v) blocking reagent (Roche) in MAB, rotating, for 2 hrs at RT. The antibody incubation for detecting DIG-marked RNA probes was done with an anti-DIG-AP (anti-Digoxigenin with conjugated with alkaline phosphatase) (Roche). Anti-DIG-AP was diluted 1:4000 in 1% (w/v) blocking reagent in MAB and incubated under rotation, overnight at 4 °C. On the next day, 12 x 30 min washing steps were carried out under rotation at RT. A 13th washing step was done afterward rotating, overnight at 4 °C. The Hydras were washed on the next day 2 x 10 min with fresh NTMT (50 ml NTMT: 35 ml in DNAse/RNAse free water, 5 ml 1 M Tris pH 9.5, 5 ml 0.5 M $MgCl_2$, 5 ml 1 M NaCl, 50 µl Tween-20). The Hydras were transferred within the second washing step into a 24 well plate. The color reaction solution was prepared as follows: 4325 µl NTMT, 50 µl NBT (Roche), 37.5 µl BCIP (Roche) were vortexed for 30 sec. The NTMT on the Hydras in the 24-well plate was exchanged with 300 µl per well with color reaction solution. The well plate was covered in aluminum foil to avoid light exposure. The reaction was done at RT until the antisense probe sample shows a clear signal or the sense probe shows background (for conventional in situ hybridization). For LNA one scrambled control was run for all used LNAs. The reaction for the LNA was run until the LNA probe samples showed a signal. A coloring of the scrambled LNA was never detected (coloring reaction for 5 days at 37 °C sealed with parafilm to avoid liquid evaporation). The coloring reactions were stopped by sucking up the coloring reaction and adding 100% Ethanol absolute. The 100% Ethanol absolute was replaced after 3 min by 100% Ethanol absolute which was incubated for 15 min. The Hydras were afterward washed 3 x 5 min with 1 x PBS and kept in 1 x PBS until mounting. Mounting was done with Mowiol solution (Mowiol solution: 12 ml 0.2 M Tris-HCL pH 8.5, 6 g Glycerol, 2.4 g Mowiol 4-88 (Carl Roth)) following the “Instructions for use” with changes: The hydras were given unto the glass slides and arranged using a lash sword (self-crafted). All remaining liquid was removed and one drop of Mowiol solution was carefully applied (with no air bubbles) on top of the hydras. Onto the coverslip, a “T” shape of Mowiol was applied (total of 200 µl) (with no air bubbles). The coverslip was lowered unto the animals by carefully bending the coverslip with the help of a thin-tipped forceps starting at the shorter Mowiol-“T” side. The samples were dried overnight at 4 °C and on the next day the coverslip sides were sealed with Fixogum (Marabu). After drying, the samples were ready for documentation. The documentation was done with a Nikon Eclipse 80i with an applied

DIC contrast using the NIS Elements software. The animals were imaged completely by several images to gain a higher definition after stitching. The image stitching was done by Adobe Photoshop as well as the background filling.

Plasmids and constructs

Constructs used for *in situ* hybridization probe synthesis or used in cell culture were cloned by Jutta Tennigkeit. The cDNA of the genes of interests were subcloned into pCEP-Pu (Thermo Fisher) mammalian expression vectors for cell culture approaches or into pGEMT-easy vector for *in situ* hybridization. Plasmids used for caped mRNA synthesis for *Xenopus laevis* injection were ordered from BIOMATIK and subcloned into pGEMT-easy vector.

Protein Stability Assay

Human cell lines handling

Human embryonic kidney 293-T cells (HEK293-T cells) (Invitrogen) were cultured in 10 ml full DMEM Media (Gibco®, Life technologies; containing 1 µg/ml Penicillin/Streptomycin and 10% (w/v) FBS (PAA, The cell culture company) in 100 ml flasks (Greiner) at 37 °C with 5% CO_2 in a cell incubator (Herecell 150i CO2 Incubator (set to 37 °C with 5% CO_2). All cell handling was done under a safety hood (Hera Safe (Heraeus)) and pipetted with a Brand Accu-jet ® pro pipetboy with attached long filter pipet tips (Costar ® Stripette sterile Serological pipet (Corning Incorporated)). Two to three times a week, when the cells were ~100% confluent, the medium was replaced by 1 ml 0,05% Trypsin (Gibco®) (37 °C) to de-attach the cells from the flask surface. After an incubation of 3 min at 37 °C, 9 ml of preheated full DMEM Media was added to the cells and the suspension was gently pipetted up and down five times to avoid cell clumps. This cell suspension was either used for the production of recombinant proteins (see "Recombinant proteins produced by HEK cells") or to infect a fresh bottle. If a new bottle was infected with HEK 293-T cells, 9 ml full DMEM Media (37 °C) was

pipetted beforehand into a new bottle and infected with 1 ml of the cell suspension. The bottle was immediately put back into the 37 °C heated cell incubator.

Recombinant proteins produced by HEK cells

1800 µl full DMEM Media (preheated to 37 °C) was pipetted into each well of a 6-well plate. 200 µl of the cell suspension (see "Human cell lines handling") was added and the cells were allowed to grow until they were ~70% confluent. The cells were transfected following the TransIT® - LT1 (Mirus® Bio) Transfection Reagent protocol with changes: Per well 7 µl TransIT (at RT) was mixed with respective 1 µg of plasmid, briefly vortexed and centrifuged, and incubated for 5 min at RT. Afterward, 200 µl of DMEM reduced media (without FBS and Penicillin/Streptomycin) was given to the mix, pipetted up and down and incubated for 15 min at RT. The 200 µl transfection mix was dropwise given unto all areas of the well and gently rocked to all sides several times. The plate was immediately put back into the cell incubator for 48 h. After 48 hrs the cells and the supernatant were harvested. Secreted His-tagged proteins were purified using Ni-NTA sepharose (Qiagen) (Hochuli, Bannwarth, Döbeli, Gentz, & Stüber, 1988). To 1 ml supernatant 40 µl Ni-NTA beads (vortexed and washed beforehand 3 times with 1 x PBS, centrifugation 1 min at 500 rpm) was given and incubated under rotation for 1 hr at 4 °C. Afterward 2 x 2 min washing steps with 500 µl 1 x PBS with subsequent centrifugation steps for 1 min at 500 rpm were performed at RT. The proteins were eluted using 40 µl 250 mM Imidazole while rotating for 15 min at RT (Crowe et al., 1994). In the final step, the beads were centrifuged at 10000 rpm for 3 min and the supernatant containing the His-tagged protein immediately snap-frozen by liquid nitrogen and stored at -80 °C. Eluted proteins were tested before using in a Western blot assay (10% SDS-PAGE) (see "Wnt proteolysis assay").

Hydra body part lysates

100 hydras were cut into four different parts using a scalpel: Tentacles, head, upper and lower body column part (Fig. 3 a), kept on ice and separately washed 2 x 2 min with 1 x PBS. Afterward, the hydra body parts were in a final volume of 250 µl PBS on ice. The samples were sonicated (Sonificator: Branson, sonifier 250, Settings: Timer: Hold; Duty cycle: 10%; Output control: 1.5) on ice until no tissue parts were visible.

The samples were centrifugated 1 min at 10000 rpm at RT and the supernatant was snap-frozen by liquid nitrogen and stored in aliquots at -80 °C. The total protein concentration was controlled by NanoDrop (see "NanoDrop") and diluted to ~4 mg/ml.

Wnt proteolysis assay

All described incubations were stopped after the respective time points by adding 3 µl 5 x reducing samples buffer (10.5 ml 5 x reducing loading dye: 4 ml 10% SDS in ddH_2O, 2.5 ml 0.5 M Tris pH6.8, 2 ml 86% (v/v) Glycerol, 1 ml ddH_2O, 1 ml β- Mercaptoethanol (Carl Roth)) and incubation for 5 min at 96 °C. Afterward, the samples were briefly spin down and stored at -20 °C until analyzing on an SDS-PAGE.

~5 ng of purified HyWnt-His, HyDkk1/2/4-His or mWnt3a was incubated with 15 µg of the respective Hydra body part lysates in a total volume of 12 µl in PBS for 0, 1, 2, 4, 6, 8 and 24 hrs at RT. Fractions from the ion exchange chromatography were prepared for Western blotting for HAS-7 detection or incubated with recombinant HyWnt3 for 0 or 6 hrs.

The final reaction concentrations of tested inhibitor: 200 µM Batismatate (Sigma-Aldrich), 200 µM EDTA (AppliChem), 200 µM 1, 10-Phenanthroline (Sigma-Aldrich) or Fetuin-B (provided by Stöcker Lab, University of Mainz, Germany) (different concentration, see Figure 3 e) were diluted in 1 x PBS and applied as described above. For the BSA stability assay, one reaction per time point contained 1 µg BSA in 8 µl PBS and 5 µl Hydra HL. The BSA stability assay samples were afterward analyzed by blue gel (see "Blue Gel").

SDS-PAGE

The 0.75 mm gap glass plates (Bio-Rad) were cleaned, sealed and fixated into the gel assemble structure (Bio-Rad). 10 % separating as well as 4% stacking SDS-PAGE gels were prepared accordingly (add TEMED and APS directly before applying the respective gel part) starting with the separating SDS-PAGE gel:

For 4 gels:

10% separating SDS PAGE	4% stacking SDS PAGE

11.12 ml ddH_2O	7.5 ml ddH_2O
6 ml 1.5 M Tris pH 8.8	3 ml 0.5 M Tris pH 6.8
400 µl 10% (w/v) SDS (Serva) in ddH_2O	200 µl 10% (w/v) SDS in ddH_2O
6.6 µl 29:1 Acrylamide/Bisacrylamide	1.2 µl 29:1 Acrylamide/Bisacrylamide
40 µl TEMED (Carl Roth)	30 µl TEMED
220 µl 10% (w/v) APS (Ammonium persulphate in ddH_2O), (Carl Roth)	140 µl 10% (w/v) APS (Ammonium persulphate in ddH_2O)

The separating gel was pipetted in between the glass plates leaving a ~2 cm gap to the top of the glass plates. The gel mixture was covered with ~250 µl 2-Propanol until the gel polymerized (~20 min). The 2-Propanol was tilted out and the polymerized gel surface was washed 2 x briefly with 2-3 ml ddH_2O which was tilted out as well. The remaining water was carefully sucked away with a Whatman® Cellulose filter paper. The stacking SDS-PAGE gel mixture was pipetted in between the glass plates unto the separating SDS-PAGE gel up to the top of the lower glass plate. Subsequently, a 0.75 mm comb for 10 gel pockets was inserted into the unpolymerized stacking SDS-PAGE gel avoiding air bubbles. When the gel was polymerized the assembling frame was disassembled, the glass plates with the gels were wrapped into wet paper towels and wrapped into cling film to avoid drying out and stored at 4 °C for up to two weeks. Two SDS-PAGE gels were inserted into each SDS-PAGE running chamber and the space in between both gels was filled up with 1 x SDS-PAGE running buffer (10 x SDS-PAGE running buffer: 1.92 M Glycine, 250 mM Tris, 0.1% (w/v) SDS in ddH_2O). The rest of the running chamber was filled with ~5 cm 1 x SDS-PAGE running buffer. The samples which were test by SDS-PAGE with a possible subsequent Western blot or Blue gel were pipetted into the pockets which were caused by the removed comb. To determine the kDA size of the tested proteins a page ruler (PageRuler™ pre-stained, Thermo Fischer) was given into one pocket. The gels were connected to a power supply (Bio-Rad) and ran at 125 V for ~1.5 hrs or until the blue running front ran out of the gel.

Blue Gel

After the SDS-PAGE run was completed and the gel has to be analyzed for all its protein the gel was stained with Coomassie staining solution (1 l Coomassie staining solution: 500 ml Methanol, 400 ml ddH_2O, 100 ml anhydrous acetic acid, 1 g

Coomassie Brilliant Blue) rocking for 30 min. The gel was afterward washed briefly with Destaining solution (Destaining solution: 700 ml ddH_2O, 200 ml Methanol, 100 ml anhydrous acetic acid) and in fresh Destaining solution in the microwave 30-40 sec boiled at the highest program. Afterward, the gel was incubated on the rocker in the destaining solution until protein bands were visible. The blue gel was documented on a white surface using a smartphone camera.

Western blotting

For Western blotting, no blue gel was performed. The Western blot technique allows to blot proteins from SDS-PAGEs unto membranes, here I used a PVDF membrane (Merck), with Transfer blotting buffer (2 l Transfer blotting buffer: 25 mM Tris, 150 mM Glycine, 10% (v/v) Methanol, fill up with ddH_2O up to 2 l) using the wet blotting chamber for 2 gels (Bio-Rad) for 1 hr set to 360 mA per transfer chamber at 4 °C. The membranes were afterwards blocked for 1 hr while rocking at RT with the respective blocking solution: His-detection (5% (w/v) BSA in 1 x PBS-T), α-Tubulin-detection (5% (w/v) Milk powder in 1 x PBS-T), mWnt3a (5% (w/v) BSA in 1 x PBS-T) and HAS-7-detection (5%(w/v) Milk powder in 1 x PBS-T). After the blocking step the first specific antibody for protein detection was given in a 1:1000 dilution onto the membrane which was carefully rocked overnight at 4°C (mouse anti-His (Thermo Fisher) (in 1% (w/v) BSA in 1 x PBS-T), rabbit anti-α-Tubulin (Sigma-Aldrich) (in 1% (w/v) Milk powder in 1 x PBS-T), rabbit anti-mWnt3a (Abcam((EPR4920(2)) (ab172612)))(in 1% (w/v) BSA in 1 x PBS-T), rabbit α HAS-7 (Eurogentec) (in 1% (w/v) Milk powder in 1 x PBS-T). The following day, the membranes were washed 3 x 5 min with 1 x PBS-T. Afterward, the secondary antibody incubation was done rocking for 1 hr at RT. The secondary antibody binds to the first antibody and is conjugated with a peroxidase and was either 1:10000 anti-mouse horseradish peroxidase-conjugated antibody (Abcam) in 5% (w/v) BSA in 1 x PBS-T or 1:5000 peroxidase-conjugated anti-rabbit antibody (Jackson ImmunoResearch Laboratories, Inc.) in 5% (w/v) Milk powder in 1 x PBS-T. After the secondary antibody incubation, 2 x 5 min washing steps were performed with 1 x PBS-T on the rocker at RT. Two further 5 min washing steps were performed with 1 x PBS. The documentation was done using 500 μl of a 1:1 mix of ECL-1 and ECL-2 (ECL-1: 17 ml ddH_2O, 2.5 ml 1 M Tris pH 8, 200 mM Luminol (Sigma-Aldrich), 90 mM Coumaric acid (Sigma-Aldrich); ECL-2: 18 ml ddH_2O, 2 ml 1 M Tris pH 8, 12 μl H_2O_2) (Haan & Behrmann, 2007) which was mixed right before pipetting in onto the membrane. This

detection method functions by visualizing the peroxidase reaction product. The membrane was completely soaked in a 1:1 mix of ECL-1 and ECL-2 and documented right away using an Intas imager (INTAS®). To document the page ruler a single picture with focus light on for 20 ms was taken. Blots were arranged and the page ruler sizes indicated using Adobe Illustrator or Inkscape.

Single-cell sequencing data

Single-cell sequencing data provided from the Juliano Lab (University of California, Davis, USA) was obtained using the public available homepage: https://singlecell.broadinstitute.org/single_cell/study/SCP260/stem-cell-differentiation-trajectories-in-hydra-resolved-at-single-cell-resolution
Gene of interest IDs (see Table 2: "Single cell sequencing IDs") were generated using https://research.nhgri.nih.gov/hydra/sequenceserver/ (For Transcripts select: Juliano aepLRv2; For Protein select: Augustus Protein Models). All genes of interest just showed activity in the i-cell cluster so just the i-cell cluster was used for further investigation in scatter plot format.

Ion exchange chromatography

1000 *Hydra vulgaris,* which starved for 24 hrs, were dissolved by sonification (see "Hydra body part lysates") in 1 ml HEPES(-) buffer (HEPES (-) buffer: 50 mM HEPES in ddH_2O pH 7.4). The hydra lysate was centrifugated at maximum speed for 15 min in the cooling centrifuge. Samples of the supernatant were taken and treated like all following samples. 500 µl supernatant was injected onto an anion exchange chromatography column (Thermo Fischer Scientific) attached to an Äkta™ Laboratory-scale Chromatography Systems (GE Healthcare Life Sciences). The system ran at 1 ml/min speed starting at 0% conductivity. All collected samples were snap-frozen in liquid nitrogen and stored at -80 °C. The Flowthrough was collected and HEPES (+) buffer (HEPES (+) buffer: 1 M NaCl, 50 mM HEPES in ddH_2O pH 7.4) was connected to the system to increase the conductivity. 1 ml fractions were collected during the salt concentration raise and 15 x 1 ml fractions were collected after the conductivity

reached 100%. Fractions were used in HyWnt stability assay and for HAS-7 detection using Western blotting.

Functional assay in *Xenopus laevis*

Sample preparation

Used constructs for HyHAS-7 and HyWnt3 were codon-optimized for *Xenopus laevis* by using the BIOMATIK service. The constructs used for XWnt8 and a Scrambled control were received by the Niehrs Lab (University of Heidelberg, DKFZ, Germany). The mRNA synthesis was done with mMESSAGE mMACHINE T7 (Invitrogen by Thermo Fisher Scientific) Kit according to the provided instruction protocol with changes.

M13 PCR amplification

To generate linearized DNA a M13 PCR amplification was done according to "M13 PCR amplification".

PCR product clean-up

The PCR product clean-up was done with Wizard ® SV Gel and PCR Clean-Up System Kit from Promega with changes as described in "PCR product clean-up".

Caped mRNA synthesis and purification

The caped mRNA synthesis was done with T7 mMESSAGE mMACHINE (Invitrogen by Thermo Fisher Scientific) following the provided instruction protocol with changes Depending on the orientation of the gene the sp6 or T7 mMESSAGE mMACHINE Kit should be used. All reaction components were thaw on RT except 2x NTP/CAP and the "Enzyme Mix" were kept on ice. All reactions were pipetted at RT in the following order into a 1.5 ml Eppendorf tube:

- 5 µl DNAse/RNAse free water (total reaction volume up to 20 µl)
- 10 µl 2x NTP/CAP
- 1 µl PCR product (1 µg/µl)
- 2 µl 10x Reaction Buffer

- 2 µl Enzyme Mix

The samples were gently flicked and briefly centrifugated. The reactions were incubated for 1.5 hrs at 37 °C. An optional DNAse step was skipped. Right after the synthesis a Phenol-Chloroform extraction, a 2-propanol precipitation was done to purify the freshly synthesized capped mRNA. To the 20 µl caped mRNA synthesis reaction 115 µl of DNAse/RNAse free water and 15 µl Ammonium Acetate was added and mixed by flicking the tube. The mixture was briefly centrifugated. 150 µl Phenol/Chloroform/Isoamyl alcohol was added and mixed by slowly pipetting up and down several times. The sample was centrifuged at 13000 rpm for 5 min at RT. The upper aqueous phase was transferred into a new 1.5 ml Eppendorf tube and the lower organic phase was discarded. To the upper aqueous phase, 80 µl Chloroform/Isoamyl alcohol (24:1 (v/v)) was added and mixed by pipetting up and down several times and centrifuged again at 13000 rpm for 10 min at RT. The upper aqueous phase was again pipetted into a new 1.5 ml Eppendorf tube and the lower organic phase was discarded. The caped mRNA was precipitated by adding to the upper aqueous phase 1 volume of 2-Propanol (to 30 µl aqueous phase add 30 µl 2-Propanol). The samples were kept overnight at -20 °C. The next day, the sample was centrifugated at maximal speed for 30 min at 4 °C in the cooling centrifuge. The liquid was carefully pipetted away and discarded. The well visible pellet was dissolved in 20 µl DNAse/RNAse free water. The sample was frozen away at -80 °C. The purified and precipitated capped mRNA was checked on a 1% (w/v) Agarose gel (see "Agarose gel") and the quantity was checked by NanoDrop (see "NanoDrop") to estimate the concentration for further dilution calculation.

In vito fertilization of *Xenopus laevis*

Female *Xenopus laevis* were injected with 50 U of hCG (Human chorionic gonadotropin) and kept at 18 °C overnight. The next day, prior to the injection, female *Xenopus laevis* were squeezed to induce physically ovulate into an empty glass petri dish. The *in vitro* fertilization was done with a *Xenopus laevis* male testes suspension. The fertilized eggs were defolliculated using 2% (w/v) L-Cysteine in 0.1% (v/v) Marc's Modified Ringer's Solution (10x Stock: 1 M NaCl, 50 mM HEPES, 20 mM KCl, 20 mM $CaCl_2 \cdot 2H_2O$, 10 mM $MgSO_4 \cdot 7H_2O$; pH 8) by rotating the eggs in the solution by hand

and pipetting the eggs carefully up and down with a plastic pipette to separate them. The hormonal injection, the squeezing, the in vitro fertilization and the defolliculation process were done by members of the Niehrs' Lab (University of Heidelberg, DKFZ, Germany). The euthanizing of the male *Xenopus laevis* to generate the testes and the storage of the testes was not given.

Xenopus laevis 4-cell stage injection

Fertilized *Xenopus laevis* eggs were kept in 0.3 x MBS, 2% (w/v) Ficoll (Oocyte medium; 10x MBS: 880 mM NaCl, 100 mM HEPES, 24 mM NaHCO3, 10 mM KCl , 8.2 mM $MgSO_4.7H_2O$, 4.1 mM $CaCl_2.6H_2O$, 3.3 mM $Ca(NO_3)_2.4H_2O$, pH 7.5) in a coated petri dish. The coating consisted out of 1% (w/v) Agarose in 1 x $MBS^{(-)}$ (without calcium and magnesium). The agarose coating prevents the oocytes from sticking to the bottom of the petri dish. The *Xenopus laevis* eggs were kept at 18 °C until the 4-cell stage was reached during developmental progression. 5 nl of the capped mRNA were microinjected into both ventral blastomeres (2 of 4 bigger and darker cells) of the 4-cell stage into the equatorial region (2 x 5 nl; a total of 10 nl with 10 or 100 pg caped mRNA per blastula, as stated in results). The embryos were kept after the injection in 0.1 x MBS at 18 °C. 24 hpf (hours post fertilization) the 0.1 x MBS was exchanged with fresh 0.1 x MBS. ~ 48 hpf the embryos were staged after Nieuwkoop & Faber, 1994 (https://www.xenbase.org/anatomy/alldev.do) (Gurdon, 1995).

At stage 24 (tail bud stage) they were fixed with 37% (w/v) Paraformaldehyde in PBS at 4°C for 3 hrs. Afterward, the 37% (w/v) Paraformaldehyde in PBS was exchanged with fresh 37% (w/v) Paraformaldehyde in PBS and the embryos were stored at 4 °C until documentation. The embryos were documented with a Nikon SMZ 25 microscope using a 0.5x AHR Plan Apo objective with a Nikon DS-Ri2 camera attached. The light source was self-applied to get light from the top. The embryos were later aligned using the software Adobe Photoshop and Adobe Illustrator. The phenotypical aberrations were classified according to the dorso-anterior index after Kao & Elinson, 1988 (Kao & Elinson, 1988).

Chromatin immunoprecipitation

Chromatin immunoprecipitation analysis was done by the Hartl Lab (University of Innsbruck, Austria) and "carried out as described recently by using sheared extracts from formaldehyde-treated *Hydra* animals, which have been treated without or with 5 µM Alp in DMSO (48 hrs) and an antiserum directed against a recombinant *Hydra* TCF protein (Lommel et al., 2018) (Gufler et al., 2018). PCR of precipitated DNA was done using specific primers flanking the potential TCF binding sites in the 5'-regulatory regions of the *Hydra HAS-7* or the *TSP* gene. PCR primer sequences:
TCF binding motif in *HAS-7* (5'-GCTGTTATCTGTCCGCTTTC-3'/5'-CCATATAGAGGCCACACACC-3'), and the proximal TCF binding motif in *TSP* (5'-TTGAAGGCATTTAACAACTTGC-3'/5'-TGCCCAAATGTAAAGTTCTGTG-3')."
((Ziegler et al., 2020) in preparation)

Structural modeling

The structural modeling was designed and done by Walter Stöcker (Institute of Molecular Physiology, Cell and Matrix Biology, Johannes Gutenberg University Mainz, Germany) and Jörg Stetefeld (Department of Chemistry, University of Manitoba, Canada). "Protein-Protein docking experiments were performed in ClusPro2 (Kozakov et al., 2017) using the crystal structures of *Xenopus* Wnt8 (pdb-code:4F0A) and pro-meprin-ß (pdb-code: 4GWM). The propeptide E25-G66 blocking access to the active site cleft and disordered loop segments in Wnt8 were removed to allow for proper structural analysis. Targeted search matrices were chosen by selecting the zinc-binding site of pro-meprin-ß (H132-H136-H142) and the putative cleavage site of HyWnt3 (K186-D187-P188) as attractive search targets. Based on Lennart-Jones potentials, distance metrices and electrostatic evaluations the best 100 docking hits were subject to gradient energy minimization in the Crystallography and NMR system. 14 The lowest energy structures were further subject to 500 cycles of unrestrained Powell minimization. Harmonic restraints were imposed on the target molecule (2 kcal/mol $Å^2$) with increased weight (25 kcal/mol $Å^2$). Protein structure and model assessment tools were used to verify the quality of the modeled structure. Additionally, HAS-7 modeling was performed using Modeller (Sali & Blundell, 1993) implemented

in Chimera (Pettersen et al., 2004) with astacin complexed to a transition state analog inhibitor (pdb-code: 1QJI) and zebrafish hatching enzyme (3LQB), the latter being the most closely HAS-7-related astacin with a known structure to date." (Ziegler et al., 2020)

Mathematical simulation

Mathematical simulations were designed and executed, and results were provided by Moritz Mercker and Anna Marciniak-Czochra from the Institute for Applied Mathematics, Interdisciplinary Center for Scientific Computing (University of Heidelberg, Germany).

Material

Sequences and nucleotides

siRNA sequences

Table 1: siRNA sequences

Gene name	siRNA Sequence (anti-sense)
HAS-7	GUCUCCUUCAAACAGAUUGUUUU (siRNA1) AAUGUUAUUCCAUAUAAUAUUUU (siRNA2) UGAUUUGCAAUAACCUGUAUUUU (siRNA3)
HMP1	UCACUGCAGAUAUGUAUGCUUUU (siRNA1) UCCAGUGACACCGCUACACUUUU (siRNA2)
HAS-1	ACUAUUGGAGUAUAGAGAUCUUU (siRNA1) AUCGUAUGGAACAACAUUGUUUU (siRNA2)
HyDKK1/2/4	GCAACGAAUGCAGCUACAACUUU (siRNA1) UUUCGCAGUCUGCAUCCUUAUUU (siRNA2)
GFP	AAUUGGCCAUGGAACAGGUAGUUUU
Scrambled GFP	AAACCGGUGUGAAUCGAUGAGUUUU
HyWnt3	AAATGGAGTTTCTATACAAAGUU
β-catenin	AAGGUUAUGAUGAUGAUGAAGUU
HyNdr	GUCUCUCCGGAUGUGGUUAUU (siRNA1) AGCAAUCAAGACGAAUCGUUU (siRNA2)
HyWnt8	GUCUCUCCGGAUGUGGUUAUU (siRNA1) AGCAAUCAAGACGAAUCGUUU (siRNA2)

RT-qPCR Primer

Table 2: RT-qPCR primer

Gene name	qPCR Primer Sequence
EF1α	Fw: TATTGATAGACCTTTTCGACTTTGC
	Rev: CTGTACAGAGCCACTTTCAACTTTT
HAS-7	Fw: GGATGTGAAATCAAATGGTTATGCT
	Rev: TGATGAACTCATTCTTCGAAGATCG

Single cell sequencing IDs

Table 3: Single cell sequencing IDs and HAS Accession numbers

Trivial name	Transcript ID	Accession number
HAS-1	t20535aep	XP_012565441.1
HAS-2	t18494aep	XP_002162822.1
HAS-3	t22149aep	XP_002166229.3
HAS-4	t11453aep	XP_002162738.1
HAS-5	t596aep	XP_002164800.1
HAS-6	t19593aep	XP_002157397.2
HAS-7	t16296aep	XP_012560086.1
HAS-8	t22154aep	XP_002153855.1
HAS-9	t3416aep	XP_002161766.1
HAS-10	t10258aep	XP_002159980.2
HAS-11	t19316aep	XP_012561076.1
HMP-1	t1098aep	NP_001296695.1
HyDkk1/2/4	t8678aep	AM182483.1

Accession numbers can be used to obtain protein amino acid sequences by blasting the accession number:
https://blast.ncbi.nlm.nih.gov/Blast.cgi?PROGRAM=blastp&PAGE_TYPE=BlastSearch&BLAST_SPEC=&LINK_LOC=blasttab&LAST_PAGE=blastn
Transcript IDs were obtained by https://research.nhgri.nih.gov/hydra/sequenceserver/ and used to gain single sequencing data https://portals.broadinstitute.org/single_cell/study/stem-cell-differentiation-trajectories-in-hydra-resolved-at-single-cell-resolution.

In situ probes

Table 4: LNA and conventional *in situ* probes used in WISH

	Accession Number	LNA or in situ probe sequence
HAS-1	XP_012565441.1	Full length antisense mRNA (1-717)
HAS-2	XP_002162822.1	ATCACGGTCAGGACGGCATTGT
HAS-3	XP_002166229.3	TAGTGACATATCTATCTCTGT
HAS-4	XP_002162738.1	ATTGTTCAGGTGTCAATTGTA
HAS-5	XP_002164800.1	TCAGACAAGTGTAGGTGTGATA
HAS-6	XP_002157397.2	TCTAAGGCAAGTGTAAGTGTGA
HAS-7	XP_012560086.1	Full length antisense mRNA (1-1021)
HAS-8	XP_002153855.1	TATGACGTAAGGTACAACAGCA
HAS-9	XP_002161766.1	ACGGCAAGATCTGCGGCAAGAT
HAS-10	XP_002159980.2	TACTGTACCAAGTCGCAAGCAA
HAS-11	XP_012561076.1	ACATGACTTGCAGCATAGCTGA
HMP-1	NP_001296695.1	Full length antisense mRNA (1-858)

Chemicals

Table 5: Used chemicals

Chemical Name	Company
0,05% Trypsin	Gibco, Life technologies
10-Phenanthroline	Sigma-Aldrich
2-Propanol (experimental use)	Merck
2-Propanol (Hydra cleaning)	provided by the Zentrallager
Acetic anhydride	Grüssing
Acrylamide/Bisacrylamide 29:1	Carl Roth
Agarose	Carl Roth
Ammonium acetate	Grüssing
Ammonium persulfate (APS)	Carl Roth
anhydrous Acetic Acid	Honeywell
Batismatate	Sigma-Aldrich
BCIP	Roche
Blocking reagent	Roche
Bovine serum albumin (BSA)	Carl Roth
Bromphenol blue	Sigma-Aldrich
Calcium Chlorid (CaCl2)	Carl Roth
Chaps	Roche
Chloroform	Honeywell
Coumaric acid	Sigma-Aldrich
ddH2O	provided by the institute
Dimethylsulfoxid (DMSO)	Merck
DMEM Media	Gibco, Life technologies
DNA 5 x loading dye	Thermo Fisher
Ethanole, 100 % absolute	Merck
Fetal Bovine Serum (FBS)	PAA, The cell culture company
Ficoll 400	Sigma-Aldrich
Fixogum	Marabu
Formamide	VWR chemicals
Glycerol	Sigma-Aldrich
Glycine	Labochem international
Heparin	Carl Roth
HEPES	Sigma-Aldrich
Hydrogen peroxide solution (H2O2)	Merck
Isoamylalcohol	Sigma-Aldrich
Kalium Chliride (KCl)	Sigma-Aldrich
Linanool	Sigma-Aldrich
Luminol	Sigma-Aldrich
Magnesium Chloride (MgCl2)	Applichem, Merck

Magnesium sulfate ($MgSO_4$)	Merck, Millipore
Maleic acid	Merck
Methanol	VWR chemicals
Midori Green	NIPPON genetics EUROPE
Milk powder	Carl Roth
Mowiol 4-88	Carl Roth
NBT	Roche
Ni-NTA sepharose	Quiagen
PageRule, pre stained	Thermo Fisher
Paraformaldehyde (PFA)	Sigma-Aldrich
Phenol-Chlorophorm-Isoamylalcohol mixture	Merck, BioUltra
Polyvinylpyrrolidone	Sigma-Aldrich
Proteinase K	Sigma-Aldrich
Pyruvate	Carl Roth
RNAse/DNAse free water	Braun
Sodium Acetat	Sigma-Aldrich
Sodium chloride (NaCl)	Sigma-Aldrich
Sodium Citrate (Na-Citrate)	Sigma-Aldrich
Sodium dodecyl sulfate (SDS)	Serva
TEMED	Carl Roth
TES	Applichem
TransIT® - LT1	Mirus® Bio
Triethanolamine (TEA)	Merck
Tris	Carl Roth
TRIzol	Thermo Fisher Scientific
Tween-20	Carl Roth
Urethan	Sigma-Aldrich
Xylen Cyanol	Serva
Yeast RNA	Carl Roth
β- Mercaptoethanol	Carl Roth

Chemicals and material used for Xenopus experiments were provided by the Niers Lab and are not given.

Antibiotics

Table 6: Used antibiotics

Antibiotic	Company
Ampicilin	Sigma-Aldrich
Kanamycin	Carl Roth
Penicillin	Sigma-Aldrich
Rifampicin	Sigma-Aldrich
Streptomycin	Serva

Antibodies

Table 7: Used antibodies

First Antibody	Company
anti Digoxigenin, conjugated with alkaline phosphatase	Roche
mouse anti His-Tag	Thermo Fisher
rabbit anti mWnt3a	Abcam ((EPR4920(2)) (ab172612))
rabbit anti HAS-7	Eurogentec
rabbit anti Tubulin	Sigma-Aldrich
rabbit anti CPP1	Eurogentec

Second Antibody	Company
anti mouse, horseradish peroxidase-conjugated	Abcam
anti rabbit, horseradish peroxidase-conjugated	Jackson ImmunoResearch Laboratories, Inc.
anti rabbit Alexa 488	Eurogentec

Inhibitors

Table 8: Used inhibitors

Inhibitor	Company
Alsterpaullone (Alp)	Sigma-Aldrich
Azakenpaullone (Azk)	Sigma-Aldrich
Batimastat	Sigma-Aldrich
Dimethyl sulfoxide (DMSO)	Serva
EDTA disodium salt	Carl Roth
1, 10-Phenanthroline	Sigma-Aldrich

Materials

Table 9: Used material

Material	Brand and additional information
1.5 ml and 2 ml Tubes	Sarstedt
10 µl, 20 µl, 200 µl and 1 ml Pipette tips	Kisker (with or without filter as stated)
15 ml and 50 ml Tube	Falcon
24-well plate for ISH	Greiner
5 ml, 10 ml and 25 ml long filter pipete tips	Costar ® Stripette sterile Serological pipet (Corning Incorporated)
96-well plates for qPCR	96 Fast PCR-Platte half skirt DNA-/DNAse-/RNAse-/PCR inhibitor free (Sarstedt)
Electroporation Cuvette	Bio Rad, 0.4 cm gap cuvette
Glas plates, short and with 0.75mm spacer plate	Bio Rad
Gloves	TouchNTuff (Ansell)

Lid for 96-well plates for qPCR	MicroAmp ™ Optical Adhesive Film PCR/REAL-time PCR compartible (applied biosystems by Themo Fisher Scientific)
Pasteur glas pipettes	Pasteur capillary pipettes short size 150 mm (Neo Lab)
Petri dish	Greiner
SDS-PAGE assemby and running chamber	Bio Rad

Machines

Table 10: Used Machines

Machine	*Brand Name of Machine*
0.5x AHR Plan Apo objective	Nikon
2 µl, 20 µl, 200 µl and 1 ml Pipettes	Gilson
Bench Binocular	Schott KL 200 LED
Cell hood	Hera Safe (Heraeus)
Cell incubator	Herecell 150i CO2 Incubator (set to 37 °C or 27 °C with 5% CO2)
Centrifuge	Thermo scientific Herdeus Pico 17 centrifuge
Cooling Centrifuge	Heraeus (Biofuge fresco)
Electroporator	Bio Rad Gene Pulser Xcell
Heating Stirrer	Carl Roth, MH15 Rotilabo® Magnitic stirrer with heat
Intas Imager	INTAS® UV-Systems Gel Imager
Nano Drop	Nano Drop ® ND-1000 Spectrophotometer (peQLab) Biotechnologie GmbH
Nikon DS-Ri2 camera	
Nikon SMZ 25 microscope	
PCR machine	Bio Rad S1000™ Thermal Cycler
pH Meter	Sartorius PB-11 (glas electrode strored in 3M KCL)
Pipetboy	Brand accu-jet ® pro
Plate centrifuge	PeQLab Perfect Spin P

Power supply	Bio Rad
RT-qPCR machine	Applied Biosystems StepOnePlus ™ Instrument
Safe Imager Blue-Light Transilluminator	Thermo Fisher
Sonicator	Branson (Sonifier 250)
Thermomixer	Eppendorf Thermomixer comfort
Vortexer	Heidolph
Wet blotting machine	Bio Rad

Kits

Table 11: Used Kits

Kit	*Company*
NucleoSpin® Plasmid/Plasmid (NoLid) Miniprep	Macherey-Nagel
SensiFAST cDNA Synthesis Kit	Bioline
SensiFAST SYBR-Hi-ROX Kit	Bioline
sp6 or T7 mMESSAGE mMACHINE	Invitrogen by Thermo Fisher Scientific
Wizard ® SV Gel and PCR Clean-Up System Kit	Promega

Software

Table 12: Used Software

Software	*Company*
Adobe Illustator	Adobe
Adobe Photoshop	Adobe
Excel	Microsoft
Fiji	
Geneious	
Inkscape	
Mendeley	
NanoDrop Software	
NIS Elements	Nikon
Prism	
SerielCloner	
Word	Microsoft

Acknowledgments

I would like to express my very great appreciation to Suat Özbek for giving me the opportunity to work on this project, as well as for his patient guidance and enthusiastic encouragement. You are a great supervisor and person.
Furthermore, I want to thank the Deutsche Forschungsgemeinschaft for funding this project and giving me the chance to work on my own project, increase the knowledge in such an interesting research field and in the end improve myself in various research fields. I also want to thank the Schmeil-foundation for awarding me with the "Doctoral Dissertation Award 2020", acknowledging my work.
I would like to express my deep gratitude to Thomas Holstein, Jan Lohmann, Sergio Acebrón and Gary Davidson for taking the time to be part in my thesis advisory committee and for their useful and constructive recommendations on this project.
For their friendship even outside of the lab and for a lot of refreshing tea breaks I want to thank Marie, Niha and Gideon.
A big thanks for teaching me certain experimental technics goes to Steffi Höger, Benjamin Trageser, Mark Lommel and my Bachelor thesis supervisor Anna Beckmann.
I would also like to extend my thanks to our former lab technician Jutta Tennigkeit and our present lab technician Maike Fath for helping me with my experiments, as well as having helping hands and ears during all of my laboratory work – you are the hearts and souls of the lab! I also wish to thank all members of the Holstein, Guse and Acebrón Labs which I did not mention above as well as the whole COS-Institute community.
I would like to express my very great appreciation to Walter Stöcker who gave us the opportunity to brainstorm together and for his input in terms of structural modeling together with Jörg Stetefeld. Furthermore, I want to thank Moritz Mercker and Anna Marciniak-Czochra for contributing to this project by building a mathematical model to show the project from a different point of view. I want to thank Sumit Kumar for doing initial experiment to this project, Uwe Warnken and Martina Schnölze for doing the mass spectrometry, Markus Hartl for the ChIP analysis and Alexander Hirth from the Niehrs lab.
I also want to thank my former students, especially Svenja Kling and Jana Röder for their good work and active participation but I also want to thank all other students which I supervised may their work be part of this thesis or not.
I wish to thank my family and parents for their support and encouragement throughout my study.
I want to thank my friends very much for their support in finding a healthy work-life balance as well as for their open ears all the time.
Finally, I want to thank Constantin for everything good in my life.

Publications

Parts of this thesis were published or communicated

Poster presentations

B. Ziegler, et al. „An astacin metalloprotease involved in Wnt-dependent patterning in Hydra “ | Annual Wnt SFB 1324 meeting 2019

B. Ziegler, et al. „An astacin metalloprotease involved in Wnt-dependent patterning in Hydra” | “Old Questions and New Frontiers” COS Symposium 2019

B. Ziegler, S. Özbek „An astacin metalloprotease involved in Wnt-dependent patterning in Hydra“ | European Society for Evolutionary Developmental Biology (EvoDevo) conference 2018, Galway, Ireland

B. Ziegler, S. Özbek „An astacin metalloproteaseinvolved in Wnt-dependent patterning in Hydra“ | European Wnt meeting 2018, Heidelberg, Germany

B. Ziegler, et al. „An astacin metalloprotease involved in Wntdependent patterning in Hydra” | International Workshop “The diversification of early emerging metazoans” 2017, Tutzing, Germany

Talks

Flashtalk: B. Ziegler, S. Özbek „An astacin metalloprotease involved in Wnt-dependent patterning in Hydra “ | European Wnt meeting, Heidelberg, Deutschland

Flashtalk: B. Ziegler, et al. „An astacin metalloprotease involved in Wnt-dependent patterning in Hydra “ | Annual Wnt SFB 1324 meeting 2019

Publications

D. K. Shoemark, **B. Ziegler**, H. Watanabe, J. Strompen, R. P. Tucker, S..zbek, and J. C. Adams. Emergence of a Thrombospondin Superfamily at the Origin of Metazoans; Mol Biol Evol. 2019 Jun 1; 36(6):1220-1238.

In preparation: **B. Ziegler**, Irene Yiallouros, Benjamin Trageser, Sumit Kumar, Moritz Mercker, Svenja Kling, Maike Fath, Uwe Warnken, Martina Schn.lzer, Thomas W. Holstein, Markus Hartl, Anna Marciniak-Czochra, J.rg Stetefeld, Walter Stöcker, Suat Özbek. A Wnt-specific astacin proteinase controls head formation in Hydra. Available at bioRxiv.

References

Augustin, R., Franke, A., Khalturin, K., Kiko, R., Siebert, S., Hemmrich, G., & Bosch, T. C. G. (2006). Dickkopf related genes are components of the positional value gradient in Hydra. *Developmental Biology*, *296*(1), 62–70. https://doi.org/10.1016/j.ydbio.2006.04.003

Augustin, R., Fraune, S., & Bosch, T. C. G. (2010). *Seminars in Immunology How Hydra senses and destroys microbes*. *22*, 54–58. https://doi.org/10.1016/j.smim.2009.11.002

Beattie, G. J., Young, H. A., & Smyth, J. F. (1994). Phase I study of intraperitoneal metalloproteinase inhibitor BB-94 in patients with malignant ascites (Abstract). 8th NCI-EORTC Symposium on New Drug Development. *Amsterdam, March*.

Becker-Pauly, C., Barré, O., Schilling, O., auf dem Keller, U., Ohler, A., Broder, C., … Overall, C. M. (2011). Proteomic Analyses Reveal an Acidic Prime Side Specificity for the Astacin Metalloprotease Family Reflected by Physiological Substrates. *Molecular & Cellular Proteomics*, *10*(9), M111.009233. https://doi.org/10.1074/mcp.M111.009233

Becker, C., Kruse, M., Slotty, K. A., Köhler, D., Robin, J., Rösmann, S., … Tierphysiologie, M. (2003). *Differences in the Activation Mechanism between the _ and ⁄ Subunits of Human Meprin*. *384*(May), 825–831.

Beninga, J., Rock, K. L., & Goldberg, A. L. (1998). Interferon-gamma can stimulate post-proteasomal trimming of the N terminus of an antigenic peptide by inducing leucine aminopeptidase. *The Journal of Biological Chemistry*, *273*(30), 18734–18742. https://doi.org/10.1074/jbc.273.30.18734

Blader, P., Rastegar, S., & Fischer, N. (1997). *Cleavage of the BMP-4 Antagonist Chordin by Zebrafish Tolloid*. *278*(December), 0–4.

Bode, H., Lengfeld, T., Hobmayer, B., & Holstein, T. W. (2008). Detection of expression patterns in Hydra pattern formation. *Methods in Molecular Biology (Clifton, N.J.)*, *469*, 69–84. https://doi.org/10.1007/978-1-60327-469-2_7

Bode, H. R., Heimfeld, S., Chow, M. A., & Huang, L. W. (1987). *Gland Cells Arise by Differentiation from Interstitial Cells in Hydra attenuata*. *577585*. https://doi.org/122,577585

Bode, W., Gomis-Rüth, F. X., Huber, R., Zwilling, R., & Stöcker, W. (1992). Structure of astacin and implications for activation of astacins and zinc-ligation of collagenases. *Nature*, *358*(6382), 164–167. https://doi.org/10.1038/358164a0

Bode, W., Gomis-Rüth, F. X., & Stöckler, W. (1993). Astacins, serralysins, snake venom and matrix metalloproteinases exhibit identical zinc-binding environments (HEXXHXXGXXH and Met-turn) and topologies and should be grouped into a common family, the “metzincins”. *FEBS Letters*, *331*(1–2), 134–140. https://doi.org/10.1016/0014-5793(93)80312-i

Bond, J. S., & Beynon, R. J. (1995). The astacin family of metalloendopeptidases. *Protein Science*, *4*(7), 1247–1261. https://doi.org/10.1002/pro.5560040701

Bosch, T. C., & David, C. N. (1987). *Stem Cells of Hydra magnipapillata Can Differentiate into Somatic Cells and Germ Line Cells*. *191*, 182–191.

Broun, M. (2005). Formation of the head organizer in hydra involves the canonical Wnt pathway. *Development*, *132*(12), 2907–2916. https://doi.org/10.1242/dev.01848

Broun, M., & Bode, H. R. (2002). *Characterization of the head organizer in hydra*. *884*, 875–884.

Browne, E. N. (1909). The production of new hydranths in hydra by the insertion of

small grafts. *J Exp Zool*, *7*(1), 1–23.
Buzgariu, W., Crescenzi, M., & Galliot, B. (2014). Robust G2 pausing of adult stem cells in Hydra. *Differentiation*, *87*(1–2), 83–99. https://doi.org/10.1016/j.diff.2014.03.001
Campbell, R. D. (1967). Tissue dynamics of steady state growth in Hydra littoralis. II. Patterns of tissue movement. *J. MORPR.*, *121*, 19–28.
Carter, J. A., Hyland, C., Steele, R. E., & Collins, E. S. (2016). Article Dynamics of Mouth Opening in Hydra. *Biophysj*, *110*(5), 1191–1201. https://doi.org/10.1016/j.bpj.2016.01.008
Chang, P. C., & Lee, Y. H. (1992). Extracellular autoprocessing of a metalloprotease from Streptomyces cacaoi. *The Journal of Biological Chemistry*, *267*(6), 3952–3958.
Chomczynski, P., & Sacchi, N. (1987). Single-step method of RNA isolation by acid guanidinium thiocyanate-phenol-chloroform extraction. *Analytical Biochemistry*, *162*(1), 156–159. https://doi.org/10.1006/abio.1987.9999
Clevers, H. (2006). Wnt/beta-catenin signaling in development and disease. *Cell*, *127*(3), 469–480. https://doi.org/10.1016/j.cell.2006.10.018
Crowe, J., Dobeli, H., Gentz, R., Hochuli, E., Stiiber, D., & Henco, K. (1994). *6xHis-Ni-NTA Chromatography as a Superior Technique in Recombinant Protein Expression/Purification BT - Protocols for Gene Analysis* (A. J. Harwood, Ed.). https://doi.org/10.1385/0-89603-258-2:371
Cummings, S. G., & Bode, H. R. (1984). *Roux ' s Archives of Developmental Head regeneration and polarity reversal in Hydra attenuata can occur in the absence of D N A synthesis*. 79–86.
David, C. N. (2012). *Interstitial stem cells in Hydra : multipotency and decision-making*. *497*(June), 489–497. https://doi.org/10.1387/ijdb.113476cd
De, A. (2011). Wnt/Ca2+ signaling pathway: a brief overview. *Acta Biochimica et Biophysica Sinica*, *43*(10), 745–756. https://doi.org/10.1093/abbs/gmr079
Detry, B., Erpicum, C., Paupert, J., Blacher, S., Maillard, C., Bruyère, F., … Noël, A. (2012). Matrix metalloproteinase-2 governs lymphatic vessel formation as an interstitial collagenase. *Blood*, *119*(21), 5048–5056. https://doi.org/10.1182/blood-2011-12-400267
Dumermuth, E., Sterchis, E. E., Jiang, W., Wolz, R. L., Bond, J. S., Flannery, A. V, & Beynon, R. J. (1991). The Astacin Family of Metalloendopeptidases. *The Journal of Biological Chemistry*, 21381–21385. https://doi.org/10.1182/blood-2011-12-400267. Epub 2012 Apr 6.
Eldering, J. A., Grünberg, J., Hahn, D., Croes, H. J., Fransen, J. A., & Sterchi, E. E. (1997). Polarised expression of human intestinal N-benzoyl-L-tyrosyl-p-aminobenzoic acid hydrolase (human meprin) alpha and beta subunits in Madin-Darby canine kidney cells. *European Journal of Biochemistry*, *247*(3), 920–932. https://doi.org/10.1111/j.1432-1033.1997.00920.x
Fraser, H. B., Hirsh, A. E., Steinmetz, L. M., Scharfe, C., & Feldman, M. W. (2002). Evolutionary rate in the protein interaction network. *Science (New York, N.Y.)*, *296*(5568), 750–752. https://doi.org/10.1126/science.1068696
Gajendrareddy, P. K., Engeland, C. G., Junges, R., Horan, M. P., Rojas, I. G., & Marucha, P. T. (2013). MMP-8 overexpression and persistence of neutrophils relate to stress-impaired healing and poor collagen architecture in mice. *Brain, Behavior, and Immunity*, *28*, 44–48. https://doi.org/10.1016/j.bbi.2012.10.016
Garrigue-Antar, L., François, V., & Kadler, K. E. (2004). Deletion of epidermal growth

factor-like domains converts mammalian tolloid into a chordinase and effective procollagen C-proteinase. *The Journal of Biological Chemistry*, *279*(48), 49835–49841. https://doi.org/10.1074/jbc.M408134200
Ge, G., Hopkins, D. R., Ho, W.-B., & Greenspan, D. S. (2005). GDF11 forms a bone morphogenetic protein 1-activated latent complex that can modulate nerve growth factor-induced differentiation of PC12 cells. *Molecular and Cellular Biology*, *25*(14), 5846–5858. https://doi.org/10.1128/MCB.25.14.5846-5858.2005
Gierer, A., & Meinhardt, H. (1972). A Theory of Biological Pattern Formation. *Kybernetik by Springer-Verlag*, *39*, 30–39.
Goel, T., Wang, R., Martin, S., Lanphear, E., & Collins, S. (2019). *Linalool acts as a fast and reversible anesthetic in Hydra*.
Gomis-Rüth, F. X., Stöcker, W., Huber, R., Zwilling, R., & Bode, W. (1993). Refined 1.8 Å X-ray crystal structure of astacin, a zinc-endopeptidase from the crayfish Astacus astacus L.: Structure determination, refinement, molecular structure and comparison with thermolysin. *Journal of Molecular Biology*, Vol. 229, pp. 945–968. https://doi.org/10.1006/jmbi.1993.1098
Gomis-Rüth, F. X., Trillo-Muyo, S., & Stöcker, W. (2012). Functional and structural insights into astacin metallopeptidases. *Biological Chemistry*, *393*(10), 1027–1041. https://doi.org/10.1515/hsz-2012-0149
Gomis-Rüth, F. Xavier. (2003). *Structural Aspects of the Metzincin Clan of Metalloendopeptidases*. *24*, 18–26.
Gomis-Rüth, F Xavier. (2009). Catalytic domain architecture of metzincin metalloproteases. *The Journal of Biological Chemistry*, *284*(23), 15353–15357. https://doi.org/10.1074/jbc.R800069200
Gordon, M. D., & Nusse, R. (2007). *Wnt Signaling : Multiple Pathways , Multiple Receptors ,*. *281*(32), 22429–22433. https://doi.org/10.1074/jbc.R600015200
Grasso, G., & Bonnet, S. (2014). *Metal complexes and metalloproteases : targeting conformational diseases*. 1346–1357. https://doi.org/10.1039/c4mt00076e
Grens, A., Gee, L., Fisher, D. A., & Bode, H. R. (1996). CnNK-2, an NK-2 homeobox gene, has a role in patterning the basal end of the axis in hydra. *Developmental Biology*, *180*(2), 473–488. https://doi.org/10.1006/dbio.1996.0321
Guder, C., Pinho, S., Nacak, T., Schmidt, H., Hobmayer, B., Niehrs, C., Holstein, T. W. (2006). An ancient Wnt-Dickkopf antagonism in Hydra. *Development*, *133*(5), 901–911. https://doi.org/10.1242/dev.02265
Guder, C., Philipp, I., Lengfeld, T., Watanabe, H., Hobmayer, B., & Holstein, T. W. (2006). *The Wnt code : cnidarians signal the way*. 7450–7460. https://doi.org/10.1038/sj.onc.1210052
Guevara, T., Yiallouros, I., Kappelhoff, R., Bissdorf, S., Stöcker, W., & Gomis-Rüth, F. X. (2010). Proenzyme structure and activation of astacin metallopeptidase. *The Journal of Biological Chemistry*, *285*(18), 13958–13965. https://doi.org/10.1074/jbc.M109.097436
Gufler, S., Artes, B., Bielen, H., Krainer, I., Eder, M., Falschlunger, J., & Bollmann, A. (2018). *β -Catenin acts in a position-independent regeneration response in the simple eumetazoan Hydra*. *433*(August 2017), 310–323. https://doi.org/10.1016/j.ydbio.2017.09.005
Gurdon, J. B. (1995). Normal table of Xenopus laevis (Daudin): edited by PD Nieuwkoop and J. Faber Garland Publishing, 1994. In *Trends in Genetics* (Vol. 11). Elsevier.
Haan, C., & Behrmann, I. (2007). A cost effective non-commercial ECL-solution for

Western blot detections yielding strong signals and low background. *Journal of Immunological Methods*, *318*(1–2), 11–19. https://doi.org/10.1016/j.jim.2006.07.027

Hengst, J. A., & Bond, J. S. (2004). Transport of meprin subunits through the secretory pathway: role of the transmembrane and cytoplasmic domains and oligomerization. *The Journal of Biological Chemistry*, *279*(33), 34856–34864. https://doi.org/10.1074/jbc.M405774200

Hesiod, T. (1914). The Homeric Hymns and Homerica with an English Translation by Hugh G. Evelyn-White. *Cambridge, MA., Harvard University Press; London, William Heinemann Ltd.*

Hobmayer, B., Rentzsch, F., Kuhn, K., Happel, C. M., Von Laue, C. C., Snyder, P., … Holstein, T. W. (2000). WNT signalling molecules act in axis formation in the diploblastic metazoan Hydra. *Nature*, *407*(6801), 186–189. https://doi.org/10.1038/35025063

Hobmayer, E., Hatta, M., Fischer, R., Fujisawa, T., Holstein, T. W., & Sugiyama, T. (1996). Identification of a Hydra homologue of the beta-catenin/plakoglobin/armadillo gene family. *Gene*, *172*(1), 155–159. https://doi.org/10.1016/0378-1119(96)00162-x

Hochuli, E., Bannwarth, W., Döbeli, H., Gentz, R., & Stüber, D. (1988). Genetic Approach to Facilitate Purification of Recombinant Proteins with a Novel Metal Chelate Adsorbent. *Bio/Technology*, *6*(11), 1321–1325. https://doi.org/10.1038/nbt1188-1321

Holstein, T W, Hobmayer, E., & Technau, U. (2003). Cnidarians : An Evolutionarily Conserved Model System for Regeneration? *Developmental Dynamics*, 257–267. https://doi.org/10.1002/dvdy.10227

Holstein, Thomas W. (2012). The Evolution of the Wnt Pathway. *Biologypring Harbor Perspectives in Biology*, 1–18.

Huelsken, J. (2002). *The Wnt signalling pathway A Wnt Signalling Update*. *2002*(2), 3977–3978. https://doi.org/10.1242/jcs.00089

Janda, C. Y., Waghray, D., Levin, A. M., Thomas, C., & Garcia, K. C. (2012). Structural basis of Wnt recognition by Frizzled. *Science (New York, N.Y.)*, *337*(6090), 59–64. https://doi.org/10.1126/science.1222879

Janssen, R., Le Gouar, M., Pechmann, M., Poulin, F., Bolognesi, R., Schwager, E. E., … McGregor, A. P. (2010). Conservation, loss, and redeployment of Wnt ligands in protostomes: implications for understanding the evolution of segment formation. *BMC Evolutionary Biology*, *10*, 374. https://doi.org/10.1186/1471-2148-10-374

Kao, K. R., & Elinson, R. P. (1988). The entire mesodermal mantle behaves as Spemann's organizer in dorsoanterior enhanced Xenopus laevis embryos. *Developmental Biology*, *127*(1), 64–77. https://doi.org/10.1016/0012-1606(88)90189-3

Karmilin, K., Schmitz, C., Kuske, M., Körschgen, H., Olf, M., Meyer, K., … Stöcker, W. (2019). Mammalian plasma fetuin-B is a selective inhibitor of ovastacin and meprin metalloproteinases. *Scientific Reports*, *9*(1), 1–12. https://doi.org/10.1038/s41598-018-37024-5

Kessler, E, Takahara, K., Biniaminov, L., Brusel, M., & Greenspan, D. S. (1996). Bone morphogenetic protein-1: the type I procollagen C-proteinase. *Science (New York, N.Y.)*, *271*(5247), 360–362. https://doi.org/10.1126/science.271.5247.360

Kessler, Efrat, Takahara, K., Biniaminov, L., Brusel, M., & Greenspan, D. S. (1996). *Bone Morphogenetic Protein-1 : The Type I Procollagen C-Proteinase*. *271*(January), 17–20.

Kondo, S. (2017). An updated kernel-based Turing model for studying the mechanisms of biological pattern formation. *Journal of Theoretical Biology*, *414*(November 2016), 120–127. https://doi.org/10.1016/j.jtbi.2016.11.003

Kondo, S., Miura, T., & Turing, T. (2010). Reaction-Diffusion Model as a Framework for Understanding Biological Pattern Formation. *Science*, *329*(September), 1616–1621.

Kozakov, D., Hall, D. R., Xia, B., Porter, K. A., Padhorny, D., Yueh, C., … Vajda, S. (2017). The ClusPro web server for protein-protein docking. *Nature Protocols*, *12*(2), 255–278. https://doi.org/10.1038/nprot.2016.169

Kramps, T., Peter, O., Brunner, E., Nellen, D., Froesch, B., Chatterjee, S., … Basler, K. (2002). Wnt/wingless signaling requires BCL9/legless-mediated recruitment of pygopus to the nuclear beta-catenin-TCF complex. *Cell*, *109*(1), 47–60. https://doi.org/10.1016/s0092-8674(02)00679-7

Kühl, M., Sheldahl, L. C., Malbon, C. C., & Moon, R. T. (2000). Ca(2+)/calmodulin-dependent protein kinase II is stimulated by Wnt and Frizzled homologs and promotes ventral cell fates in Xenopus. *The Journal of Biological Chemistry*, *275*(17), 12701–12711. https://doi.org/10.1074/jbc.275.17.12701

Kunick, C., Lauenroth, K., Leost, M., & Lemcke, T. (2004). *1-Azakenpaullone is a selective inhibitor of glycogen synthase kinase-3*. *14*, 413–416. https://doi.org/10.1016/j.bmcl.2003.10.062

Kusserow, A., Pang, K., Sturm, C., Hrouda, M., Lentfer, J., Schmidt, H. A., … Holstein, T. W. (2005). *Unexpected complexity of the Wnt gene family in a sea anemone*. *433*(January), 65–69.

Lengfeld, T., Watanabe, H., Simakov, O., Lindgens, D., Gee, L., Law, L., … Holstein, T. W. (2009). Multiple Wnts are involved in Hydra organizer formation and regeneration. *Developmental Biology*, *330*(1), 186–199. https://doi.org/10.1016/j.ydbio.2009.02.004

Li, S. W., Sieron, A. L., Fertala, A., Hojima, Y., Arnold, W. V, & Prockop, D. J. (1996). The C-proteinase that processes procollagens to fibrillar collagens is identical to the protein previously identified as bone morphogenic protein-1. *Proceedings of the National Academy of Sciences of the United States of America*, *93*(10), 5127–5130. https://doi.org/10.1073/pnas.93.10.5127

Lommel, M., Stromp, J., Hellewell, A. L., Prakash, G., Christofidou, E. D., Thomson, A. R., … Özbek, S. (2018). *Hydra Mesoglea Proteome Identifies Thrombospondin as a Conserved Component Active in Head Organizer Restriction*. (September 2017), 1–18. https://doi.org/10.1038/s41598-018-30035-2.

MacDonald, B. T., Tamai, K., & He, X. (2009). Wnt/beta-catenin signaling: components, mechanisms, and diseases. *Developmental Cell*, *17*(1), 9–26. https://doi.org/10.1016/j.devcel.2009.06.016

Maéno, M., Xue, Y., Wood, T. I., Ong, R. C., & Kung, H. F. (1993). Cloning and expression of cDNA encoding Xenopus laevis bone morphogenetic protein-1 during early embryonic development. *Gene*, *134*(2), 257–261. https://doi.org/10.1016/0378-1119(93)90103-a

Meinhardt, H. (1993). *A model for pattern formation of hypostome , tentacles and foot in Hydra : how to form structures close to each other , how to form them at a*

distance. 321–333.
Meinhardt, H. (2012). Turing's theory of morphogenesis of 1952 and the subsequent discovery of the crucial role of local self enhancement and long-range inhibition. *Interface Focus*, *2*(4), 407–416. https://doi.org/10.1098/rsfs.2011.0097
Meinhardt, H., & Gierer, A. (2000). *Pattern formation by local self-activation and lateral inhibition*. 753–760.
Miljkovic-Licina, M., Chera, S., Ghila, L., & Galliot, B. (2007). *Head regeneration in wild-type hydra requires de novo neurogenesis*. *1201*, 1191–1201. https://doi.org/10.1242/dev.02804
Miller, J. R. (2002). The Wnts. *Genome Biology*, *3*(1), REVIEWS3001. https://doi.org/10.1186/gb-2001-3-1-reviews3001
Möhrlen, F., Maniura, M., Plickert, G., Frohme, M., & Frank, U. (2006). Evolution of astacin-like metalloproteases in animals and their function in development. *Evolution & Development*, *8*(2), 223–231. https://doi.org/10.1111/j.1525-142X.2006.00092.x
Mosimann, C., Hausmann, G., & Basler, K. (2006). Parafibromin/Hyrax activates Wnt/Wg target gene transcription by direct association with beta-catenin/Armadillo. *Cell*, *125*(2), 327–341. https://doi.org/10.1016/j.cell.2006.01.053
Murphy, S. (1977). *Characterization of Interstitial Stem Cells in Hydra by Cloning*. *383*, 372–383.
Nakamura, Y., Tsiairis, C. D., Özbek, S., & Holstein, T. W. (2011). Autoregulatory and repressive inputs localize Hydra Wnt3 to the head organizer. *Proceedings of the National Academy of Sciences of the United States of America*, *108*(22), 9137–9142. https://doi.org/10.1073/pnas.1018109108
Nguyen, T., Jamal, J., Shimell, M. J., Arora, K., & O'Connor, M. B. (1994). Characterization of tolloid-related-1: a BMP-1-like product that is required during larval and pupal stages of Drosophila development. *Developmental Biology*, *166*(2), 569–586. https://doi.org/10.1006/dbio.1994.1338
Niehrs, C. (2012). The complex world of WNT receptor signalling. *Nature Publishing Group*, *13*(December), 25–27. https://doi.org/10.1038/nrm3470
Nishimiya-Fujisawa, C., & Kobayashi, S. (2012). *Germline stem cells and sex determination in Hydra*. *508*(June), 499–508. https://doi.org/10.1387/ijdb.123509cf
Nusse, R., Brown, A., Papkoff, J., Scambler, P., Shackleford, P., McMahon, A., … Varmu, H. (1991). A New Nomenclature for int-1 and Related Genes: The Wnt Gene Family. *Cell*, *64*, 1991. https://doi.org/10.1016/0092-8674(91)90633-a.
Nusse, Roe, & Varmus, H. E. (1982). *Many Tumors Induced by the Mouse Mammary Tumor Virus Contain a Provirus Integrated in the Same Region of the Host Genome*. *31*(November), 99–109.
Okada, A., Sano, K., Nagata, K., Yasumasu, S., Ohtsuka, J., Yamamura, A., … Tanokura, M. (2010). Crystal structure of zebrafish hatching enzyme 1 from the zebrafish Danio rerio. *Journal of Molecular Biology*, *402*(5), 865–878. https://doi.org/10.1016/j.jmb.2010.08.023
Pan, T., Gröger, H., Schmid, V., & Spring, J. (1998). A toxin homology domain in an astacin-like metalloproteinase of the jellyfish Podocoryne carnea with a dual role in digestion and development. *Development Genes and Evolution*, *208*(5), 259–266. https://doi.org/10.1007/s004270050180
Pappano, W. N., Steiglitz, B. M., Scott, I. C., Keene, D. R., & Greenspan, D. S.

(2003). Use of Bmp1/Tll1 doubly homozygous null mice and proteomics to identify and validate in vivo substrates of bone morphogenetic protein 1/tolloid-like metalloproteinases. *Molecular and Cellular Biology*, *23*(13), 4428–4438. https://doi.org/10.1128/mcb.23.13.4428-4438.2003

Paps, J., & Holland, P. W. H. (2018). Reconstruction of the ancestral metazoan genome reveals an increase in genomic novelty. *Nature Communications*, *9*(1), 1730. https://doi.org/10.1038/s41467-018-04136-5

Petersen, C., & Reddien, P. (2009). *Wnt Signaling and the Polarity of the Primary Body Axis*. https://doi.org/10.1016/j.cell.2009.11.035

Petersen, H. O., Höger, S. K., Looso, M., Lengfeld, T., Kuhn, A., Warnken, U., … Holstein, T. W. (2015). A Comprehensive Transcriptomic and Proteomic Analysis of Hydra Head Regeneration. *Molecular Biology and Evolution*, *32*(8), 1928–1947. https://doi.org/10.1093/molbev/msv079

Pettersen, E. F., Goddard, T. D., Huang, C. C., Couch, G. S., Greenblatt, D. M., Meng, E. C., & Ferrin, T. E. (2004). UCSF Chimera--a visualization system for exploratory research and analysis. *Journal of Computational Chemistry*, *25*(13), 1605–1612. https://doi.org/10.1002/jcc.20084

Philipp, I., Aufschnaiter, R., Ozbek, S., Pontasch, S., Jenewein, M., Watanabe, H., … Hobmayer, B. (2009). Wnt/ -Catenin and noncanonical Wnt signaling interact in tissue evagination in the simple eumetazoan Hydra. *Proceedings of the National Academy of Sciences*, *106*(11), 4290–4295. https://doi.org/10.1073/pnas.0812847106

Piccolo, S., Agius, E., Lu, B., Goodman, S., Dale, L., & De Robertis, E. M. (1997). Cleavage of Chordin by Xolloid metalloprotease suggests a role for proteolytic processing in the regulation of Spemann organizer activity. *Cell*, *91*(3), 407–416. https://doi.org/10.1016/s0092-8674(00)80424-9

Pseudo-Apollodorus, B. (n.d.). *Bibliotheca*. *ii.5.2*.

Rasmussen, H. S., & McCann, P. P. (1997). Matrix metalloproteinase inhibition as a novel anticancer strategy: A review with special focus on Batimastat and Marimastat. *Pharmacology and Therapeutics*, *75*(1), 69–75. https://doi.org/10.1016/S0163-7258(97)00023-5

Rijsewijk, F. (1987). *The Drosophila Homolog of the Mouse Mammary Oncogene int-1 Is Identical to the Segment Polarity Gene wingless*. *50*, 649–657.

Sali, A., & Blundell, T. L. (1993). Comparative protein modelling by satisfaction of spatial restraints. *Journal of Molecular Biology*, *234*(3), 779–815. https://doi.org/10.1006/jmbi.1993.1626

Sarras,Michael P.; Meador JR. Darrel; Zhang, A. (1991). Extracellular Matrix (Mesoglea) of Hydra Vulgaris. *Developmental Biology*, *500*, 495–500.

Sarras, M. P. J. (1996). BMP-1 and the astacin family of metalloproteinases: a potential link between the extracellular matrix, growth factors and pattern formation. *BioEssays : News and Reviews in Molecular, Cellular and Developmental Biology*, *18*(6), 439–442. https://doi.org/10.1002/bies.950180604

Sato, M., Tashiro, H., Oikawa, A., & Sawada, Y. (1992). Patterning in hydra cell aggregates without the sorting of cells from different axial origins. *Developmental Biology*, *151*(1), 111–116. https://doi.org/https://doi.org/10.1016/0012-1606(92)90218-6

Schambony, A., & Wedlich, D. (2007). Wnt-5A/Ror2 regulate expression of XPAPC through an alternative noncanonical signaling pathway. *Developmental Cell*, *12*(5), 779–792. https://doi.org/10.1016/j.devcel.2007.02.016

Schlenzig, D., Wermann, M., Ramsbeck, D., Moenke-Wedler, T., & Schilling, S. (2015). Expression, purification and initial characterization of human meprin β from Pichia pastoris. *Protein Expression and Purification*, *116*, 75–81. https://doi.org/10.1016/j.pep.2015.08.001

Schmidt, T., & David, C. N. (1986). Gland cells in Hydra: cell cycle kinetics and development. *J Cell Sci*, *85*, 197–215. Retrieved from http://www.ncbi.nlm.nih.gov/entrez/query.fcgi?cmd=Retrieve&db=PubMed&dopt=Citation&list_uids=3539952

Shimell, M. J., Ferguson, E. L., Childs, S. R., & O'Connor, M. B. (1991). The Drosophila dorsal-ventral patterning gene tolloid is related to human bone morphogenetic protein 1. *Cell*, *67*(3), 469–481. https://doi.org/https://doi.org/10.1016/0092-8674(91)90522-Z

Shimizu, H., Julius, M. A., Giarré, M., Zheng, Z., Brown, A. M., & Kitajewski, J. (1997). Transformation by Wnt family proteins correlates with regulation of beta-catenin. *Cell Growth & Differentiation : The Molecular Biology Journal of the American Association for Cancer Research*, *8*(12), 1349–1358.

Siebert, S., Anton-Erxleben, F., & Bosch, T. C. G. (2008). *Cell type complexity in the basal metazoan Hydra is maintained by both stem cell based mechanisms and transdifferentiation*. *313*, 13–24. https://doi.org/10.1016/j.ydbio.2007.09.007

Siebert, S., Farrell, J. A., Cazet, J. F., Abeykoon, Y., Primack, A. S., Schnitzler, C. E., & Juliano, C. E. (2019). *Stem cell differentiation trajectories in Hydra resolved at single-cell resolution*. *341*(July). https://doi.org/10.1126/science.aav9314

Sonneborn, H. H., Zwilling, R., & Pfleiderer, G. (1969). Evolution of endopeptidases. X. Cleavage specificity of low molecular weight protease from Astacul leptodactylus Esch. *Hoppe-Seyler's Zeitschrift fur physiologische Chemie*, *350*(9), 1097–1102.

Steinbeisser, H., De Robertis, E. M., Ku, M., Kessler, D. S., & Melton, D. A. (1993). Xenopus axis formation: induction of goosecoid by injected Xwnt-8 and activin mRNAs. *Development*, *118*(2), 499 LP – 507. Retrieved from http://dev.biologists.org/content/118/2/499.abstract

Sterchi, E. E., Naim, H. Y., & Lentze, M. J. (1988). Biosynthesis of N-benzoyl-L-tyrosyl-p-aminobenzoic acid hydrolase: disulfide-linked dimers are formed at the site of synthesis in the rough endoplasmic reticulum. *Archives of Biochemistry and Biophysics*, *265*(1), 119–127. https://doi.org/10.1016/0003-9861(88)90377-3

Stöcker, W., Sauer, B., & Zwilling, R. (2009). Kinetics of Nitroanilide Cleavage by Astacin. *Biological Chemistry*, *372*(1), 385–392. https://doi.org/https://doi.org/10.1515/bchm3.1991.372.1.385

Stöcker, Walter, & Bode, W. (1995). Structural features of a superfamily of zinc-endopeptidases: the metzincins. *Current Opinion in Structural Biology*. https://doi.org/5:383-390

Strutt, D. (2003). *Frizzled signalling and cell polarisation in Drosophila and vertebrates*. https://doi.org/10.1242/dev.00695

Technau, U., Steele, R. E., Technau, U., & Steele, R. E. (2012). *Evolutionary crossroads in developmental biology : Cnidaria Evolutionary crossroads in developmental biology : Cnidaria*. *4491*. https://doi.org/10.1242/dev.090472

Torres, M. A., Yang-Snyder, J. A., Purcell, S. M., DeMarais, A. A., McGrew, L. L., & Moon, R. T. (1996). Activities of the Wnt-1 class of secreted signaling factors are antagonized by the Wnt-5A class and by a dominant negative cadherin in early Xenopus development. *The Journal of Cell Biology*, *133*(5), 1123–1137.

https://doi.org/10.1083/jcb.133.5.1123
Trembley, A. (1744). Mémoires Pour Servir à l'Histoire d'un Genre de Polypes d'Eau Douce, à Bras en Forme de Cornes. *Chez Jean & Herman Verbeek*, 324.
Turing, A. (1952). The chemical basis of morphogenesis. *University of Manchester*, *237*(August), 37–72.
Turunen, S. P., Tatti-Bugaeva, O., & Lehti, K. (2017). Membrane-type matrix metalloproteases as diverse effectors of cancer progression. *Biochimica et Biophysica Acta. Molecular Cell Research*, *1864*(11 Pt A), 1974–1988. https://doi.org/10.1016/j.bbamcr.2017.04.002
Unterseher, F., Hefele, J. A., Giehl, K., De Robertis, E. M., Wedlich, D., & Schambony, A. (2004). Paraxial protocadherin coordinates cell polarity during convergent extension via Rho A and JNK. *The EMBO Journal*, *23*(16), 3259–3269. https://doi.org/10.1038/sj.emboj.7600332
van Tienen, L. M., Mieszczanek, J., Fiedler, M., Rutherford, T. J., & Bienz, M. (2017). Constitutive scaffolding of multiple Wnt enhanceosome components by Legless/BCL9. *ELife*, *6*. https://doi.org/10.7554/eLife.20882
Vogg, M. C., Beccari, L., Iglesias Ollé, L., Rampon, C., Vriz, S., Perruchoud, C., … Galliot, B. (2019). An evolutionarily-conserved Wnt3/β-catenin/Sp5 feedback loop restricts head organizer activity in Hydra. *Nature Communications*, *10*(1), 1–28. https://doi.org/10.1038/s41467-018-08242-2
Vogg, M. C., Galliot, B., & Tsiairis, C. D. (2019). *Model systems for regeneration : Hydra*. https://doi.org/10.1242/dev.177212
Watanabe, H., Schmidt, H. A., Kuhn, A., Höger, S. K., Kocagöz, Y., Laumann-Lipp, N., … Holstein, T. W. (2014). Nodal signalling determines biradial asymmetry in Hydra. *Nature*, *515*(7525), 112–115. https://doi.org/10.1038/nature13666
Weidinger, G., & Moon, R. T. (2003). *When Wnts antagonize Wnts*. 2002–2004. https://doi.org/10.1083/jcb.200307181
Weismann, A. (1883). Die Entstehung der Sexualzellen bei den Hydromedusen: Zugleich ein Beitrag zur Kenntniss des Baues und der Lebenserscheinungen dieser Gruppe. *Fischer, Jena*.
Wolfman, N. M., McPherron, A. C., Pappano, W. N., Davies, M. V, Song, K., Tomkinson, K. N., … Lee, S.-J. (2003). Activation of latent myostatin by the BMP-1/tolloid family of metalloproteinases. *Proceedings of the National Academy of Sciences of the United States of America*, *100*(26), 15842–15846. https://doi.org/10.1073/pnas.2534946100
Wozney, J. M., Rosen, V., Celeste, A. J., Mitsock, L. M., Whitters, M. J., Kriz, R. W., … Wang, E. A. (1988). Novel regulators of bone formation: molecular clones and activities. *Science (New York, N.Y.)*, *242*(4885), 1528–1534. https://doi.org/10.1126/science.3201241
Yan, L, Fei, K., Zhang, J., Dexter, S., & Sarras, M. P. (2000). Identification and characterization of hydra metalloproteinase 2 (HMP2): a meprin-like astacin metalloproteinase that functions in foot morphogenesis. *Development (Cambridge, England)*, *127*(1), 129–141. Retrieved from http://www.ncbi.nlm.nih.gov/pubmed/10654607
Yan, L, Pollock, G. H., Nagase, H., & Sarras, M. P. (1995). A 25.7 x 10(3) M(r) hydra metalloproteinase (HMP1), a member of the astacin family, localizes to the extracellular matrix of Hydra vulgaris in a head-specific manner and has a developmental function. *Development (Cambridge, England)*, *121*(6), 1591–1602. Retrieved from http://www.ncbi.nlm.nih.gov/pubmed/7600977

Yan, Li, Leontovich, A., Fei, K., & Sarras, M. P. (2000). Hydra metalloproteinase 1: A secreted astacin metalloproteinase whose apical axis expression is differentially regulated during head regeneration. *Developmental Biology*, *219*(1), 115–128. https://doi.org/10.1006/dbio.1999.9568

Yao, T. (1945). Studies on the organizer problem in Pelmatohydra oligactis: I. The induction potency of the implants and the nature of the induced hydranth. *Journal of Experimental Biology*, *21*(3–4), 147–150.

Yiallouros, I., Kappelhoff, R., Schilling, O., Wegmann, F., Helms, M. W., Auge, A., … Stöcker, W. (2002). Activation mechanism of pro-astacin: Role of the pro-peptide, tryptic and autoproteolytic cleavage and importance of precise amino-terminal processing. *Journal of Molecular Biology*, *324*(2), 237–246. https://doi.org/10.1016/S0022-2836(02)01102-6

Zhang, X., Abreu, J. G., Yokota, C., Macdonald, B. T., Loureiro, K., Coburn, A., … He, X. (2013). Tiki1 is required for head formation via Wnt cleavage-oxidation and inactivation. *Cell*, *149*(7), 1565–1577. https://doi.org/10.1016/j.cell.2012.04.039.Tiki1

Zhang, X., Macdonald, B. T., Gao, H., Shamashkin, M., Coyle, A. J., & Martinez, R. V. (2016). *Characterization of Tiki, a New Family of Wnt-specific*. *291*(5), 2435–2443. https://doi.org/10.1074/jbc.M115.677807

Ziegler, B., Yiallouros, I., Trageser, B., Kumar, S., Mercker, M., Kling, S., … Özbek, S. (2020). *Wnt-specific astacin proteinase controls head formation in*. 1–45.

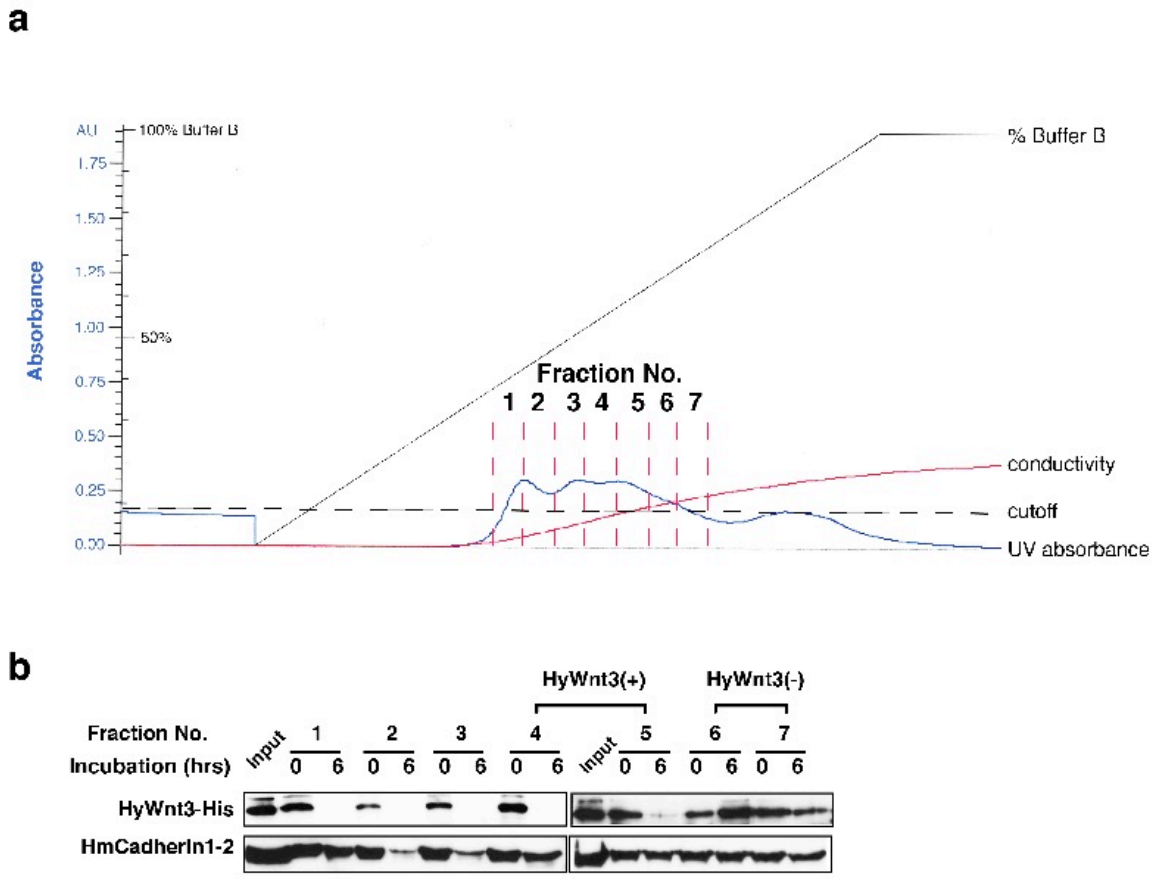

Supplementary Figure 1. Chromatogram for HyWnt3(+) and HyWnt3(-) secretome analysis. Adapted from (Ziegler et al., 2020), in preparation. (a) Chromatogram after an ion exchange of hydra HL pool. "7 fractions of 0.5 ml exceeding an absorption unit threshold of 0.175 were collected as indicated. The cut-off was chosen to provide a critical total protein concentration (> 80 μg) for the subsequent proteome analysis. (b) Peak fractions from (a) were re-screened for HyWnt3-His processing activity. A fragment of *Hydra* cadherin extracellular domain comprising the first two N-terminal cadherin repeats (HmCadherin1-2) was used as control substrate to monitor unspecific matrix metalloproteinase activity. Accordingly, fractions 4-5 were pooled and analyzed by mass spectrometry as HyWnt3-His(+) sample, fractions 6-7 as HyWnt3-His(-) sample."((Ziegler et al., 2020)in preparation)

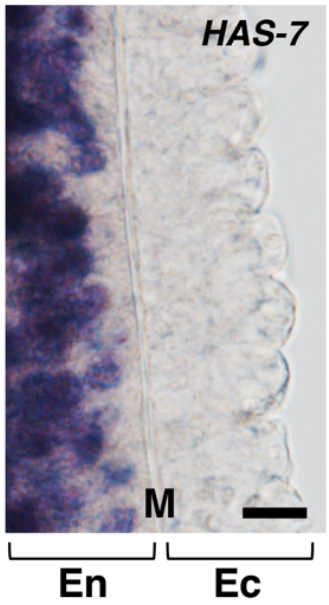

Supplementary Figure 2. Mesoglea close-up of *HAS-7* mRNA detection. Modified from (Ziegler et al., 2020), in preparation. Close up image showing the epithelial the double cell layer of *Hydra*. The endoderm (En) shows *HAS-7* expression in the gland cells. The inner endodermal cell layer is separated by the cell-free layer, the mesoglea (M), from the outer ectoderm (Ec).
Scalebar = 20 μM.

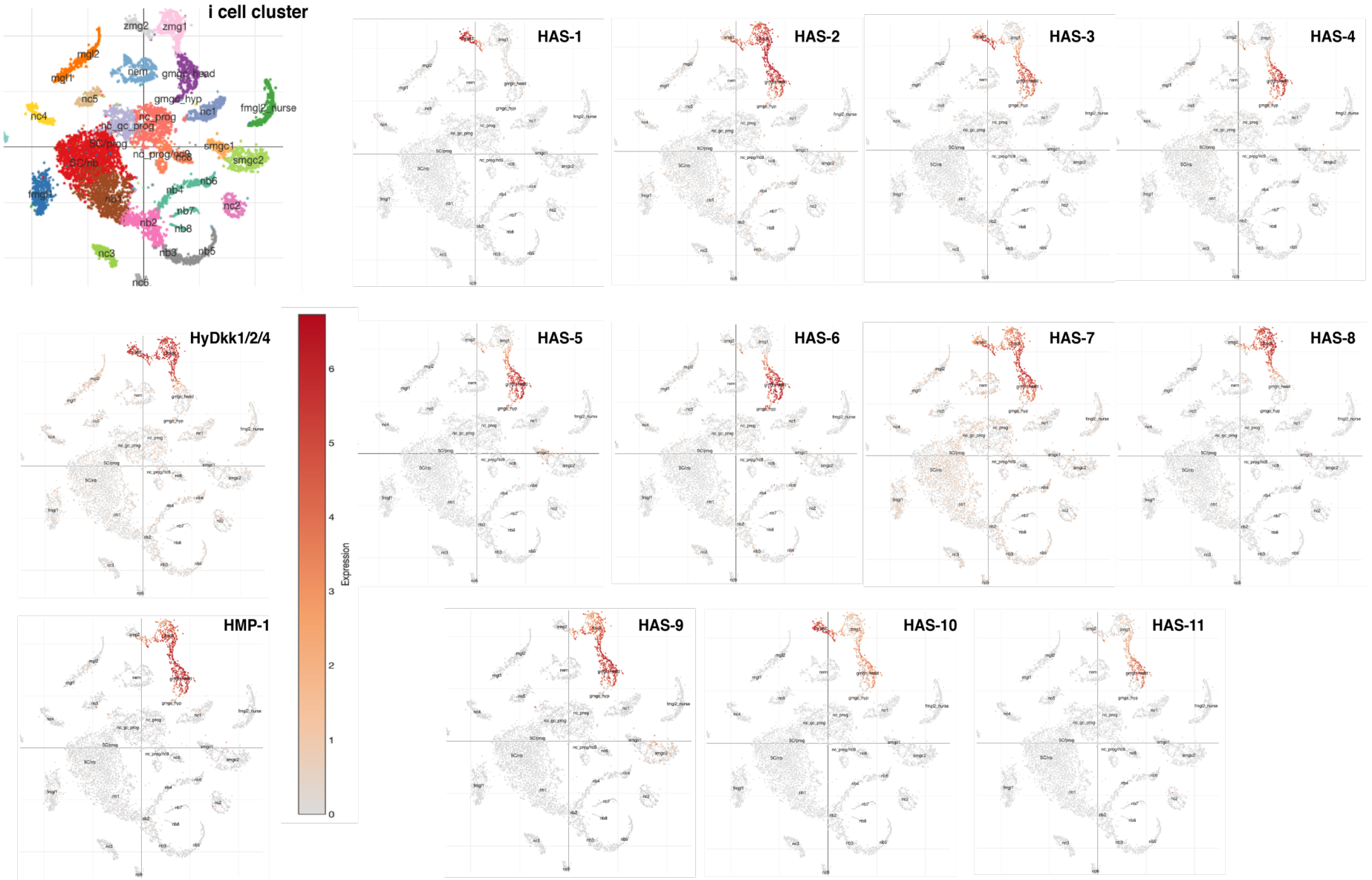
i cell cluster
zmg2
zmg1
mgl2
mgl1
nem
gmgc_head
nc5
gmgc_hyp
nc4
nc1
fmg2_nurse
nc_prog
nc_gc_prog
SC/prog
nc_prog/nc9
nc6
smgc1
SC/nb
smgc2
nb6
fmg1
nb1
nb4
nc2
nb7
nb2
nb8
nb3
nb5
nc3
HAS-1
HAS-2
HAS-3
HAS-4
HyDkk1/2/4
HAS-5
HAS-6
HAS-7
HAS-8
HMP-1
HAS-9
HAS-10
HAS-11
Expression
0
1
2
3
4
5
6

Supplementary Figure 3. Transcriptional profiles i-cell cluster overview in single cells of Hydra astacins and HyDkk1/2/4.

Singel cell sequencing t-SNE scatter blots from the i-cell cluster obtained by https://singlecell.broadinstitute.org/single_cell/study/SCP260/stem-cell-differentiation-trajectories-in-hydra-resolved-at-single-cell-resolution (Siebert et al., 2019). The transcript IDs are given in Table 2 "Single cell sequencing IDs". Transcriptional profiles of novel *Hydra* astacin metalloproteases, HMP-1 and HyDkk1/2/4. HyDkk1/2/4 (AM182483.1), HMP1 (NP_001296695.1), HAS-1 (XP_012565441.1), HAS-2 (XP_002162822.1), HAS-3 (XP_002166229.3), HAS-4 (XP_002162738.1), HAS-5 (XP_002164800.1), HAS-6 (XP_002157397.2), HAS-7 (XP_012560086.1), HAS-8 (XP_002153855.1), HAS-9 (XP_002161766.1), HAS-10 (XP_002159980.2), HAS-11(XP_012561076.1). Cluster label abbreviation key is as follows: bat: battery cell, fmgl: female germ-line, gc: gland cell, gmgc: granular mucous gland cell, hyp: hypostome, id: integration doublet, mgl: male germline, nb: nematoblast, nc: neuronal cell, nem: nematocyte, nurse: nurse cells, prog: progenitor, SC: stem cell, smgc: spumous mucous gland cell, zmg: zymogen gland cell. Numbers indicate different cell populations within a cluster.

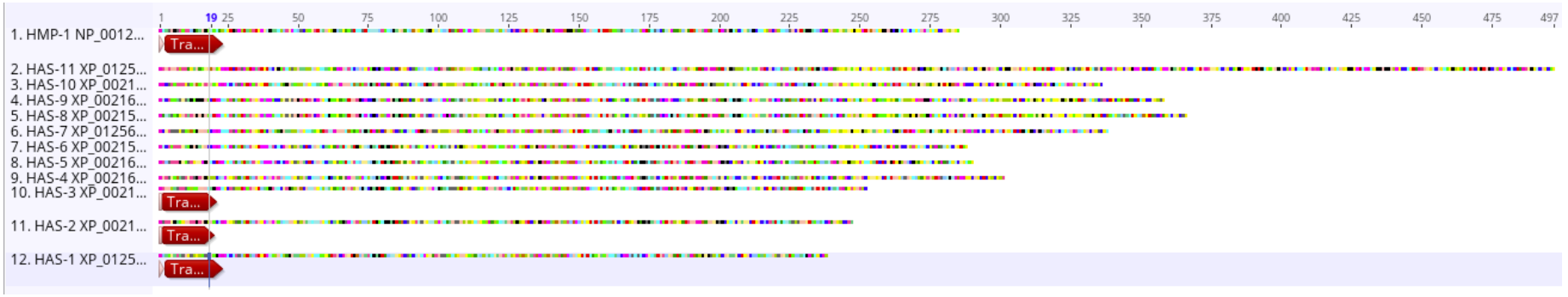

Supplementary Figure 4. Transmembrane domain prediction. Alignment and prediction of all analyzed HAS. Note that red arrows mark predicted transmembrane domains are within the signal peptide region. Accession numbers are given in Table 3.